NASA CR-
174973

DEVELOPMENT OF ADVANCED HIGH-TEMPERATURE HEAT FLUX SENSORS PHASE II VERIFICATION TESTING

by W.H. Atkinson, M.A. Cyr, and R.R. Strange

United Technologies Corporation
Pratt & Whitney Group
Engineering Division

August 1985

Prepared for

NATIONAL AERONAUTICS AND SPACE ADMINISTRATION

NASA LEWIS RESEARCH CENTER
21000 BROOKPARK ROAD
CLEVELAND, OHIO 44135

Contract NAS3-22133

NASA

UNITED TECHNOLOGIES
PRATT&WHITNEY
AIRCRAFT

400 Main Street
East Hartford, Connecticut 06108

In reply please refer to:
WHA:C:0177H: MS 116-01
Ref. No. PWA-5723-68

September 23, 1985

To: National Aeronautics and Space Administration
Lewis Research Center
21000 Brookpark Road
Cleveland, Ohio 44135

Attention: Mr. Howard Hobart, Project Manager
Mail Stop 77-1

Subject: Final Report on "Advanced High-Temperature Heat Flux Sensor Development", CR No. 174973

References: (1) Contract NAS3-22133
(2) NASA Letter, H.F. Hobart to W. Atkinson, dated August 26, 1985

Mr. Hobart:

The subject Final Report prepared under the reference (1) contract has been printed and distributed in accordance with the distribution list submitted under the reference (2) letter. Accordingly we have incorporated the changes noted in the Draft Final Report as requested by NASA.

Sincerely yours,

UNITED TECHNOLOGIES CORPORATION
Pratt & Whitney
Engineering Division

William H. Atkinson

William H. Atkinson
Program Manager

cc: Air Force Plant Representative Office
UTC/Pratt & Whitney
East Hartford, Connecticut 06108
Attn: I. Goldberg, MS 104-08

1.REPORT NO. CR 174973	2. GOVERNMENT AGENCY NASA/Lewis	3.RECIPIENT'S CATALOG NO.
4.TITLE AND SUBTITLE Development of Advanced High-Temperature Heat Flux Sensors (Phase II-Verification Testing)		5. REPORT DATE August 1985 6. PERFORMING ORG. CODE
7.AUTHOR(S) William H. Atkinson, Marcia A. Cyr and Richard R. Strange		8. PERFORMING ORG. REPT. NO. PWA 5914-39
9.PERFORMING ORG. NAME AND ADDRESS UNITED TECHNOLOGIES CORPORATION Pratt & Whitney Group Engineering Division East Hartford, CT 06108		10. WORK UNIT NO. 11. CONTRACT OR GRANT NO. NAS3-22133
12. SPONSORING AGENCY NAME AND ADDRESS National Aeronautics and Space Administration Lewis Research Center 21000 Brookpark Road		13. TYPE REPT./PERIOD COVERED Final Report 14. SPONSORING AGENCY CODE

15. SUPPLEMENTARY NOTES

Project Manager: H. Hobart, NASA Lewis Research Center

16. ABSTRACT:

A two-phase program was conducted to develop heat flux sensors capable of making heat flux measurements throughout the hot section of gas turbine engines. In Phase I, three types of heat flux sensors were selected; embedded thermocouple, laminated, and Gardon gauge sensors. Phase II, reported herein, provided for demonstration of the ability of these sensors to operate in an actual engine enviroment. A segmented liner of each of two combustors being used in the Broad Specification Fuels Combustor program was instrumented with the three types of heat flux sensors then tested in a high pressure combustor rig. Radiometer probes were also used to measure the radiant heat loads to more fully characterize the combustor environment.

Test results showed the heat flux sensors to be in good agreement with radiometer probes and the predicted data trends. In general, heat flux sensors have strong potential for use in combustor development programs.

17. KEY WORDS (SUGGESTED BY AUTHOR(S))	18. DISTRIBUTION STATEMENT
Heat Flux Sensors Combustor Liners	

19. SECURITY CLASS THIS (REPT)	20. SECURITY CLASS THIS (PAGE)	21. NO. PGS	22. PRICE *

* For sale by the National Technical Information Service, Springfield, VA 22161

FOREWORD

This Final Report presents the results of Phase II of a development program conducted by Pratt & Whitney to develop heat flux sensors capable of making heat flux measurements throughout the hot section of gas turbine engines. This effort was conducted for the National Aeronautics and Space Administration under Contract NAS3-22133. This program was conducted under the direction of Mr. Howard Hobart who served as tne NASA Program Manager. The Program Manager at United Technologies Corporation, Pratt & Whitney, was Mr. William H. Atkinson. Dick Strange and Marcia Cyr contributed significantly to the analytical effort.

TABLE OF CONTENTS

Section	Title	Page
1.0	SUMMARY	1
2.0	INTRODUCTION	2
3.0	SUMMARY OF SENSOR TYPES	3
	Overview	3
	Heat Flux Sensor Types	3
	Embedded Thermocouple Sensors	3
	Laminated Sensors	5
	Gardon Gauge Sensors	5
	Radiometer Probes	7
	Porous Plug	7
	Medtherm	7
4.0	FABRICATION	10
	Fabrication of Sensor Body Material	10
	Machining of the Sensor Bodies	10
	Instrumenting the Sensors	13
	Porous Plug Radiometer Fabrication	15
5.0	CALIBRATION OF SENSORS	16
	Calibration Fixture	16
	Quartz Lamp Bank Calibration Facility	16
	Calibration Process	19
	Sensor Calibration Results	19
	Baseline Combustor	19
	Pratt & Whitney In-House Program	28
	Radiometer Calibrations	28
6.0	INSTALLATION OF SENSORS INTO THE COMBUSTOR LINERS	37
7.0	DESCRIPTION OF TEST PLAN	44
	Test Facilities	44
	Run Program	44
8.0	TEST RESULTS	46
	Baseline Combustor-X-902 Stand	46
	Baseline Combustor-United Technologies Research Center (UTRC)	47
	Post Test Inspection of Baseline Combustor	47
	Variable Geometry Combustor-X902 Stand	52
	Radiometer Results-Variable Area Combustor	52
	Heat Flux Sensor Results Variable Geometry Combustor	56
9.0	CONCLUSIONS AND RECOMMENDATIONS	64
REFERENCES		64
DISTRIBUTION LIST		65

SECTION 1.0
SUMMARY

The overall objectives of this program were to develop and test miniature high temperature heat flux sensors suitable for making heat flux measurements in experimental combustor liners of advanced aircraft gas turbine engines. During phase I of this program, a literature search, followed by various analyses, was conducted to select the most promising candidates for this application. Based on the analyses, three types of sensors were chosen for further development: embedded thermocouple sensors, laminated sensors, and Gardon gauges. Sensors of these three types were then fabricated, calibrated, and endurance tested in the laboratory.

During phase II of the program, sensors were fabricated, calibrated, and installed in a combustor liner segment to be run in conjunction with the NASA Broad Specification Fuels Combustor Technology Contract (NAS3-12169). A second combustor liner segment was instrumented under a Pratt & Whitney in-house program. These heat flux sensors, as well as radiometers, were then run in a high pressure combustor rig to verify their ability to make heat flux measurements. Based on analysis of the data resulting from the program, the following conclusions are made:

- Sensors of the three types fabricated met the geometrical requirements and were capable of meeting the contract accuracy goal of ± 5 percent of the nominal full scale heat flux of $1X10^6$ watts per square meter.

- Both laboratory (Phase I) and high pressure combustor rig (Phase II) testing showed that the sensors are capable of surviving extended exposure to burner environmental conditions.

- Results from the total heat flux sensors in the high pressure combustor rig tests agreed well with the radiometer data trends as well as the pretest predicted data trends.

- Sensor failure rate was relatively high. The primary cause of the failures was identified as leadwire failure external to the sensors.Care must be taken due to the fine gauge leadwires. Handling of the combustor should be minimized following heat flux sensor installation.

- Miniature high temperature heat flux sensors are now available for advanced combustor development.

SECTION 2.0
INTRODUCTION

Designing combustor liners and turbine airfoils, which are durable and use a minimum amount of cooling air, requires a thorough knowledge of heat flux characteristics throughout the hot section of modern gas turbine engines. Although analytical models have been developed to predict heat fluxes, technology has not been available to measure heat flux directly on hot section components. Such measurements are necessary for modification and/or verification of analytical procedures that would lead to combustor liners and turbine airfoils having longer hot section lives, minimizing the amount of cooling required, and thus maintaining efficiency and economy. Therefore, miniature sensors which can measure the heat flux per unit area (kw/m^2), must be developed for these high temperature, high pressure applications.

The measurement of heat loads in the hot section is complicated by several factors: 1) sufficiently high temperature levels which demand use of high temperature resistant materials to fabricate the sensors and leads; 2) extreme temperature gradients along the surface of the hot section components which increase the need for small sensors; 3) the use of thermal and electrical insulation in many sensor designs to enhance one-directional heat flow; and 4) the presence of the heat flux sensor may disturb the thermal profile where it is installed and alter the heat flux relative to the unperturbed liner. Care must be exercised in selecting the material properties and geometry of the installation to minimize the surface temperature perturbation. The presence of the sensor and the installation of the sensor into the test hardware can have a pronounced effect on the sensor accuracy, so these factors must be considered during sensor design.

Phase I of this contract provided for the design, fabrication and laboratory testing of advanced high temperature steady state heat flux sensors for measuring the heat flow through combustor liner walls. Three types of sensors; embedded thermocouple, laminated sensors, and Gardon gauges, were developed and tested under thermal cycle and thermal soak conditions that are representative of actual engine environment.

The purpose of the Phase II effort, which is reported herein, was to install these sensors in a segmented combustor liner and demonstrate their use in high pressure burner rig tests. Two combustor liners used in the Broad Specification Fuels Combustor Technology Contract (NAS3-23269) were instrumented and tested in a high pressure combustor rig. Radiometer probes were also utilized to measure the radiative portion of the total incident heat load in order to more fully characterize the environment, allowing a correlation between radiometers with different fields of view as well as a comparison of the heat load incident on the liner with the heat flux transmitted through the liner.

SECTION 3.0
SUMMARY OF SENSOR TYPES

OVERVIEW

Under Phase I of this contract, three types of high temperature steady state heat flux sensors were developed and laboratory tested. These types were embedded thermocouple sensors, laminated sensors and Gardon gauge sensors. The work involved in the development of these sensors is discussed in Reference 1. Under Phase II, these sensor types were installed in segmented combustor liners and tested in a high pressure combustor rig to verify their ability to make heat flux measurements in the high pressure combustor environment. In addition to the heat flux sensors, measurements of the radiant heat load incident on the combustor wall were made with two types of radiometer probes: porous plug radiometer and Medtherm radiometer. The three types of heat flux sensors and the radiometer probes are described below.

HEAT FLUX SENSOR TYPES

Embedded Thermocouple Sensors

The embedded thermocouple sensors were fabricated in two configurations, one using dual conductor swaged wire and the other using single conductor swaged wire. A small diameter (0.025 cm) for the wire sheath was chosen to reduce the thermal perturbations. The use of single conductor swaged wire provided a heavier gauge conductor to increase durability.

The embedded thermocouple sensor fabricated with dual conductor swaged wire is shown in Figure 1. In this design, a grounded type K thermocouple is embedded in both the hot and cold sides of the sensor. The sensor output is obtained from the differential output of the Alumel wires from the two thermocouples. The type K thermocouples give reference temperatures near both the hot and cold sensor surfaces. The output, which represents the temperature differential across the combustor liner wall, can be calibrated to measure heat flux through the combustor wall.

The embedded thermocouple design utilizing single conductor swaged wire is shown in Figure 2. This design requires three leadwires rather than two, but the conductor in each of the leadwires is larger than in the dual conductor swaged wire. Sheathed Alumel wires with grounded junctions are embedded in both the hot and cold sides of the sensor. A sheathed Chromel wire with a grounded junction is also embedded in the cold side of the sensor. The sensor output is obtained from the two Alumel wires and the reference temperature is obtained from the Chromel and Alumel wires on the cold side of the sensor. The output represents the temperature difference across the liner wall and can be calibrated to measure the heat flow through the combustor wall.

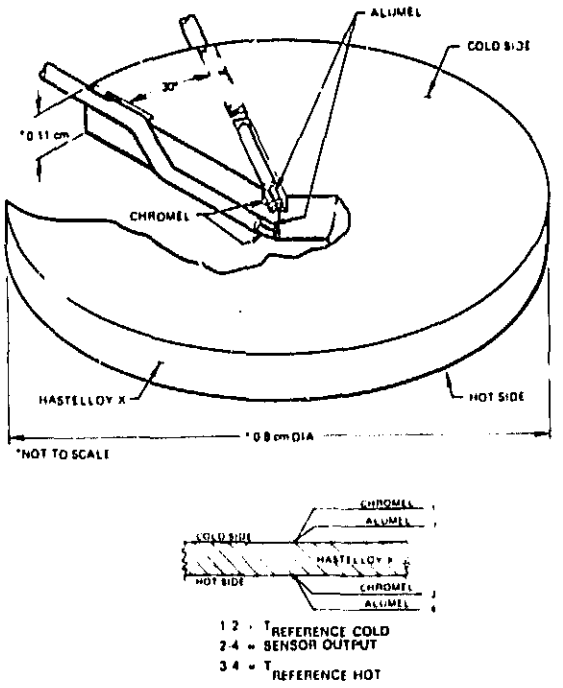

Figure 1 Schematic of an Embedded Thermocouple Heat Flux Sensor Fabricated with Dual Conductor Swaged Wires

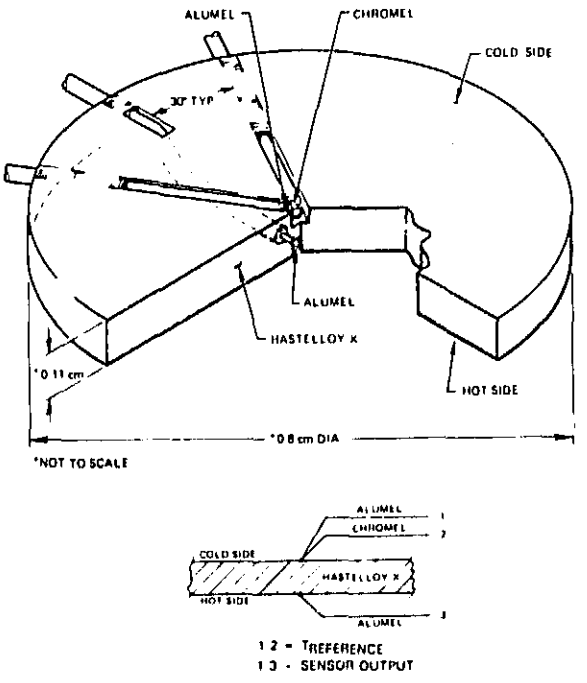

Figure 2 Schematic of an Embedded Thermocouple Heat Flux Sensor Fabricated with Single Conductor Swaged Wires

Laminated Sensors

The design of the laminated sensor is shown in Figure 3. This sensor is composed of a 0.10 centimeter thick layer of Alumel diffusion bonded between two 0.04 centimeter thick layers of Hastelloy-X. The ceramic filled groove electrically insulates the Alumel and the cold side Hastelloy-X layers in the sensor from the surrounding liner. The groove is filled with M Bond GA100 cement to restore the aerodynamic integrity of the cold side surface and to provide some oxidation resistance for the thermocouple wires. The sensor output is obtained from sheathed Hastelloy-X wires attached to the hot side Hastelloy-X layer and to the insulated cold side Hastelloy-X layer. Sensor reference temperature is obtained from a sheathed Alumel wire attached to the cold side Hastelloy-X layer and the Hastelloy-X wire from the cold side layer. The output is representative of the temperature difference across the Alumel layer and can be calibrated to measure the heat flow through the combustor wall.

Gardon Gauge Sensors

The initial design of the Gardon gauge sensor is shown in Figure 4. The Gardon gauge sensor is fabricated from the same material used for the laminated sensor. In this design, sheathed Alumel wires are attached to both the center of the Gardon gauge "foil" and the Alumel layer of the sensor. A Chromel wire is also attached to the Alumel layer of the sensor. The cavity in the sensor is filled with M Bond GA100 cement to restore the aerodynamic integrity of the cold side wall and to provide some oxidation resistance for the thermocouple wires. Sensor output is obtained from the two Alumel wires while the reference temperature is obtained from the Chromel and Alumel wires attached to the center layer of the sensor. The output represents the combination of the temperature difference between the center and the edge of the "foil" and a portion of the temperature drop across the sensor wall. This output is calibrated to measure the heat flow through the combustor wall.

Under an in-house program the design of the Gardon gauge sensor was refined to that shown in Figure 5. The laminated sensor body was replaced with a solid Hastelloy-X body to reduce cost and processing time. To improve fabricability and survivability, the three individual swaged leadwires were replaced with a special three conductor swaged wire containing two Alumel leads and one Chromel lead. The location of the Alumel wire at the side of the sensor was also moved as close to the edge of the "foil" as possible to reduce the sensitivity of the sensor output to lateral temperature gradients in the combustor liner wall.

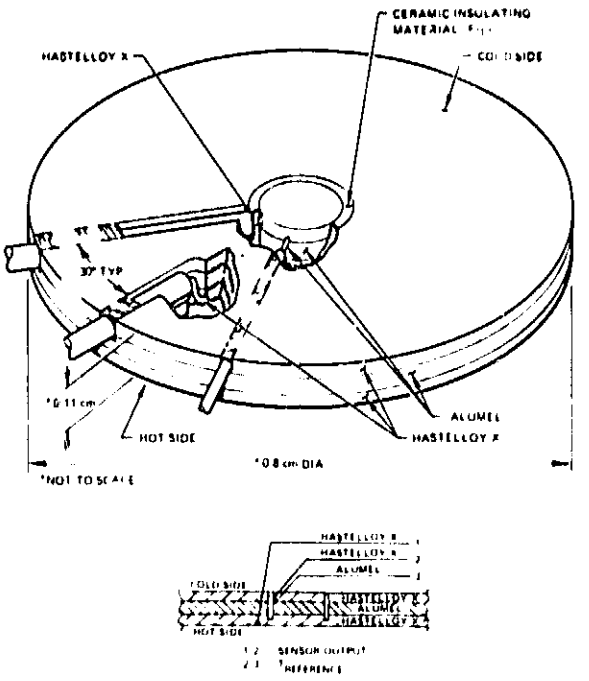

Figure 3 Schematic of Laminated Heat Flux Sensor

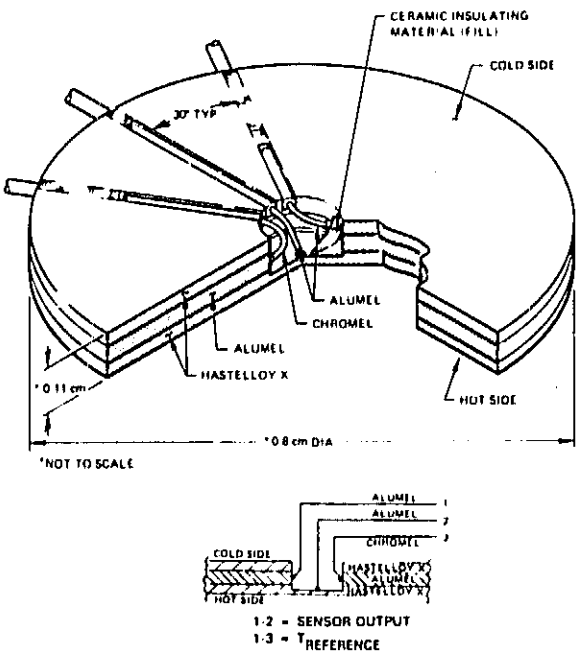

Figure 4 Schematic of Laminated Gardon Gauge Sensor

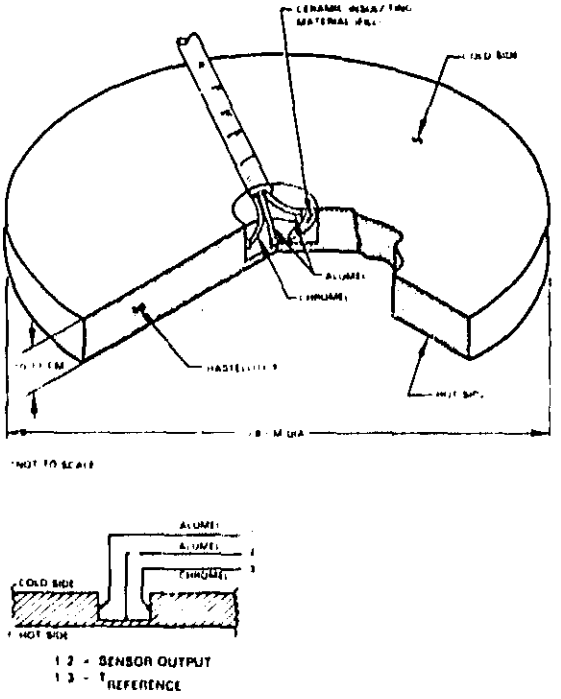

Figure 5 Schematic of Modified Gardon Gauge Sensor

RADIOMETER PROBES

Porous Plug

The porous plug radiometer probe shown schematically in Figure 6, was originally reported by Dr. Robert Moffat of Stanford University (Ref. 2) and has been further developed at Pratt & Whitney. In this design, the convective heat load on the probe screen is removed by a transpiration flow of gas through the porous material. A radiative heat load causes the porous screen to heat up and the temperature difference between the incoming purge gas and the screen temperature is calibrated to measure the incident radiant heat load. In order to measure the total radiant heat load incident on the combustor liner, the porous plug radiometer is designed to have a wide field of view (180°).

Medtherm

The Medtherm radiometer probe is a commercially available unit shown in Figure 7. The convective heat load is isolated from the sensor by the use of a sapphire window. The sensor is a Gardon gauge type sensor and is calibrated by the manufacturer. A gas purge is supplied to keep the window clean during the operation of the probe. The Medtherm radiometer has a 50 degree field of view. Figure 8 shows a comparison of the field of view of the two types of radiometers.

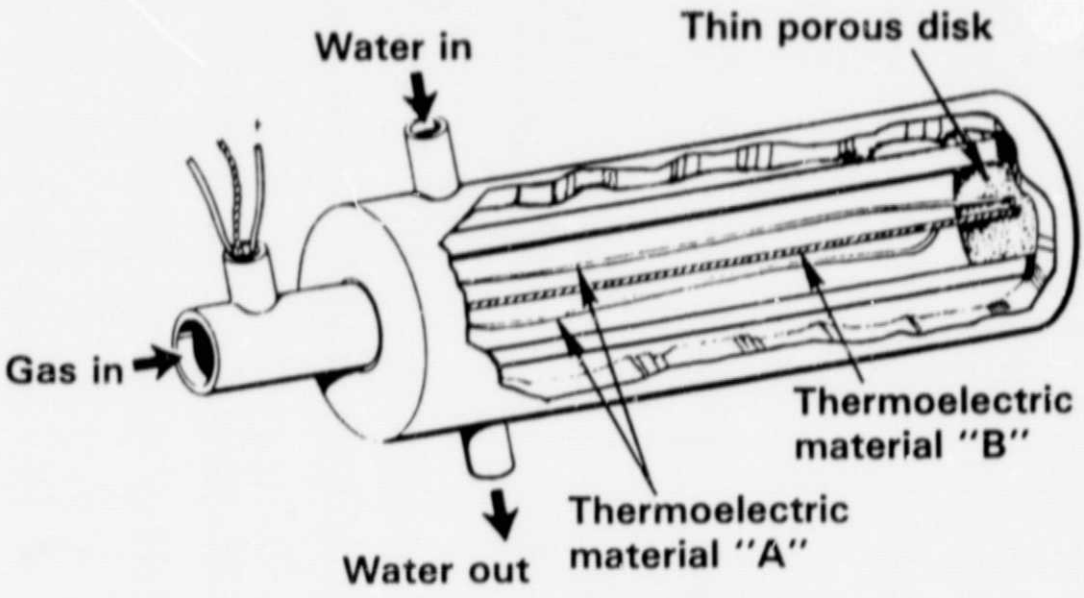

Figure 6 Porous Plug Radiometer Schematic

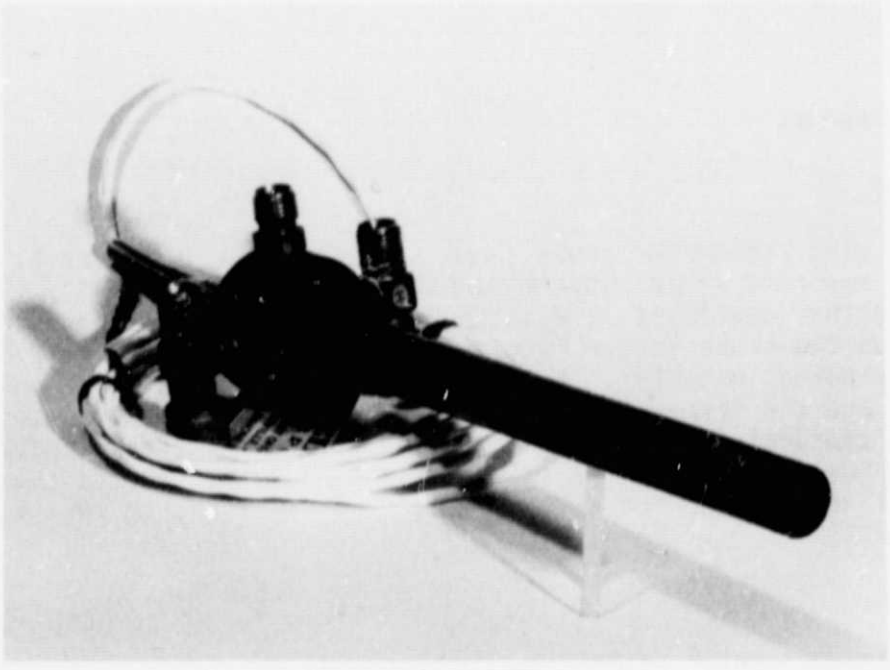

Figure 7 Medtherm Radiometer Probe

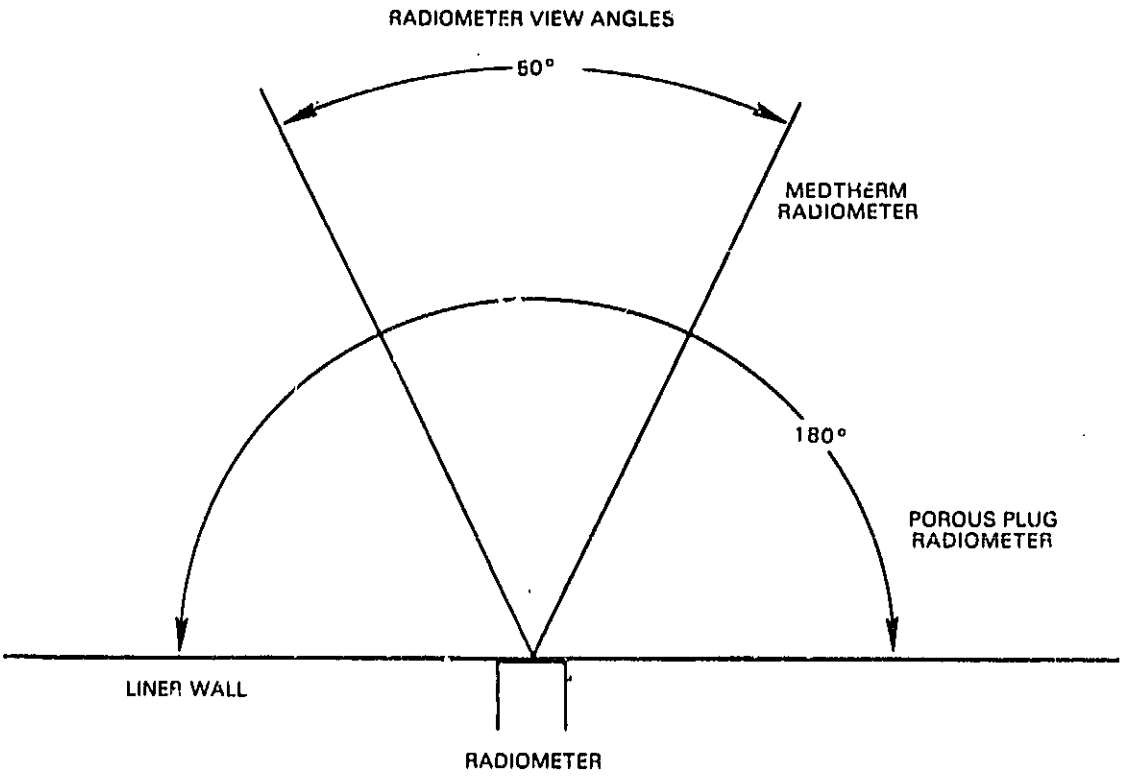

Figure 8 Comparison of the Field of View of the Two Types of Radiometers

SECTION 4.0
FABRICATION

FABRICATION OF SENSOR BODY MATERIAL

The sensor body material for the laminated sensors was formed by diffusion bonding a layer of Alumel (0.10 cm) between two layers of Hastelloy-X, each 0.04 cm thick, for a total thickness of 0.18 centimeters. Diffusion bonding was performed on square sheets approximately 2.5 cm on a side. The Alumel sheet was electrolytically plated with an 0.0005 cm thick layer of nickel to eliminate any possible oxidation problems with the Alumel material that could effect bond quality. After cleaning, the sheets were assembled in a clamping fixture, which was composed of a low thermal expansion material, that provided pressure during the bonding operation. The loaded fixture was installed in a vacuum furnace and heated to 1400K for four hours at 0.07 Pascal pressure. A photomicrograph of a bonded assembly is shown in Figure 9. The embedded thermocouple sensors and Gardon gauge sensors were produced from Hastelloy-X sheets. Round blanks with a diameter of approximately 1.0 centimeter were punched out of a Hastelloy-X sheet that was of the same thickness as the combustor liner into which the sensors were installed.

If the sensors were to be installed in a curved combustor liner where the presence of flat sensors would cause a perturbation in air flow, the sensor bodies would have been bent to the desired curvature before the lead wires were machined. However, curving of the sensors was not necessary due to the large diameter of the combustor segments used in this program.

MACHINING OF THE SENSOR BODIES

To allow for variations in the diffusion bonding process, the laminated material for the laminated sensor was made thicker than the desired final sensor thickness of 0.16 cm. Following bonding, the bonded squares were machined to a final thickness, then cut into quarters to provide material for the four sensors.

To provide ease of installation of the sensor into the combustor liner, the hole in the combustor liner was held to a close tolerance with a precision reamer. The sensor bodies were chucked between the head and tailstock of a lathe and machined to 0.8 centimeter ($\pm$0.002 cm) diameter.

The final machining operation involved producing slots for: 1) the thermocouple wires, 2) insulation ring for the laminated sensors, and 3) center cavity for the Gardon gauge sensors. Due to the small sizes and high depth-to-width ratio for the ring in the laminated sensor, the final machining operations were performed by ELOX. Photographs of completed sensor bodies for an embedded thermocouple sensor, a laminated sensor, and two Gardon gauge sensors are shown in Figures 10 to 12.

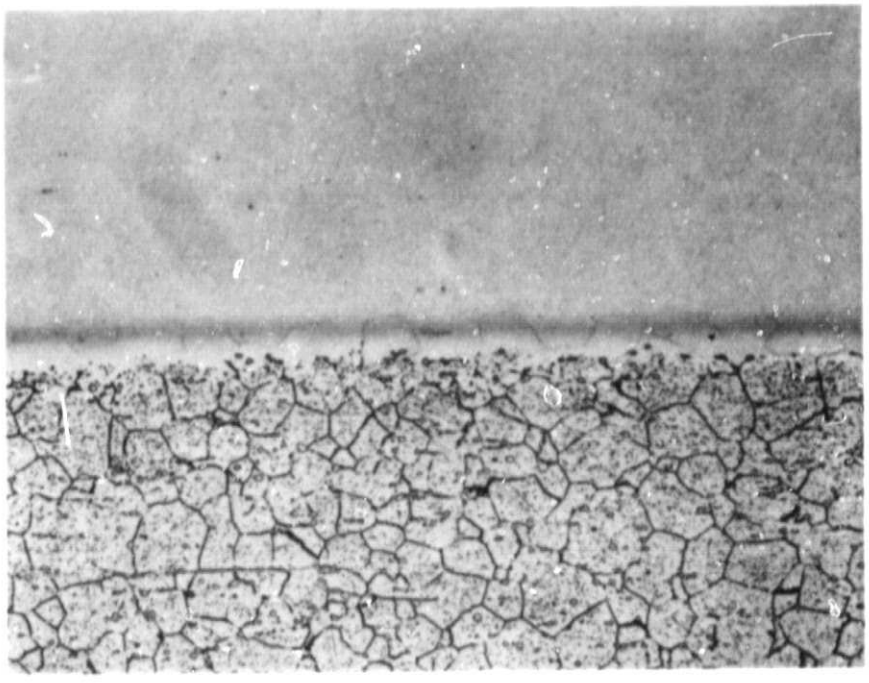

Figure 9 Photomicrograph of Alumel (Top) to Hastelloy-X (Bottom) Diffusion Bond with a 0.0005 Centimeter Nickel Plate on the Alumel Before Bonding (Mag: 200X)

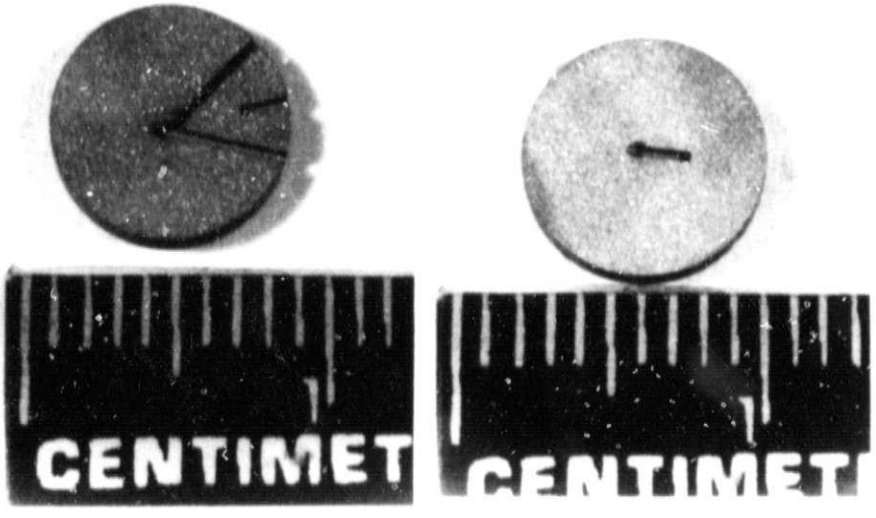

Figure 10 Embedded Thermocouple Sensor Body

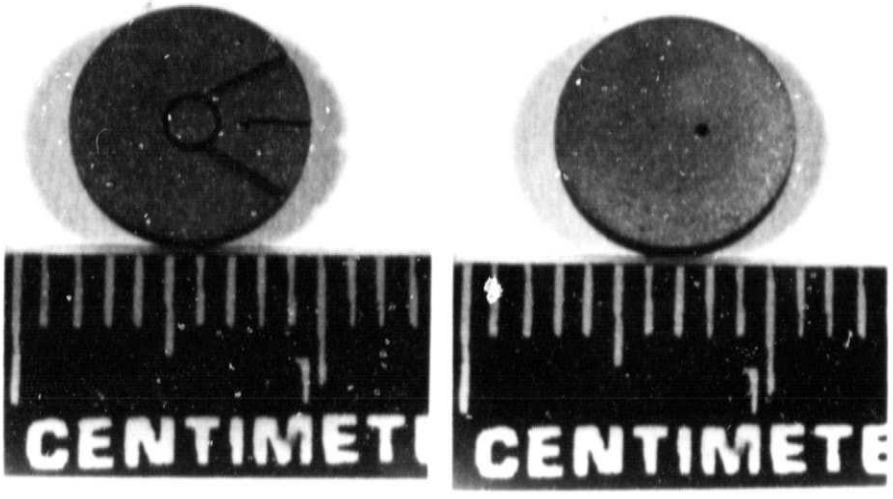

Figure 11 Laminated Sensor Body

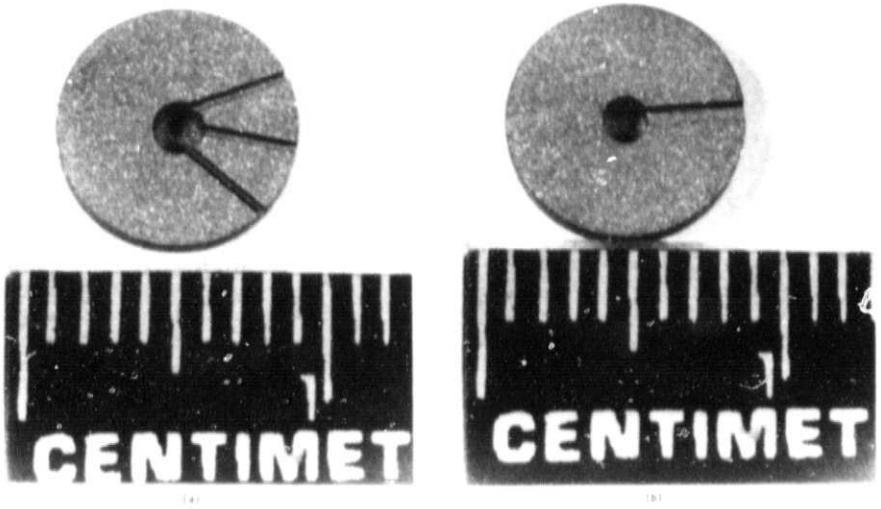

Figure 12 (a) Body for Gardon Gauge to be Fabricated with Three Single Conductor Swaged Wires, (b) Body for Gardon Gauge to be Fabricated from a Single Three Conductor Leadwire

INSTRUMENTING THE SENSORS

The sensor was instrumented by first securing it in a holding fixture. A sheathed leadwire with the sheath stripped for approximately .4 cm. was placed in a slot in the sensor and secured by taping to the holding fixture (Figure 13). The area over the sheathed leadwire in the sensor slot was then filled by resistance welding Chromel P fillet wire into the slot. After a resistance check was made to check the lead for a short to ground, the thermoelectric junction was resistance welded to the sensor body. The fillet area over the slot was then ground smooth. The remaining leadwires were installed using the same method. The sensor was cleaned and all leads checked for continuity. Figure 14 shows a sensor with one lead completed and one lead ready to be checked for short to ground.

For embedded thermocouple sensors, the areas around the thermoelectric junctions were filled with powdered MgO ceramic. Hastelloy-X caps, 0.025 cm thick, were resistance welded over the junction areas and then ground smooth.

The insulation ring (for laminated sensors) and the center cavity (for Gardon gauge sensors) were filled with M Bond GA100 ceramic cement, which was ground smooth after curing. The ceramic provided aerodynamic integrity on the cold side surface as well as some oxidation protection for the sensor leadwires. The laminated sensor nas a thermoelectric junction on the hot side which was filled with M Bond GA100 cement, then capped with Hastelloy X, 025 cm. thick, and finally ground smooth. The completed heat flux sensors were ready for calibration. Photographs of completed sensors are show in Figures 15 to 17.

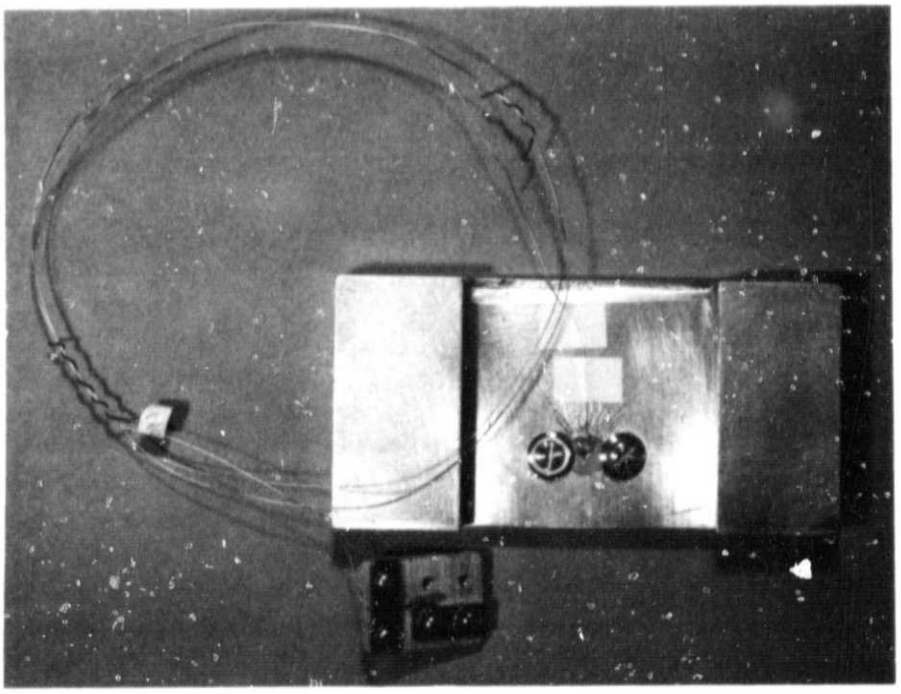

Figure 13 Sensor Secured in Holding Fixture

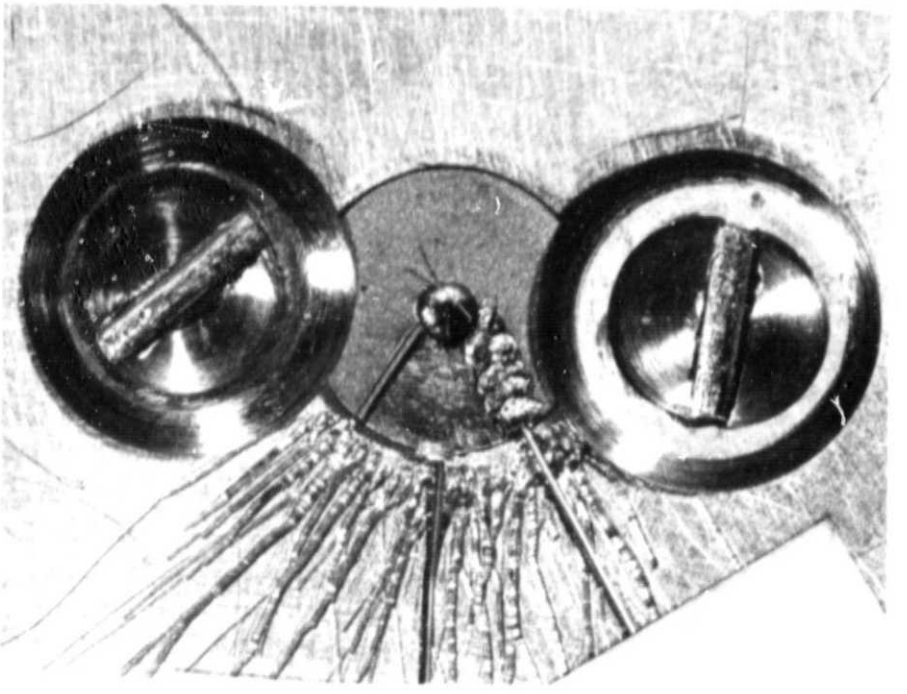

Figure 14 Sensor With One Completed Leadwire Attachment

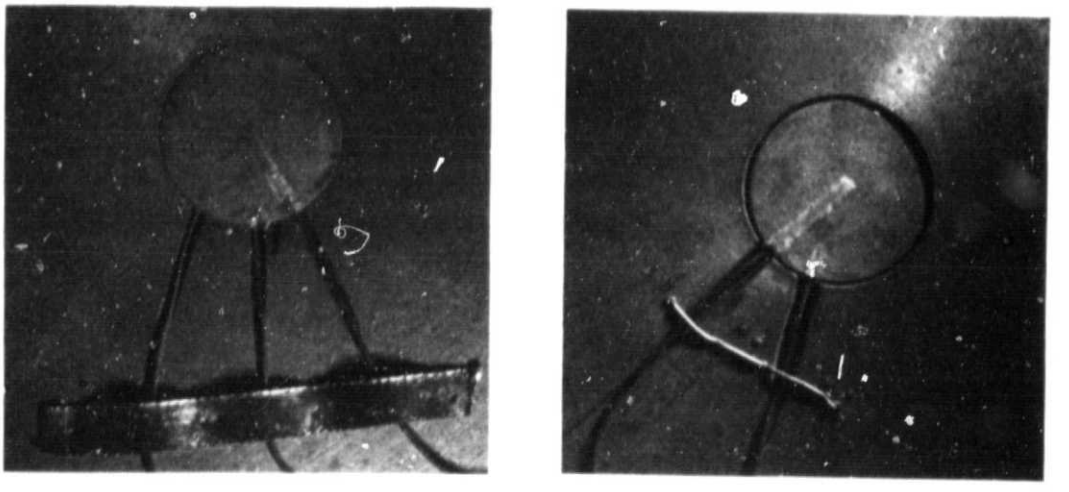

Figure 15 Completed Embedded Thermocouple Sensors

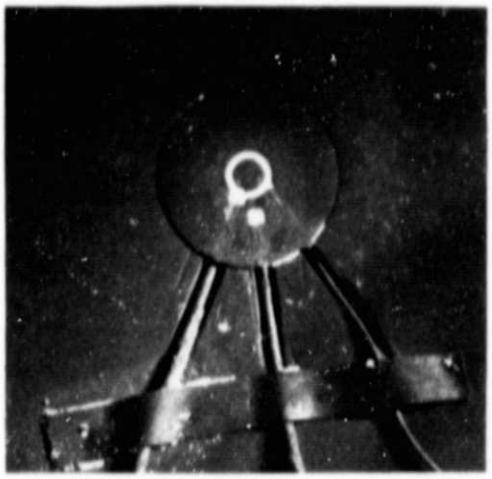

Figure 16 Completed Laminated Sensor

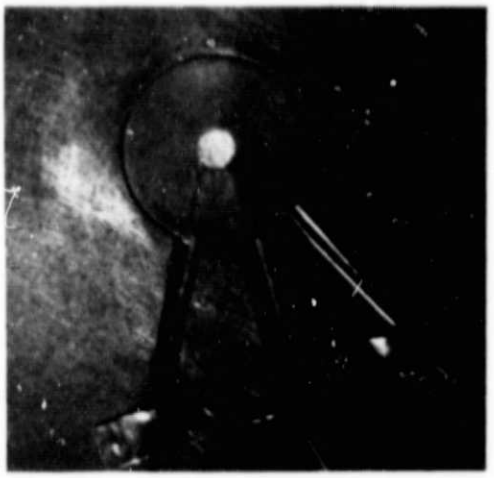

Figure 17 Completed Gardon Gauge Sensor

POROUS PLUG RADIOMETER FABRICATION

The porous plug radiometer (Figure 18) was built in a water cooled probe. First, a centering tube was installed in the probe to keep the internal gas thermocouple away from the walls of the probe. Fine wires (.008 centimeter) inside the probe were then led through the center of the tube. After the screen was cut to size, Chromel and Constantan wires were tack welded together inside the probe to form the gas thermocouple. A second Chromel wire and the Constantan wire were tack welded to the screen to form the screen thermocouple. The porous screen was attached to the probe by tack welding the periphery of the screen to the front of the probe. The installation was completed by making a transition from the fine gauge internal wires to the heavier (.025 centimeter) wires that were used for external leads and leading the heavier wire out of the probe through compression fittings. The output of the probe was obtained from the two Chromel wires. One of the Chromel wires and the Constantan wire may be used to measure either gas or screen temperature.

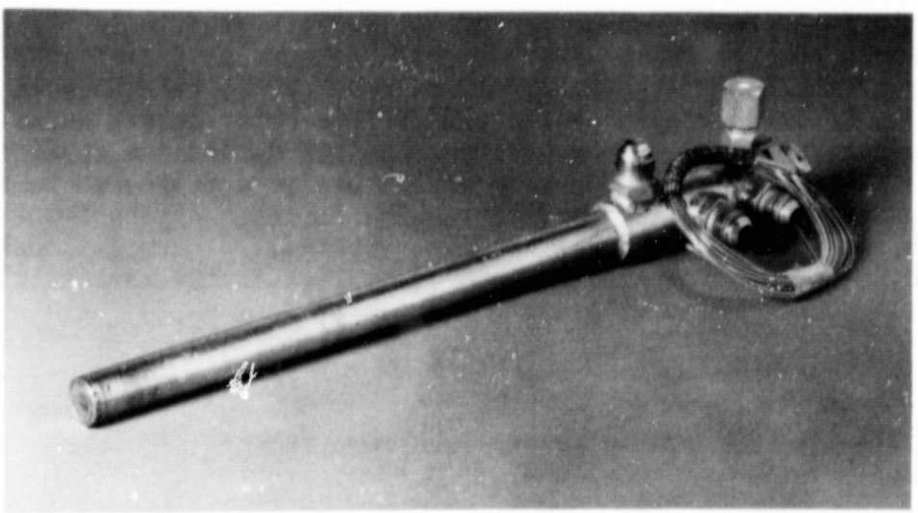

Figure 18 Porous Plug Radiometer

SECTION 5.0
CALIBRATION OF SENSORS

Due to slight variations between sensors, (such as the depth of the actual thermocouple junction, the depth of the Gardon gauge cavity, etc.) individual sensor calibrations were required to meet goals of the contract.

CALIBRATION FIXTURE

An exploded view of the calibration fixture is shown in Figure 19. The sensor was first mounted in a circular calibration plate, (7 cm in diameter). The sensor was lightly resistance welded into the plate at several positions around the circumference of the hot side surface. This was sufficient to hold the sensor in place for calibration but allowed removal of the sensor from the plate after calibration. A water cooled flange held the plate onto the body of the fixture. A metal O-ring was used as a seal. The sensor was cooled during calibration by cooling air impinging on the cold side surface of the sensor. The fixture was open at the back to allow the cooling air to exit. The sensor leadwires were led out through a fitting in the side of the fixture. The surface of the sensor was coated with "Zynolyte 1000F Hi-Temp[1]" black paint to provide a constant emittance/absorbtance of 0.89 for calibration.

QUARTZ LAMP BANK CALIBRATION FACILITY

A quartz lamp bank test facility was used for all calibrations. The heat source was a quartz lamp bank with six parallel quartz halogen bulbs, each rated at 6 kw. The bulbs were 25.4 cm long and the lamp assembly was 7.6 cm wide. The lamp assembly is capable of producing a maximum heat flux incident on the sensors of 1.7 MW/m^2. During routine operation, the lamp operation was restricted to approximately 1.0 MW/m^2 to maximize lamp life.

A photograph of the lamp face is shown in Figure 20. The reflector on the lamp was water cooled and the bulbs were air cooled to permit continuous operation. The heat flux sensor, in its calibration fixture, was positioned below the lamp through a polished water-cooled shield. Heat flux output of the lamp was monitored by a reference heat flux sensor mounted in the shield. Prior to the sensor calibrations, a second reference sensor was mounted at the same location that the heat flux sensor to be calibrated would occupy during calibration. A calibration of the assembly was then performed to determine the relationship between the heat flux measured by the reference sensor to that incident on the calibration location. This relationship was used to correct the data measured by the reference sensor during the heat flux sensor calibration. To eliminate any possible bias due to differences in the calibration of the two reference sensors, the position of the two reference sensors was exchanged and the calibration repeated. Figure 21 shows the calibration fixture and reference sensor installed in the heat shield and Figure 22 is an overview of the calibration rig.

---

1 Zynolite Products Company
15700 South Avalon
Compton, CA 90224

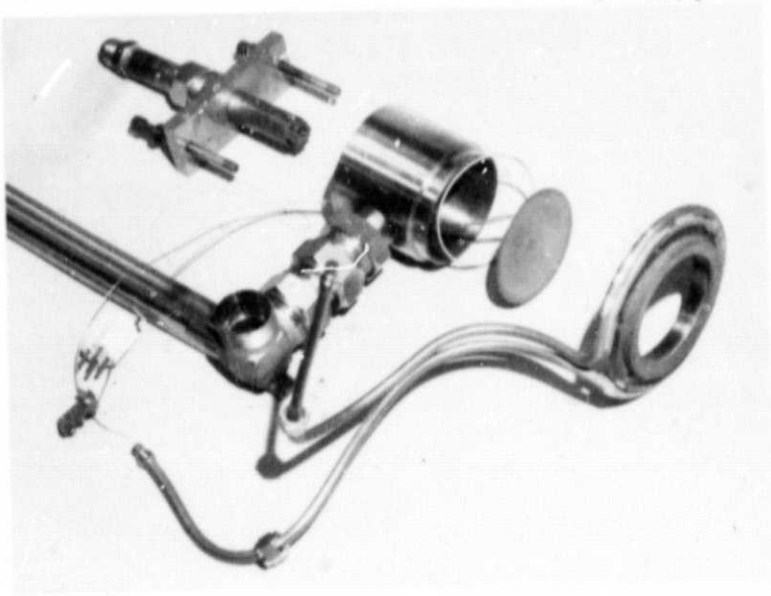

Figure 19 Exploded View of Calibration Fixture

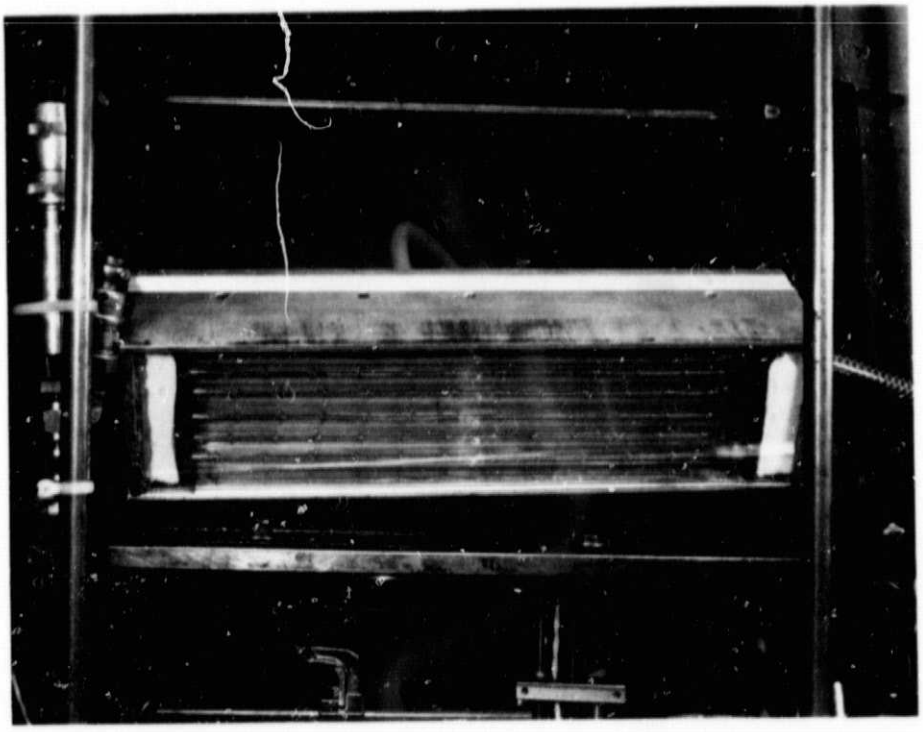

Figure 20 Calibration Rig Lamp Face

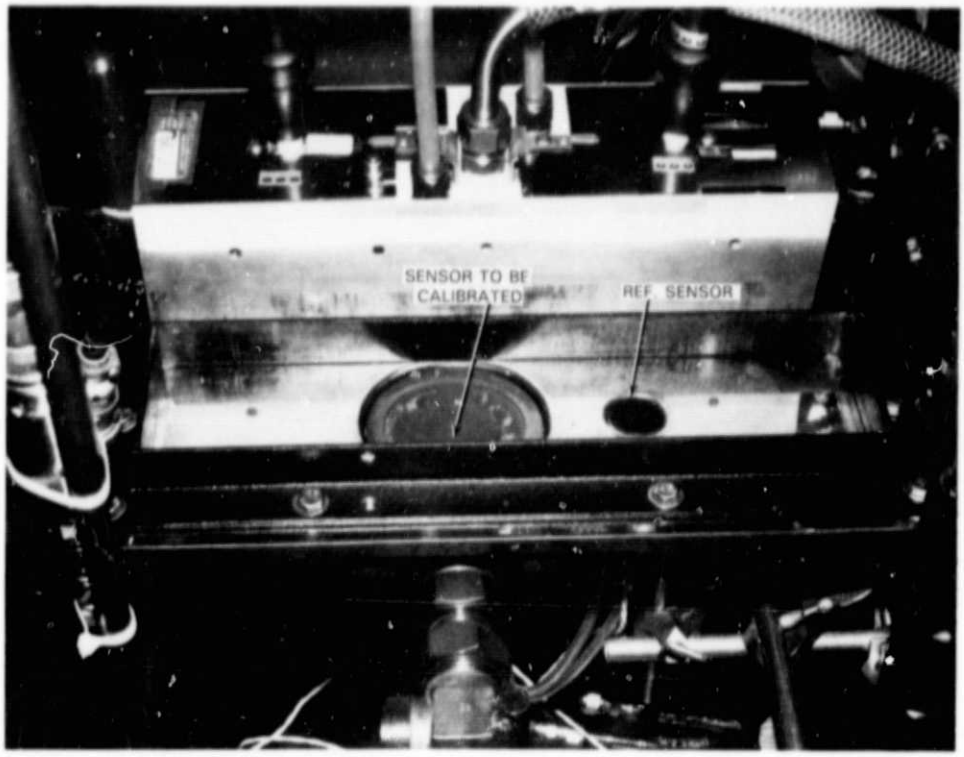

Figure 21 Calibration Fixture With Reference Sensor Installed in the Heat Shield

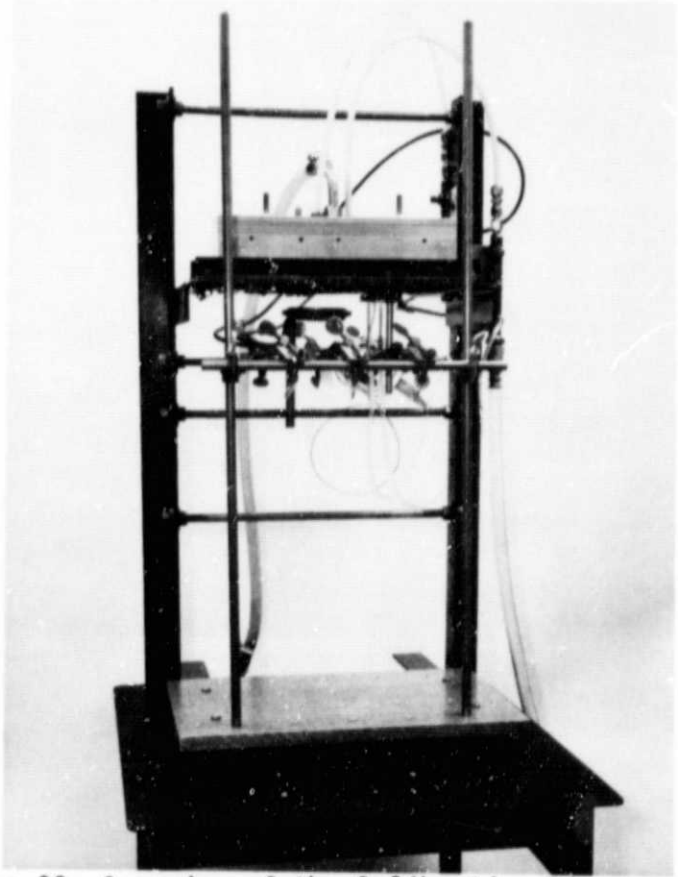

Figure 22 Overview of the Calibration Rig

CALIBRATION PROCESS

Calibrations were conducted under two sets of conditions; varying incident heat load at a constant sensor temperature and varying incident heat load with constant coolant flow impinging on the sensor. During the calibrations, data was recorded and reduced on a microcomputer based data acquisition system and stored in tabular form on floppy diskettes. This system allowed real time corrections to be applied to the calibration data. In addition, the data files on disk allowed later statistical analysis of the data, presentation of summary results in English or SI units, and automated graphical representation of test results through use of a digital plotter interfaced to the system.

At each calibration point, the heat flux incident on the sensor was calculated based on the reference sensor reading. The heat flux transmitted through the sensor was calculated by determining the heat absorbed and subtracting the heat losses from the front face by convection and re-radiation. The absorbed heat flux was equal to the incident heat flux as measured by the reference sensor, corrected to the test sensor location, times the absorbtance of the sensor surface. The convective loss was equal to the convection heat transfer coefficient (determined during an earlier program - Reference 3) times the temperature differential between the sensor surface and the ambient air temperature. The re-radiation loss was the emittance of the sensor times the Stephan-Boltzman constant times the difference in the fourth powers of the sensor surface temperature and the sink temperature. The sink temperature was experimentally determined as 400K for this calculation. A detailed error analysis of this calibration procedure was presented in Reference 1 and will not be repeated here.

SENSOR CALIBRATION RESULTS

Baseline Combustor

Under this contract a Broad Specification Fuels baseline PW2037 combustor segment was instrumented with three embedded thermocouple sensors, three Gardon gauge (three single conductor swaged wire) sensors, and two laminated sensors. The calibration data from the sensors are shown in Figures 23 to 30. The top plot in each figure shows sensor output vs. heat flux transmitted through the sensor. A least square fit was performed on this data to obtain sensor sensitivity (output per unit heat flux). The lower plot in each figure shows the variation of the calibration data from the least square line with sensor temperature.

The data from the embedded thermocouple sensors and the Gardon gauge sensors were well behaved. All the data fell within the $\pm 5\%$ of 1 megawatt per meter squared error bands. The sensor sensitivity also showed no significant variation with sensor temperature.

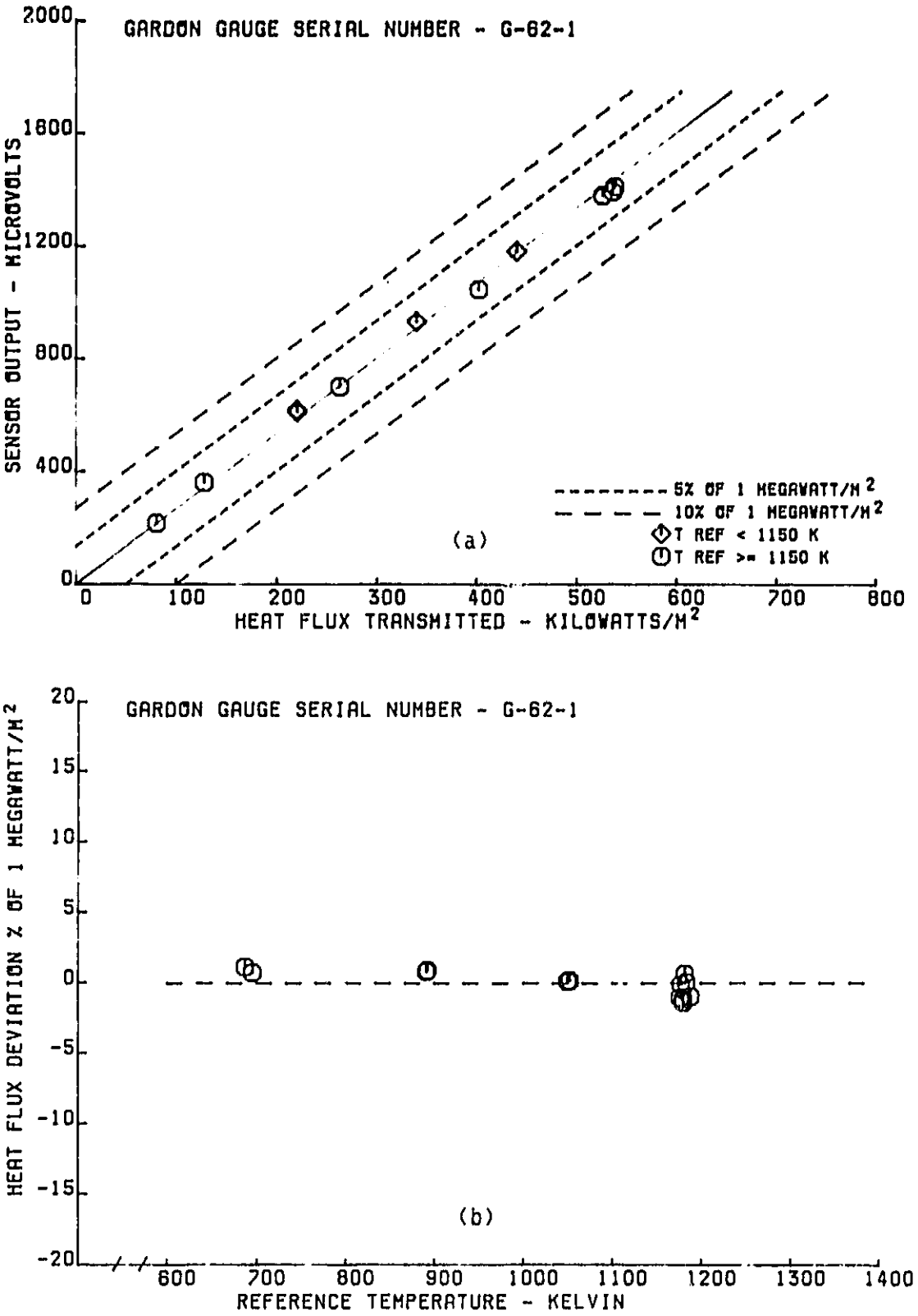

Figure 23 Gardon Gauge Serial Number G-62-1 Calibration, (a) Sensor output vs. Heat Flux Transmitted, (b) Heat Flux Deviation vs. Reference Temperature

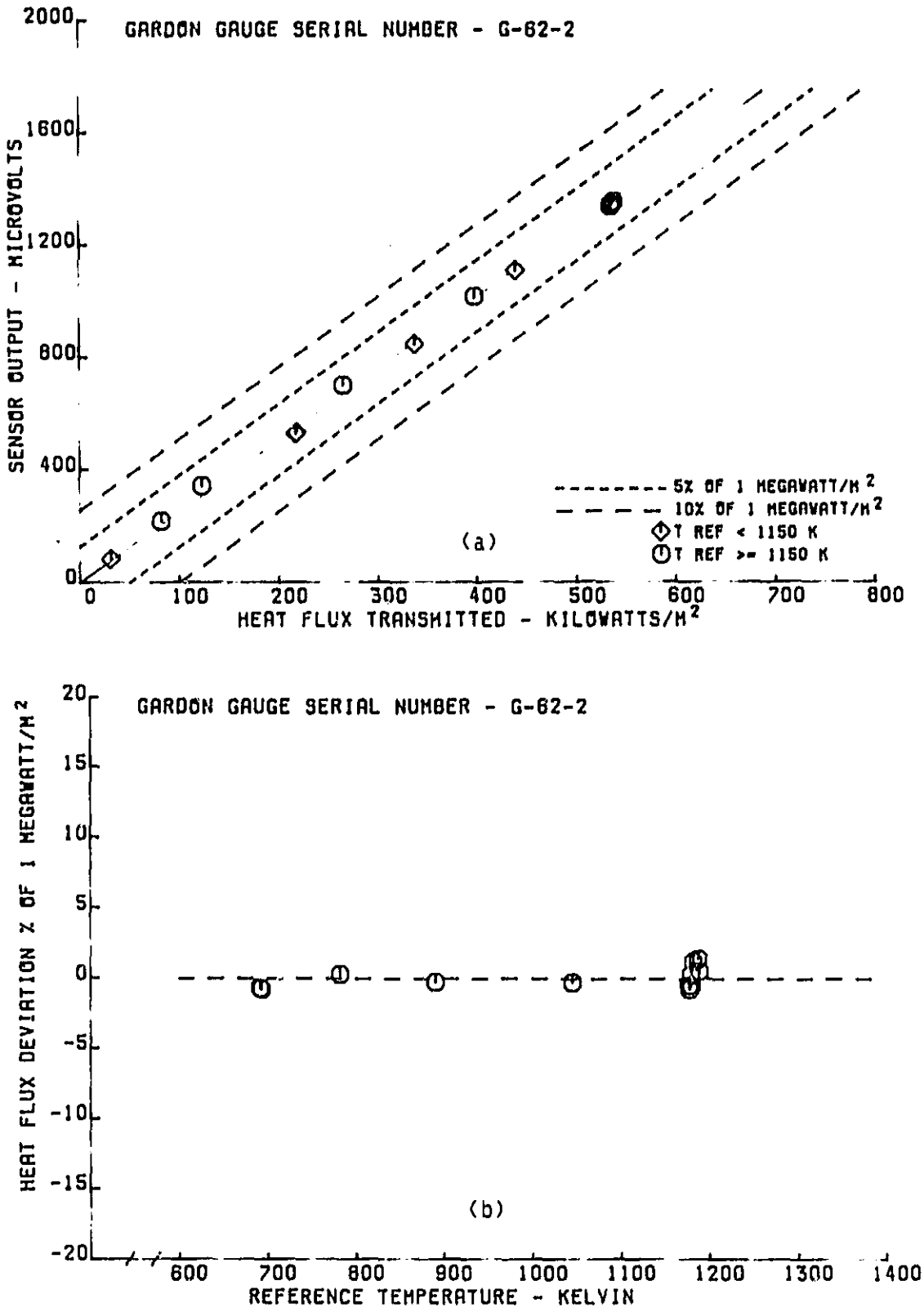

Figure 24 Gardon Gauge Serial Number G-62-2 Calibration, (a) Sensor output vs. Heat Flux Transmitted, (b) Heat Flux Deviation vs. Reference Temperature

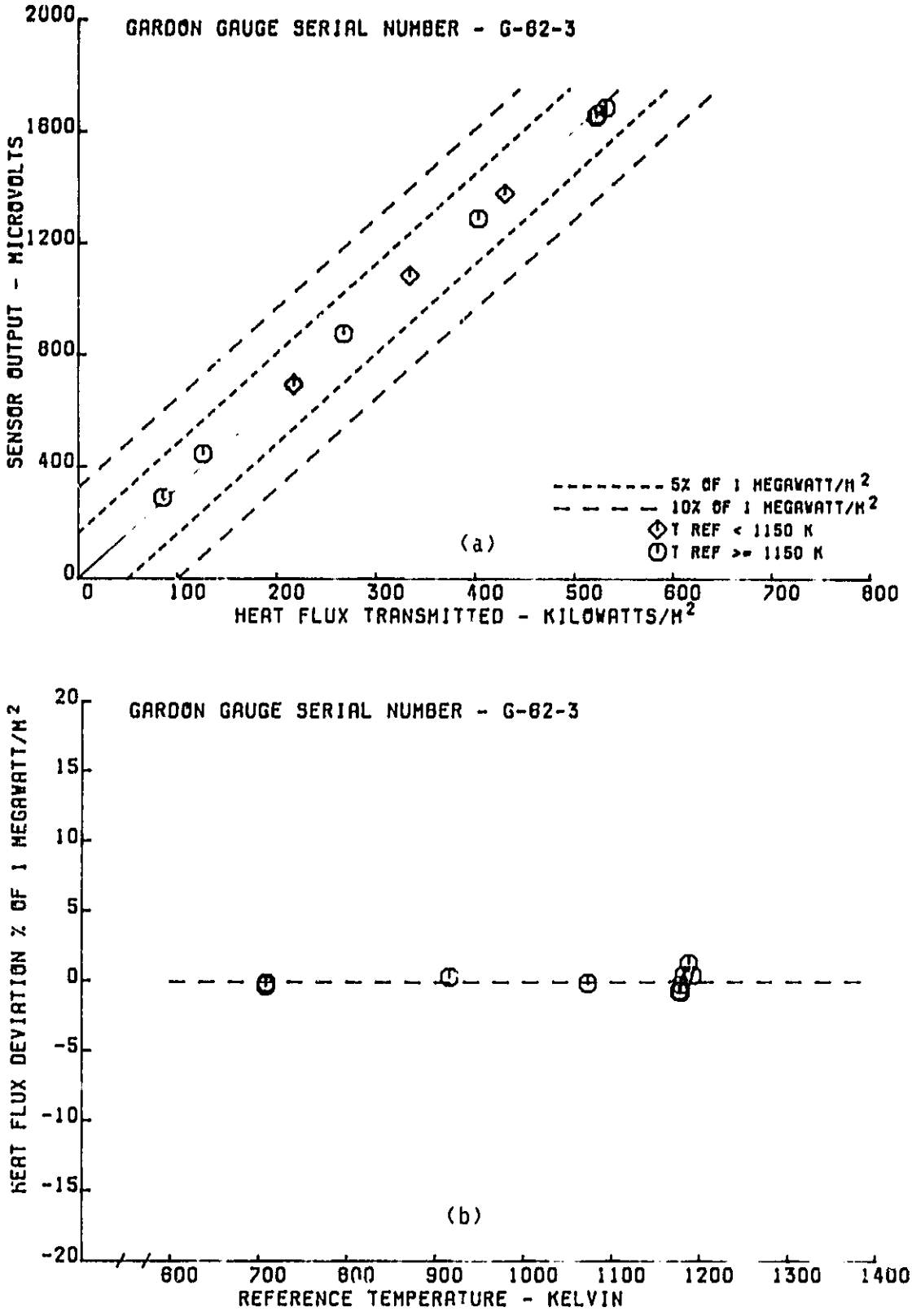

Figure 25 Gardon Gauge Serial Number G-62-3 Calibration, (a) Sensor output vs. Heat Flux Transmitted, (b) Heat Flux Deviation vs. Reference Temperature

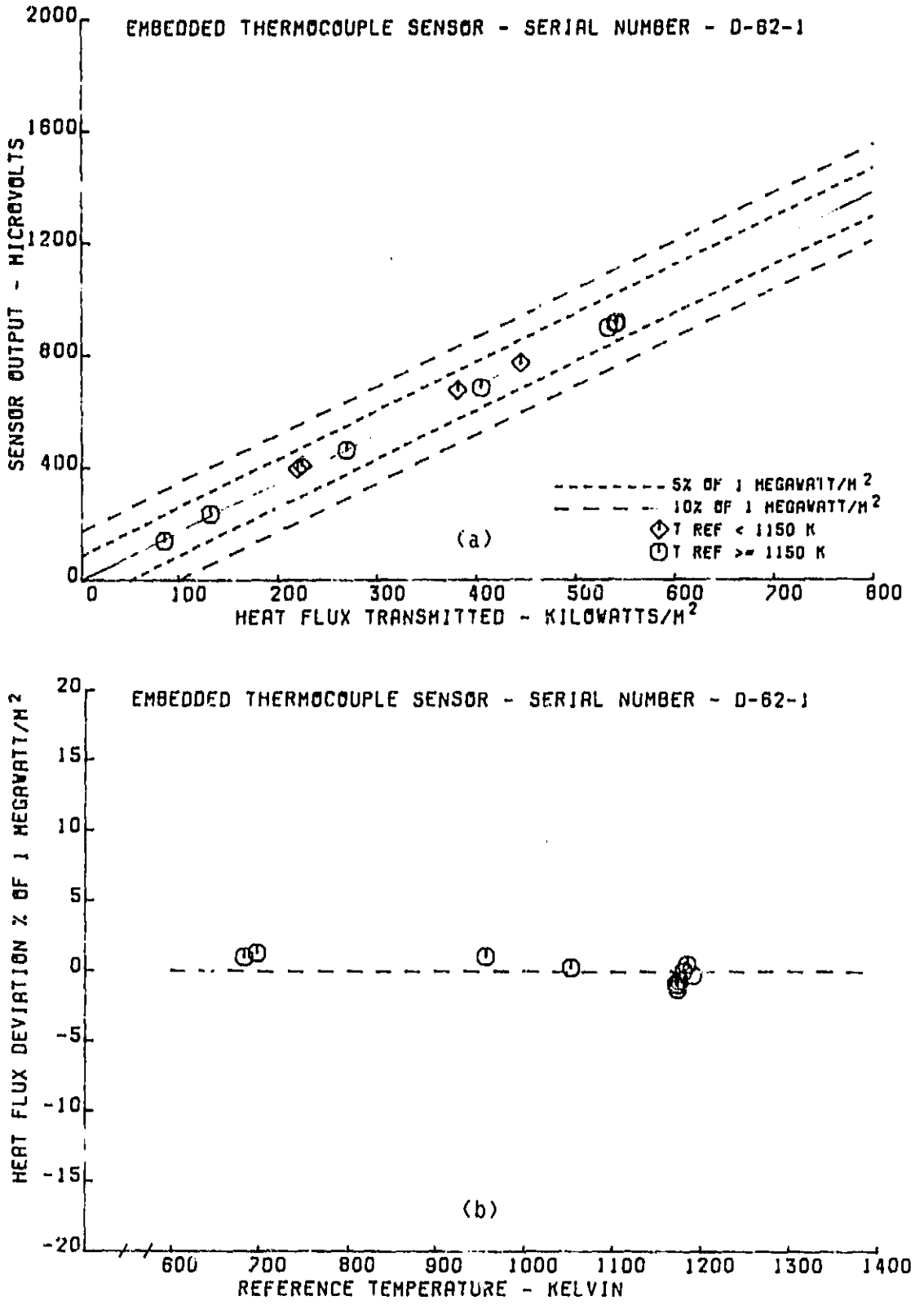

Figure 26 Embedded Thermocouple Sensor Serial Number D-62-1 Calibration, (a) Sensor output vs. Heat Flux Transmitted, (b) Heat Flux Deviation vs. Reference Temperature

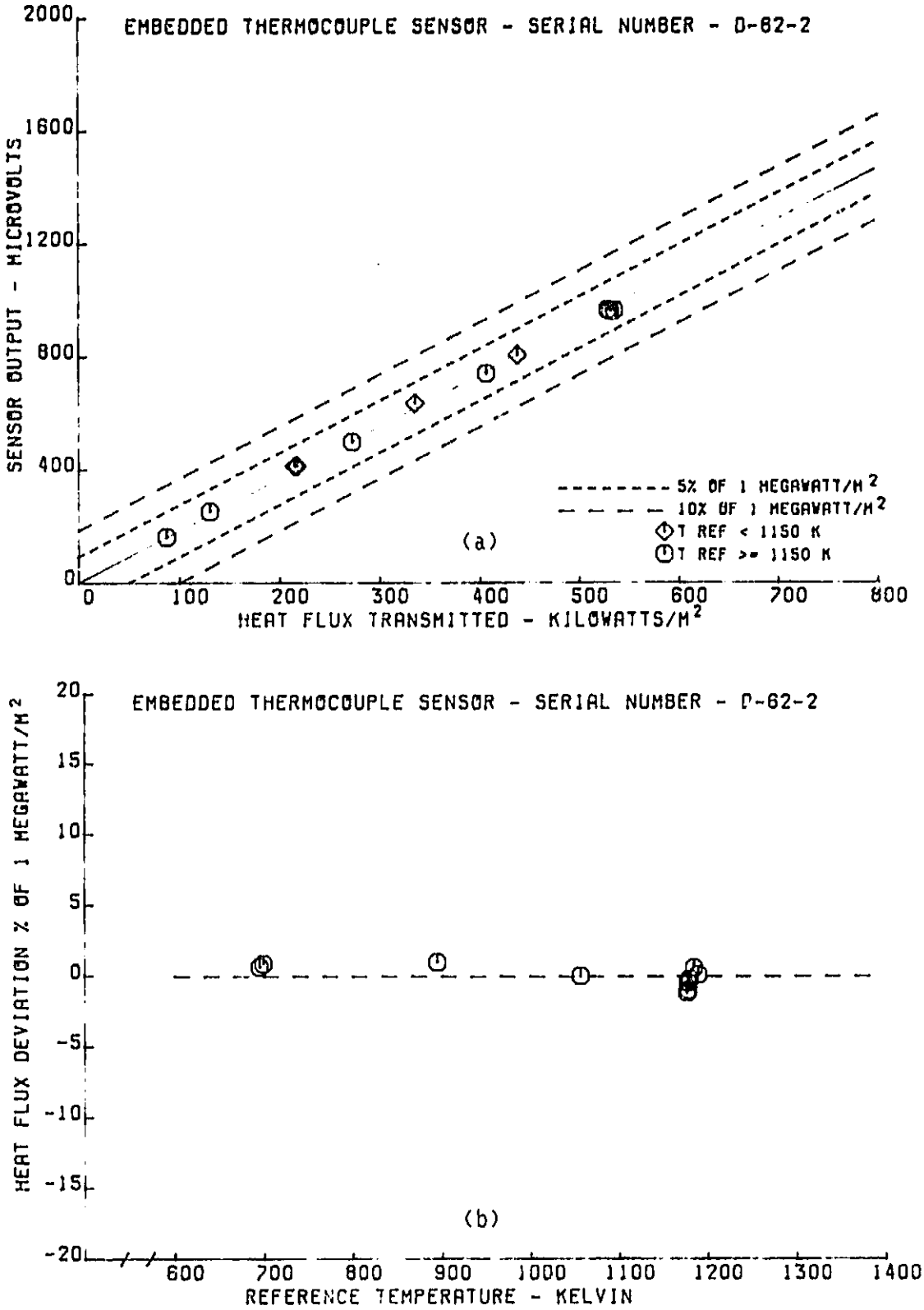

Figure 27 Embedded Thermocouple Sensor Serial Number D-62-2 Calibration, (a) Sensor output vs. Heat Flux Transmitted, (b) Heat Flux Deviation vs. Reference Temperature

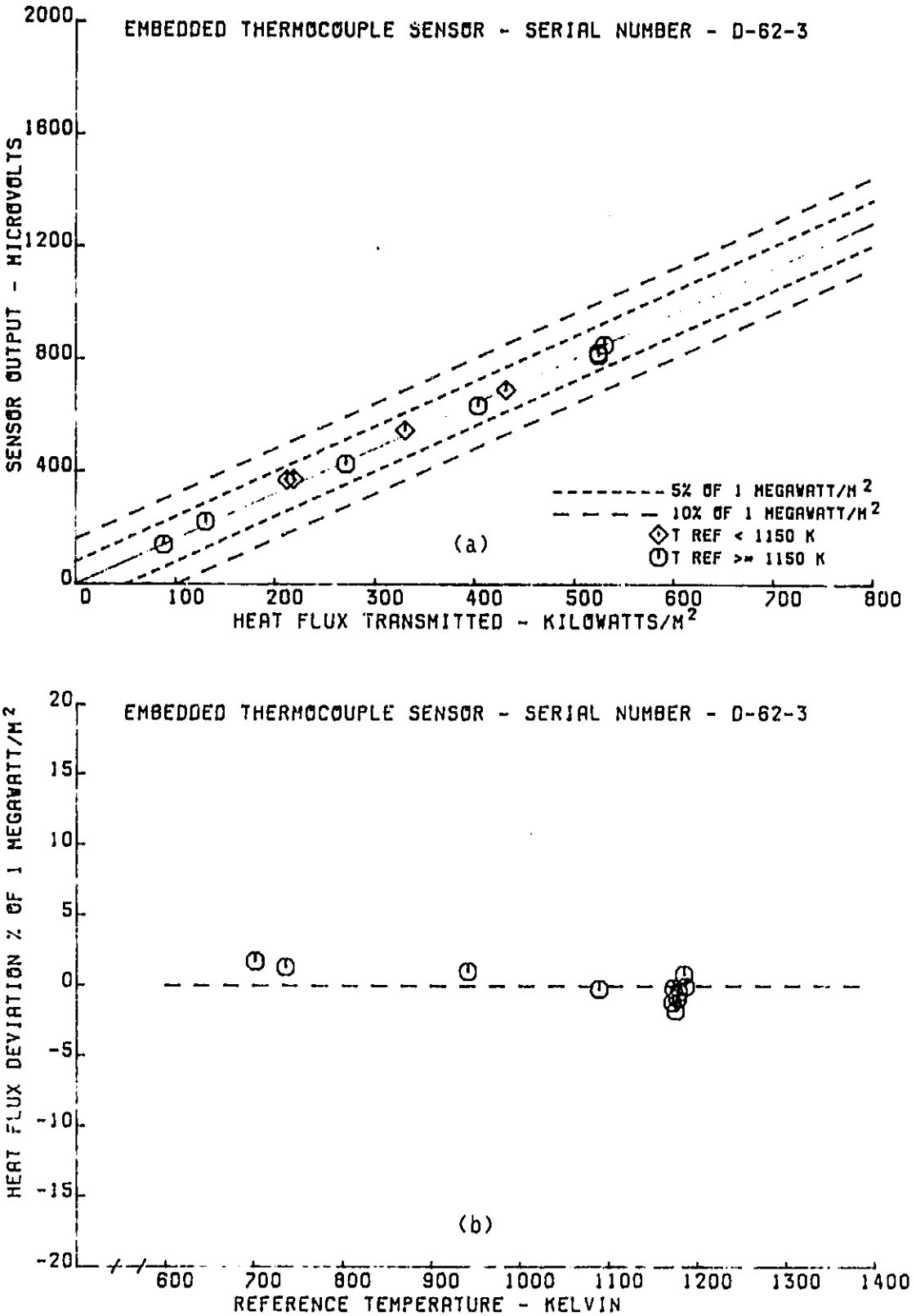

Figure 28 Embedded Thermocouple Sensor Serial Number D-62-3 Calibration, (a) Sensor output vs. Heat Flux Transmitted, (b) Heat Flux Deviation vs. Reference Temperature

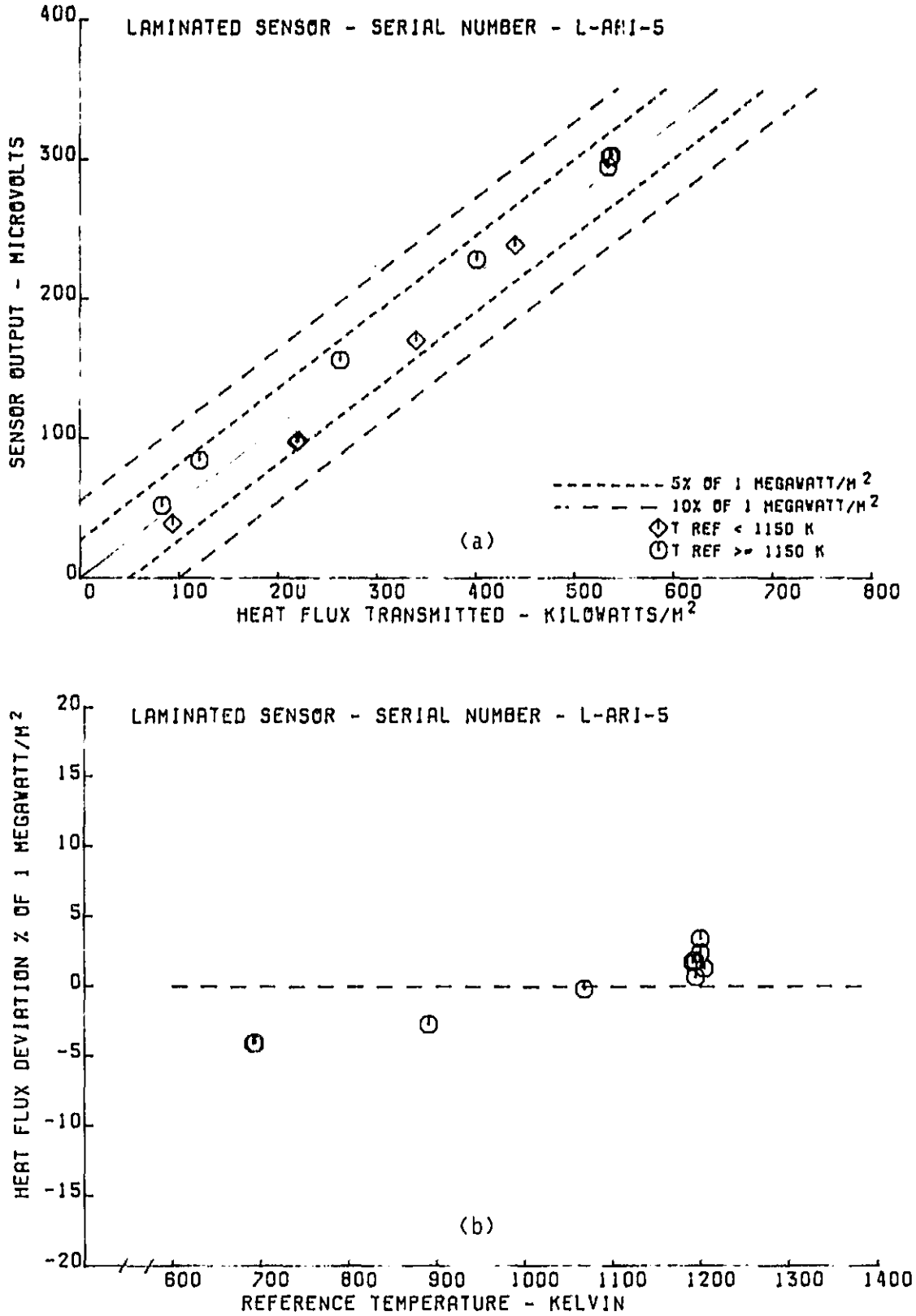

Figure 29 Laminated Sensor Serial Number L-ARI-5 Calibration, (a) Sensor output vs. Heat Flux Transmitted, (b) Heat Flux Deviation vs. Reference Temperature

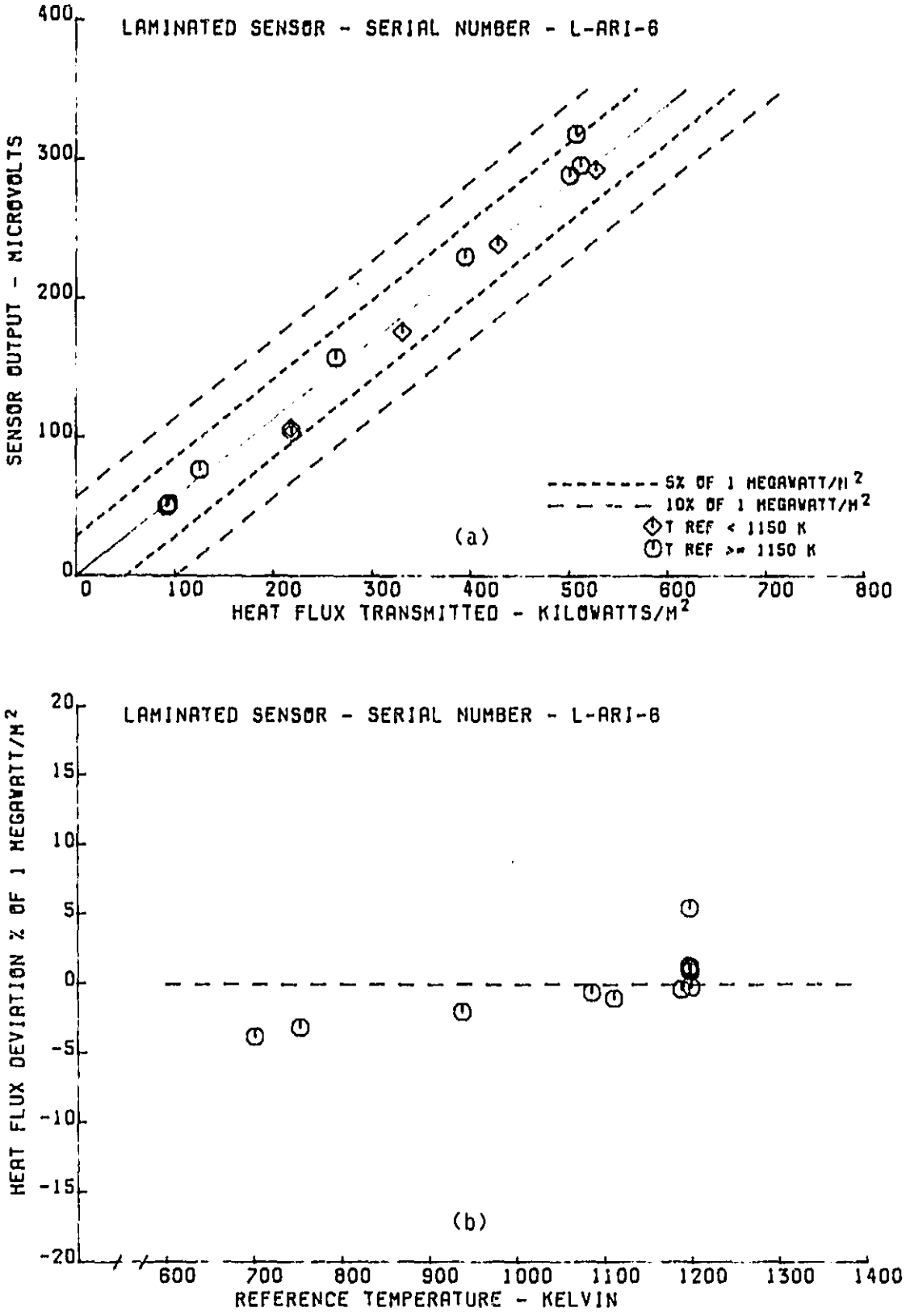

Figure 30 Laminated Sensor Serial Number L-ARI-6 Calibration, (a) Sensor output vs. Heat Flux Transmitted, (b) Heat Flux Deviation vs. Reference Temperature

The data from the laminated sensors showed significantly more scatter than the data from the other sensor types. It was also found that the sensor sensitivity varied with sensor temperature. This unexpected variation in the sensor sensitivity with temperature was first observed during the sensor development under Phase I of this contract. Research efforts at Pratt & Whitney and at NASA identified the probable cause of this variation to be circulating thermoelectric currents produced due to the dissimilar metals of the laminated sensor being in contact with each other over an extended area. The magnitude of the variation was found to depend on the location of the hot side Hastelloy-X leadwire junction. Locating the hot side junction directly above the insulating ring in the laminated sensor minimized but did not completely eliminate this variation. These sensors were constructed in that configuration. The laminated sensor sensitivity increased an average of 3.7% per 100 K increase in sensor temperature. To minimize the error due to this variation, the sensor reference temperature was used to correct the calibration data to an effective sensor temperature of 1150K. This corrected data for the laminated sensors is shown in Figures 31 and 32. It can be seen that the corrected calibration data shows much less scatter and that the variation in sensor sensitivity with temperature has been eliminated.

Pratt & Whitney In-House Program

The Pratt & Whitney in-house program used a variable geometry combustor segment run under the NASA Broad Specification Fuels program. The variable geometry combustor segment was instrumented with one embedded thermocouple sensor, two Gardon gauge (one three conductor swaged leadwire) sensors, and one laminated sensor. The calibration data from those sensors are shown in Figures 33 through 36. Again, all data from the embedded thermocouple and Gardon gauge sensors fell within the $\pm$5% error bands and the sensitivities did not vary significantly with temperature. As before, the data from laminated sensor has more scatter than the embedded thermocouple and Gardon gauge sensors and the sensor sensitivity varies with temperature. This data was corrected to an effective surface temperature of 1150K. This corrected data, which has less scatter and less variation in sensor sensitivity, is shown in Figure 37.

RADIOMETER CALIBRATIONS

Experience has shown that porous plug radiometers also require individual calibrations. Figure 38 shows a Pratt & Whitney developed pressurized radiant calibration system which allowed calibration of porous plug radiometers to heat flux levels of 300 KW/m^2 at pressures in excess of 7 atmospheres. Calibrations at elevated pressures were required to confirm probe operating characteristics with varying mass flows, volume flows, and pressure ratios across the porous screen.

The Medtherm radiometers were supplied with calibrations by the vendor. To confirm that those calibrations were reasonable, a one point check was performed at Pratt & Whitney. The radiometers were installed one at a time into the mouth of a large black body furnace (Figure 39) that had been heated to 1400K. The radiant energy, indicated by the radiometer being tested, was then compared with the calculated result based on black body temperature. These tests confirmed that the calibrations supplied by the vendor were valid.

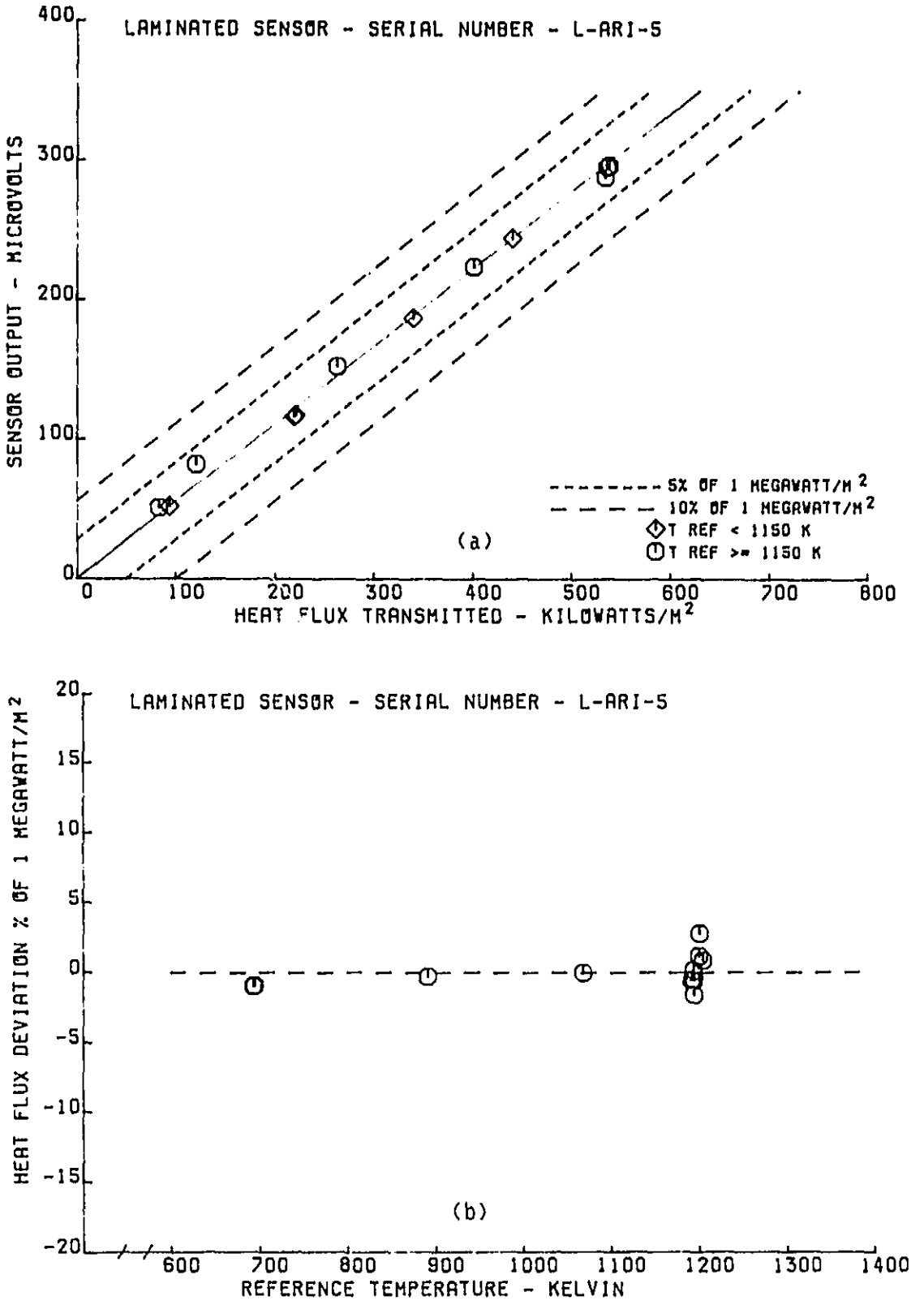

Figure 31 Laminated Sensor Serial Number L-ARI-5 Corrected Calibration, (a) Sensor output vs. Heat Flux Transmitted, (b) Heat Flux Deviation vs. Reference Temperature

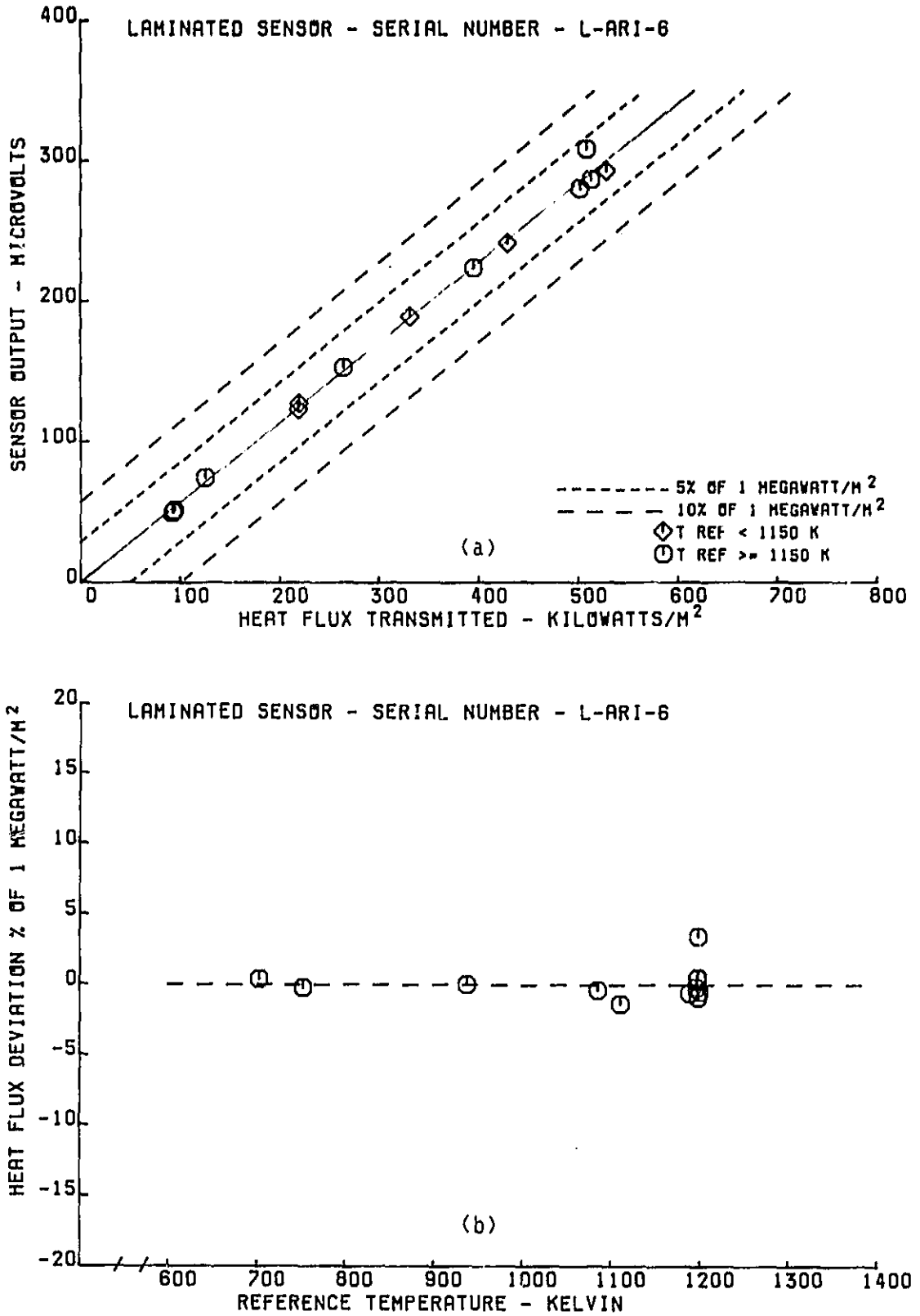

Figure 32 Laminated Sensor Serial Number L-ARI-6 Corrected Calibration, (a) Sensor output vs. Heat Flux Transmitted, (b) Heat Flux Deviation vs. Reference Temperature

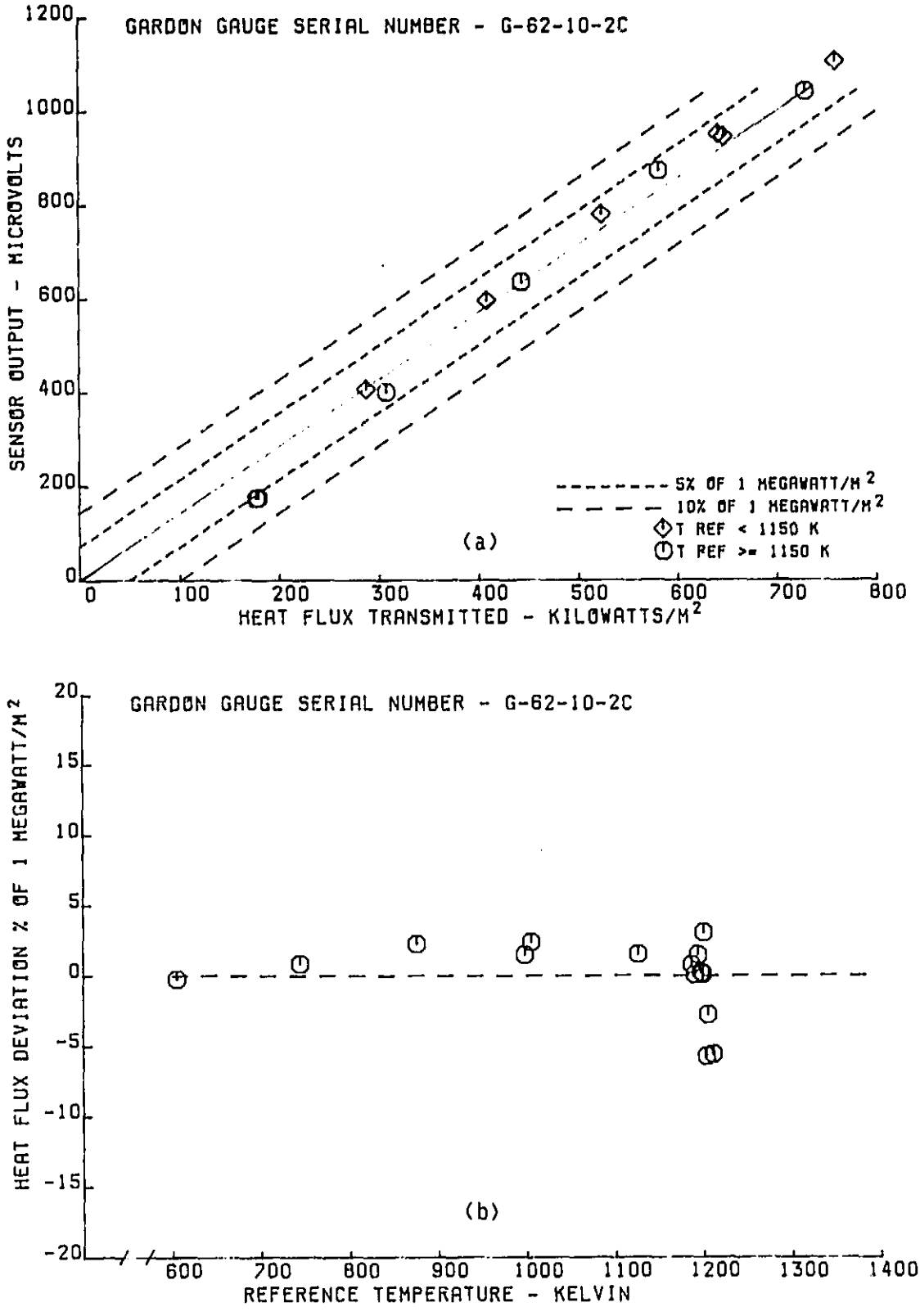

Figure 33 Gardon Gauge Serial Number G-62-10-2C Calibration, (a) Sensor output vs. Heat Flux Transmitted, (b) Heat Flux Deviation vs. Reference Temperature

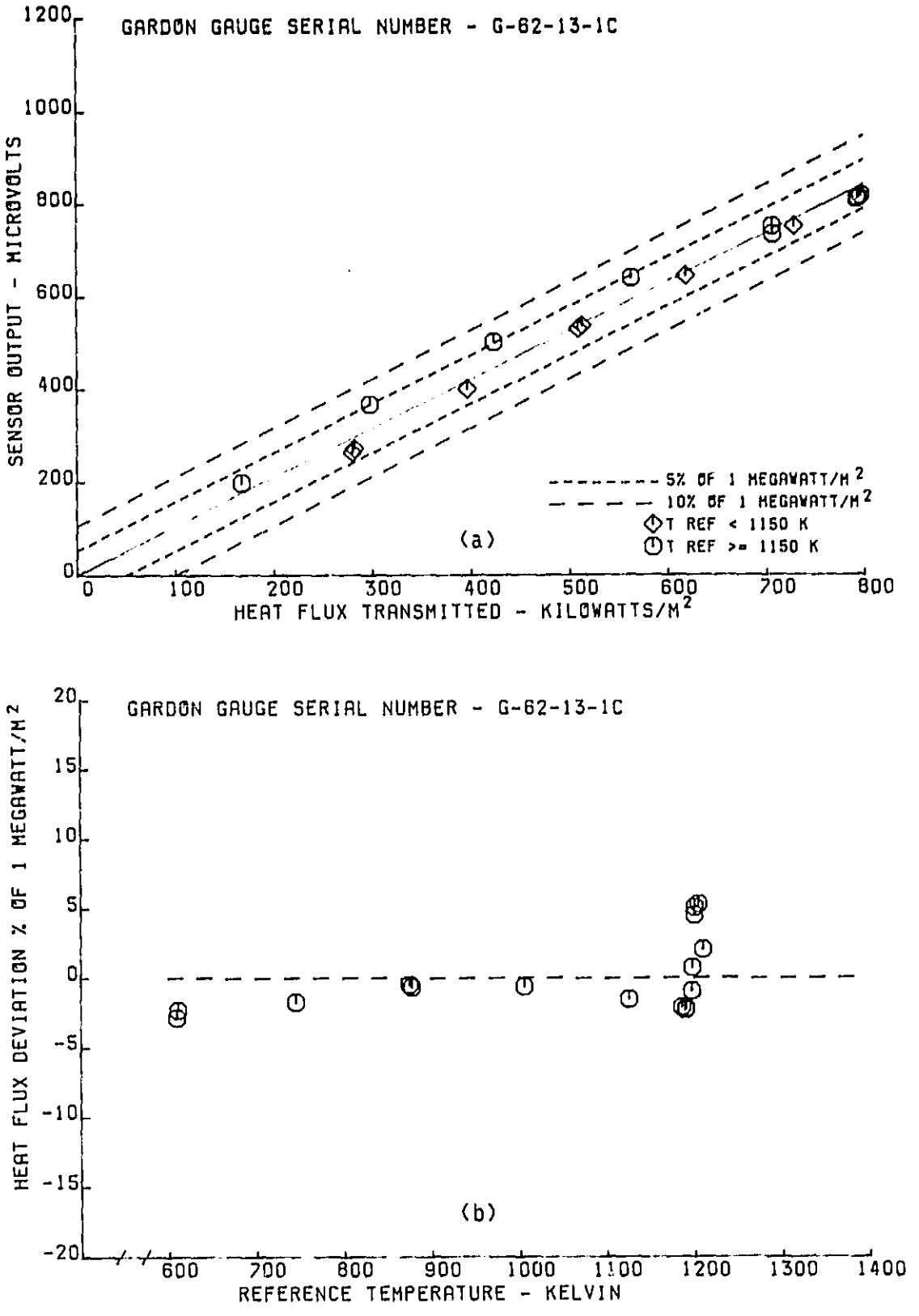

Figure 34 Gardon Gauge Serial Number G-62-13-1C Calibration, (a) Sensor output vs. Heat Flux Transmitted, (b) Heat Flux Deviation vs. Reference Temperature

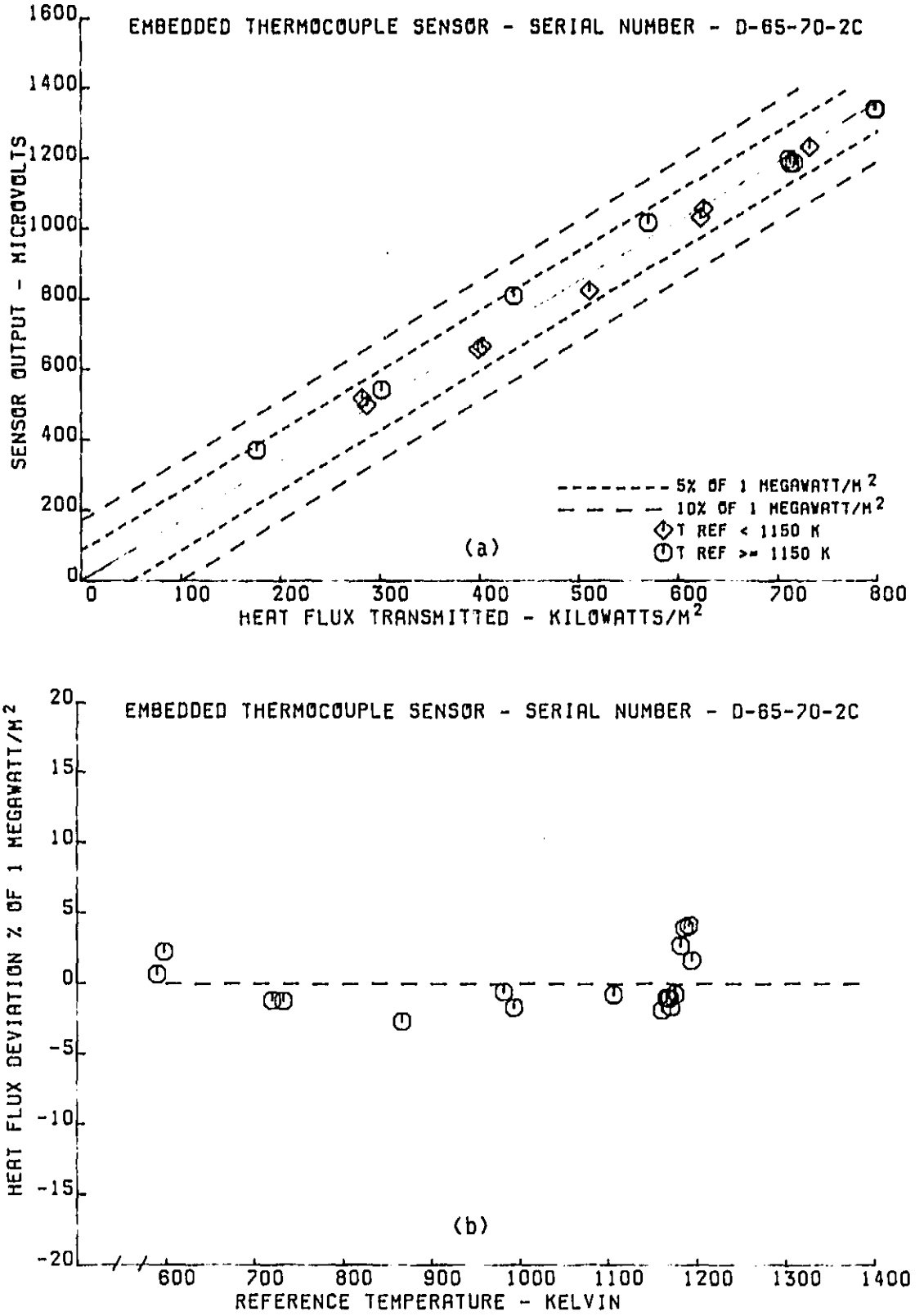

Figure 35 Embedded Thermocouple Sensor Serial Number D-65-70-2C Calibration, (a) Sensor output vs. Heat Flux Transmitted, (b) Heat Flux Deviation vs. Reference Temperature

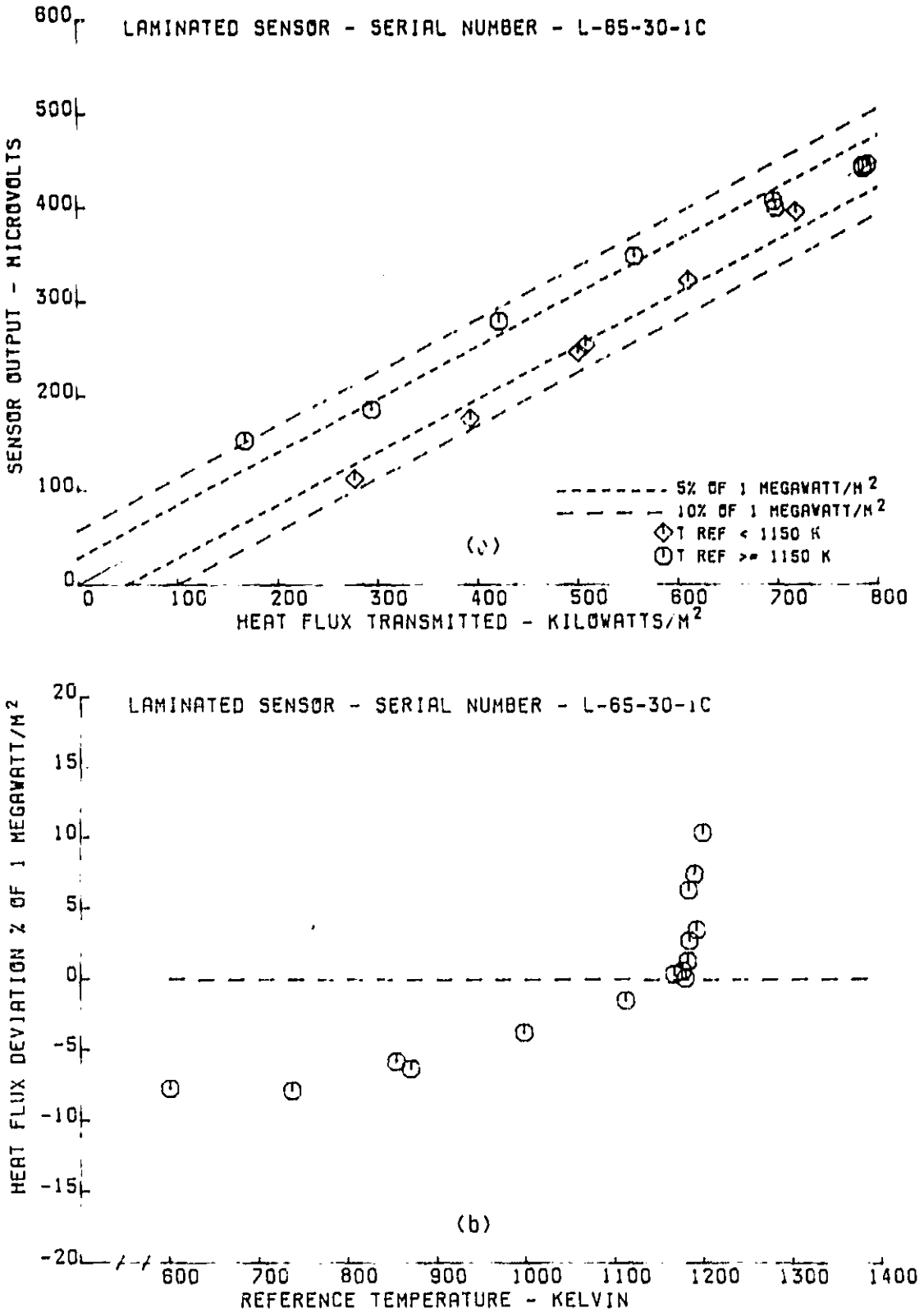

Figure 36 Laminated Sensor Serial Number L-65-30-1C Calibration, (a) Sensor output vs. Heat Flux Transmitted, (b) Heat Flux Deviation vs. Reference Temperature

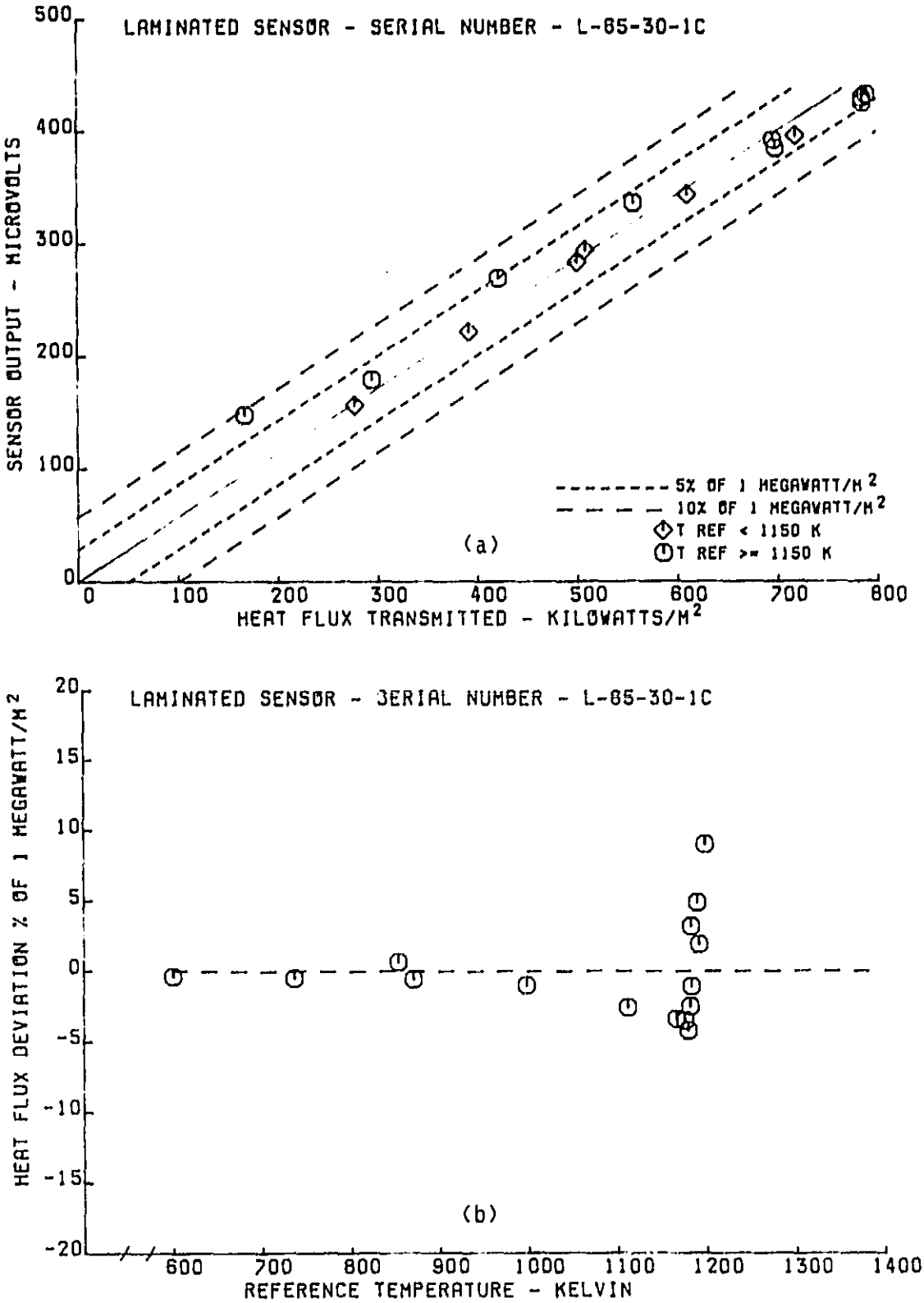

Figure 37 Laminated Sensor Serial Number L-65-30-1C Corrected Calibration, (a) Sensor output vs. Heat Flux Transmitted, (b) Heat Flux Deviation vs. Reference Temperature

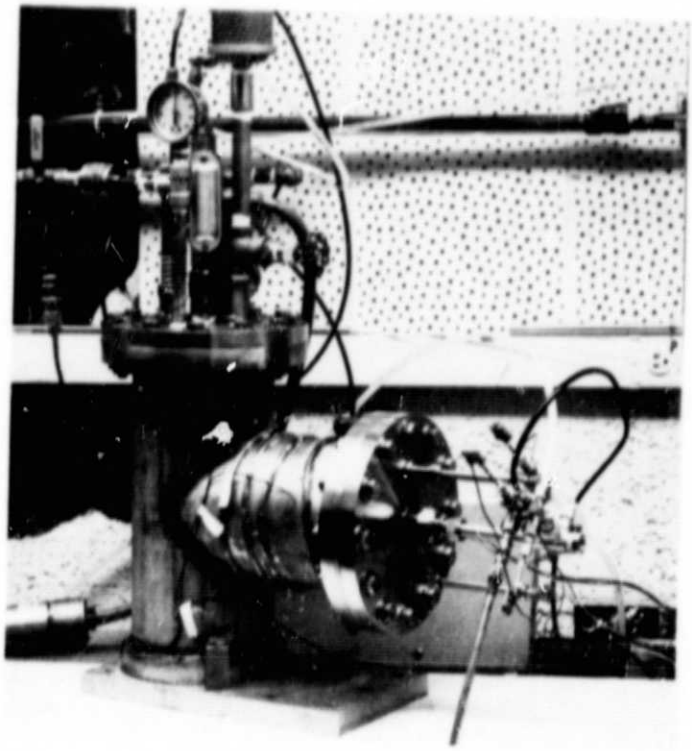

Figure 38 Porous Plug Radiometer Calibration Facility

Figure 39 Black Body Furnace

SECTION 6.0
INSTALLATION OF SENSORS INTO THE COMBUSTOR LINERS

Following calibration, the sensors were pressed out of the calibration plates and physically inspected. All sensors looked good. All leads for each sensor were identified and then strung through a piece of 1.57 mm diameter hypodermic tubing for protection. The holes were drilled and reamed in the combustor walls to accept the sensors and short grooves were cut to lead the fine leadwires away from the sensor. The hypodermic tubing containing the sensor leads was strung across the combustor and held down with straps of Hastelloy-X tack welded to the combustor. The sensors were held in place with the hot side surface of the sensor flush with the hot side combustor wall and secured in place by tack welding a fillet wire of Chromel P around the periphery of the sensor on the hot side wall. The hot side was polished to restore a flat surface. The sensors were then checked to assure that there was continuity of the leadwires. Finally, the area where the fine leads entered the hypodermic tubing was sealed with ceramic cement.

An overview of the baseline combustor is shown in Figure 40. The cold side combustor surface with an embedded thermocouple sensor and a laminated sensor installed and the cold side of a completed Gardon gauge installation is shown in Figures 41 and 42, respectiveley. A photograph, taken through a boroscope, showing the hot side of a typical installed sensor, and a schematic showing the location of each sensor installed in the baseline combustor are shown in Figures 43 and 44, respectively.

The sensors in the variable geometry combustor were installed using the same techniques as the baseline combustor. The variable geometry combustor and a schematic of the combustor are shown in Figures 45 and 46, respectively. This combustor has variable vanes between the fuel nozzles and can either be opened to allow air to enter the front of the combustor between nozzles or closed to prevent such airflow. One of the Gardon gauges and the laminated sensor are shown in Figure 47. Figure 48 shows the other Gardon gauge as well as the embedded thermocouple sensor. Figure 49 is a schematic showing the location of each sensor installed in the variable geometry combustor.

Final installation of the radiometers was done at the test cell. During the initial rig buildup, trial installations were made and locations of the radiometers where they were held on the outer rig case were marked. These locations were chosen to keep the front faces of the radiometers flush with the hot side of the combustor wall. At test, the radiometers were reinstalled and secured to the outer case with compression fittings. Figure 50 shows a schematic of a typical radiometer installation.

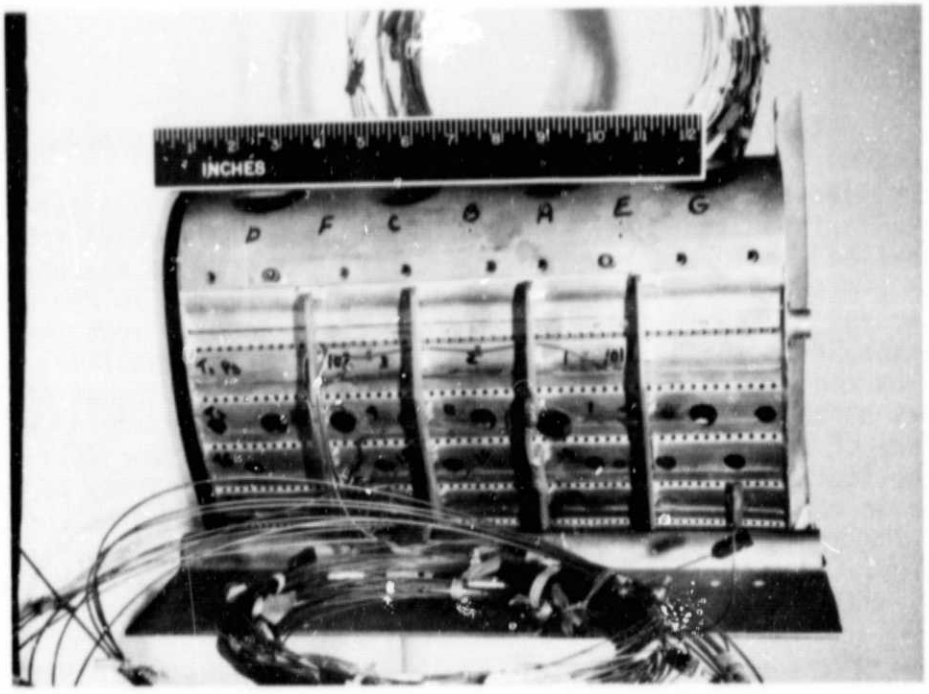

Figure 40 Overview of the Baseline Combustor

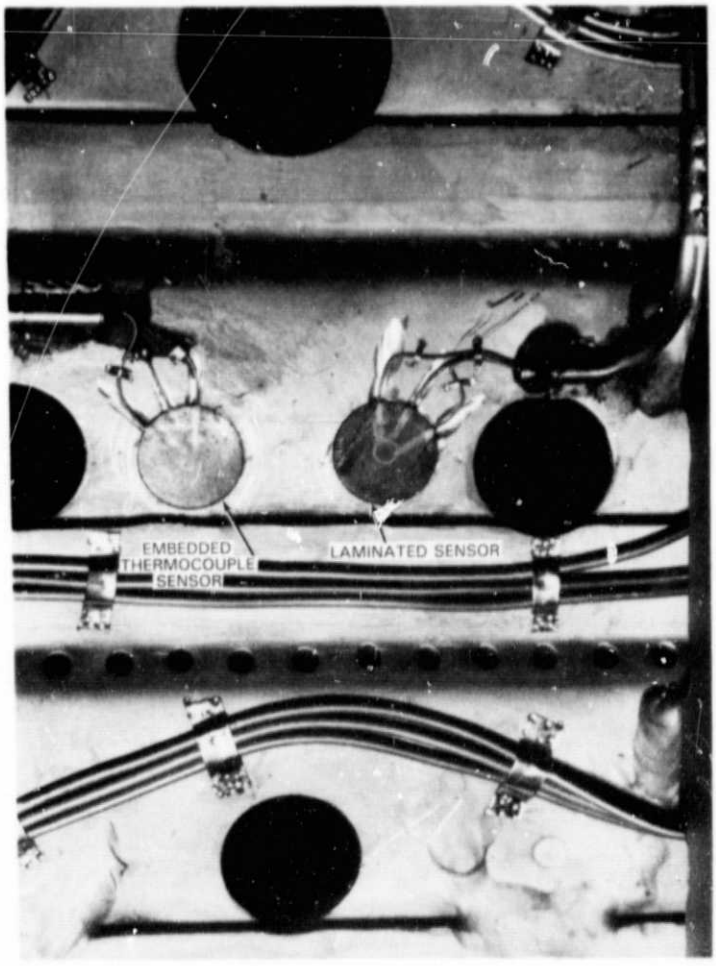

ORIGINAL PAGE IS
OF POOR QUALITY

Figure 41 Cold Side of Completed Laminated and Embedded Thermocouple Sensor Installations

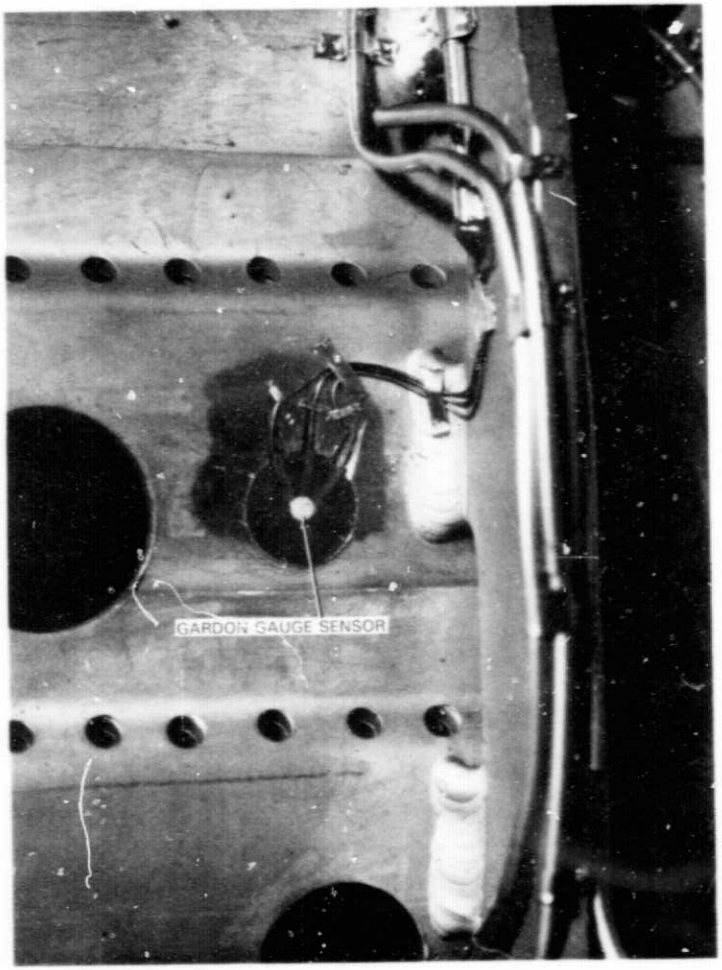

Figure 42 Cold Side of a Completed Gardon Gauge Installation

Figure 43 Photograph Taken Through a Boroscope Showing the Hot Side of a Typical Installed Sensor

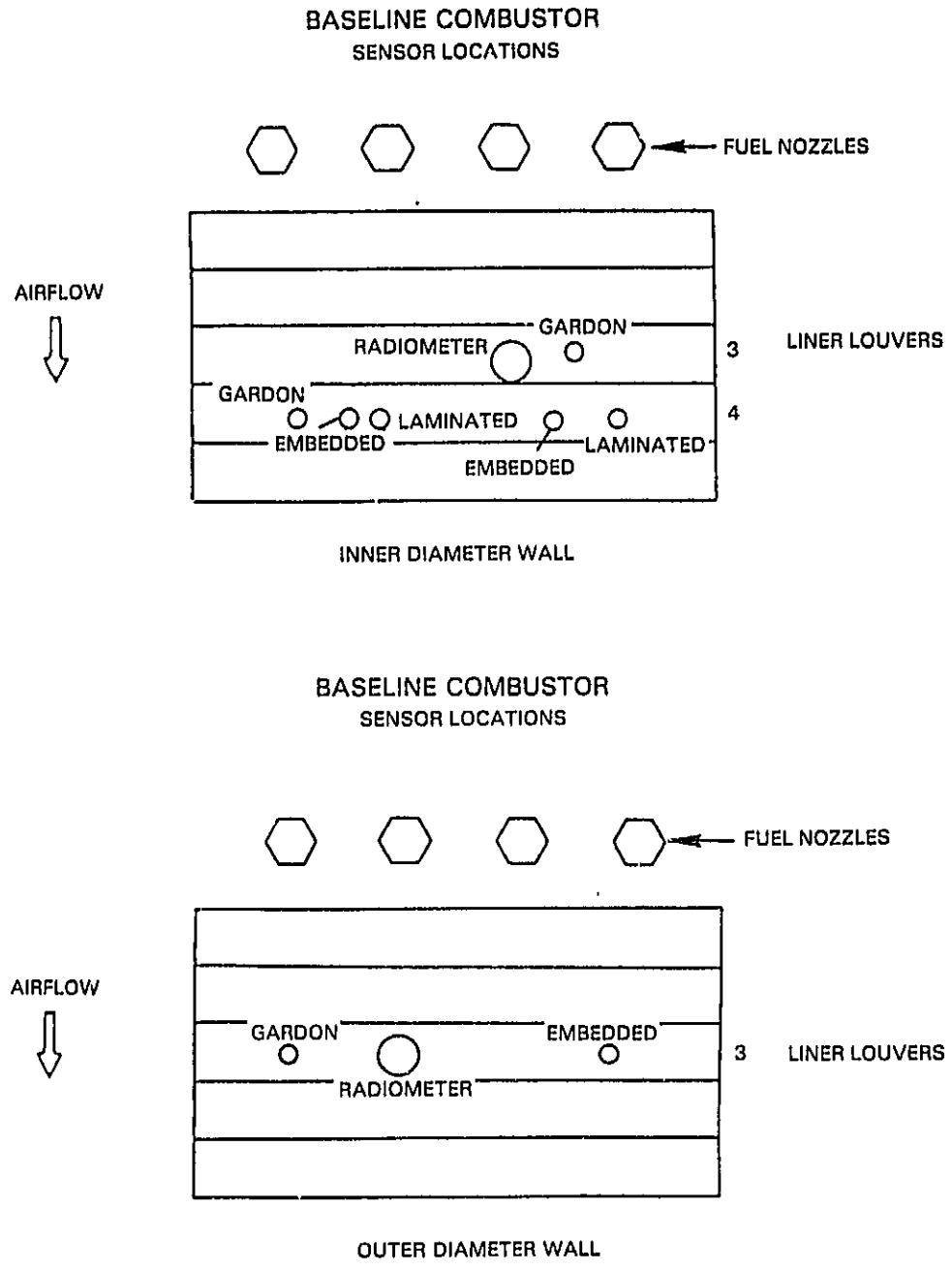

Figure 44 Schematic Showing the Location of Each Sensor Installed in the Baseline Combustor

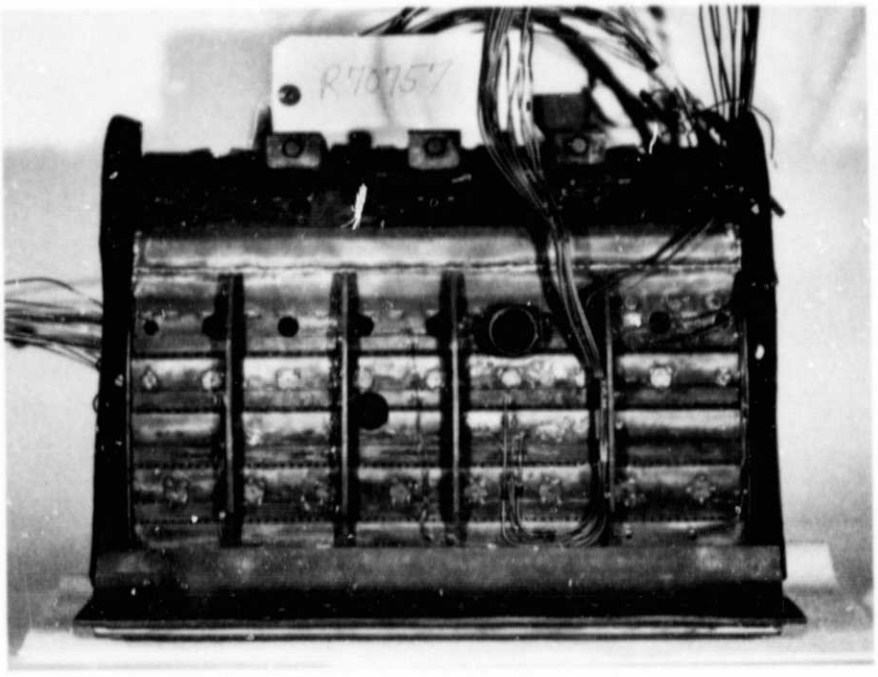

Figure 45 Overview of Variable Geometry Combustor

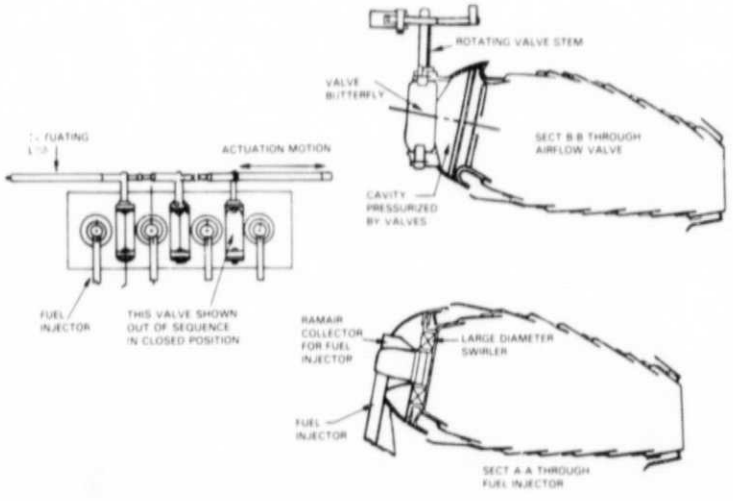

Figure 46 Schematic of Variable Geometry Combustor

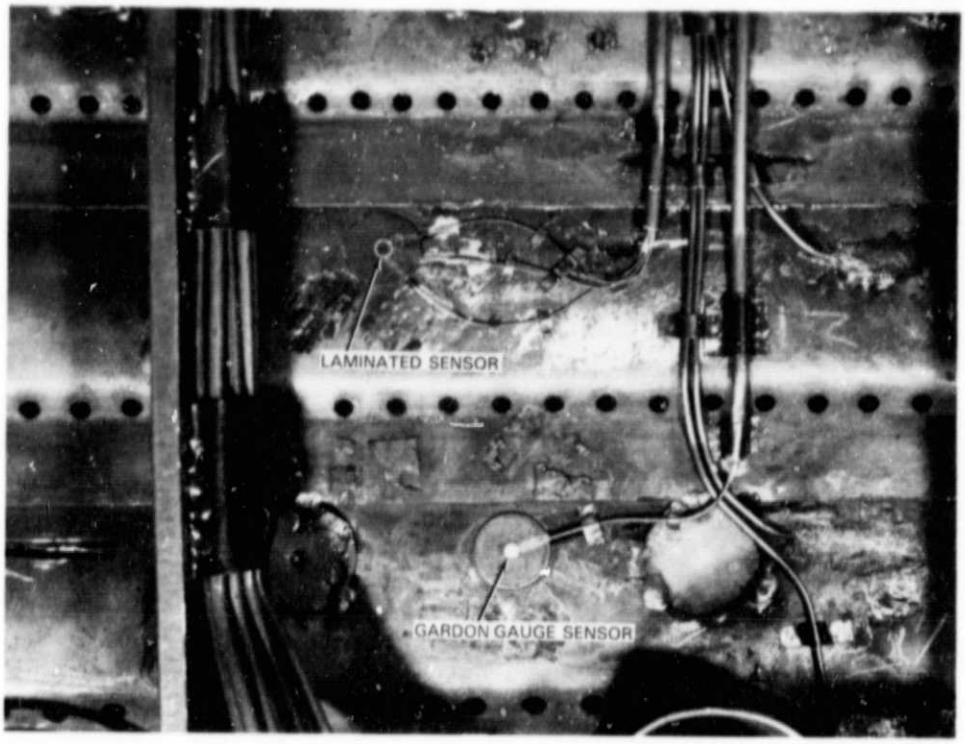

Figure 47 Cold Side of Gardon Gauge and Laminated Sensor Installations

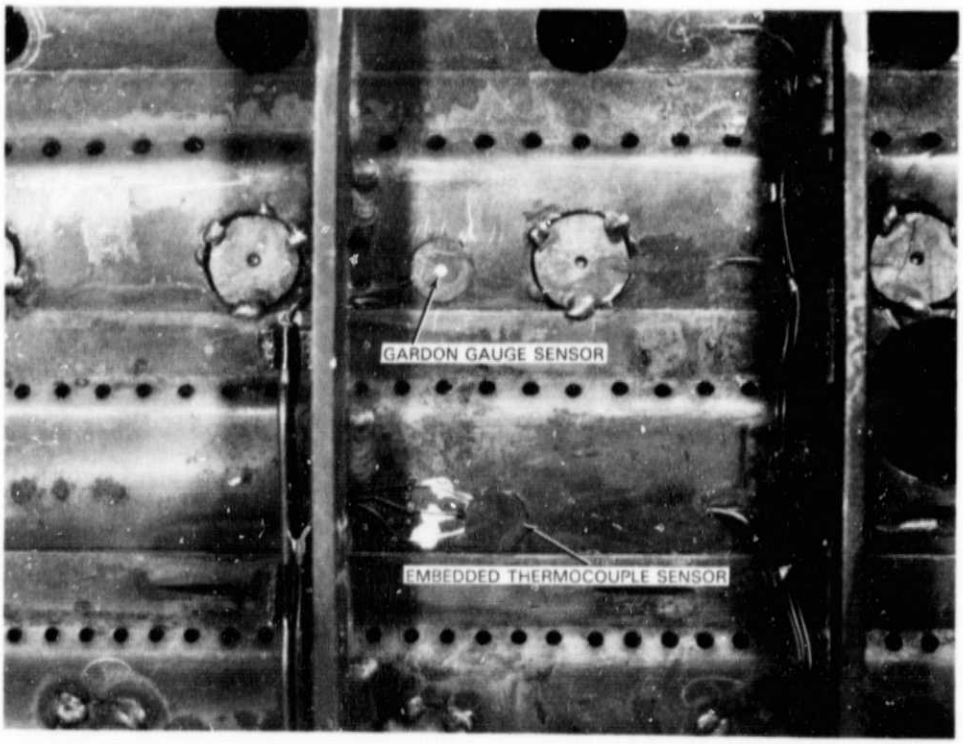

Figure 48 Cold Side Embedded Thermocouple Sensor and Gardon Gauge Installations

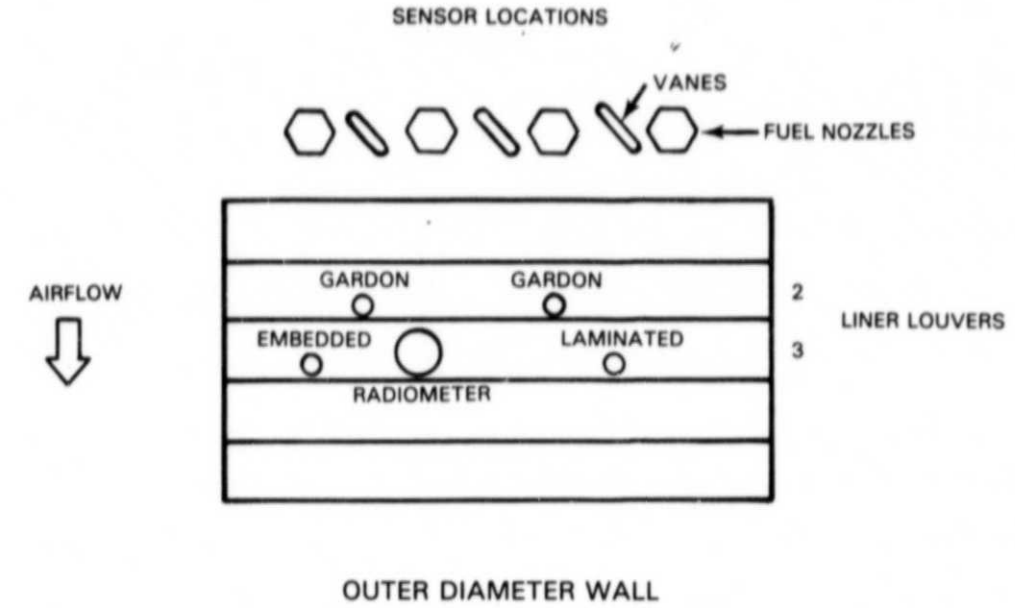

Figure 49 Schematic of Variable Geometry Combustor Showing Sensor Locations

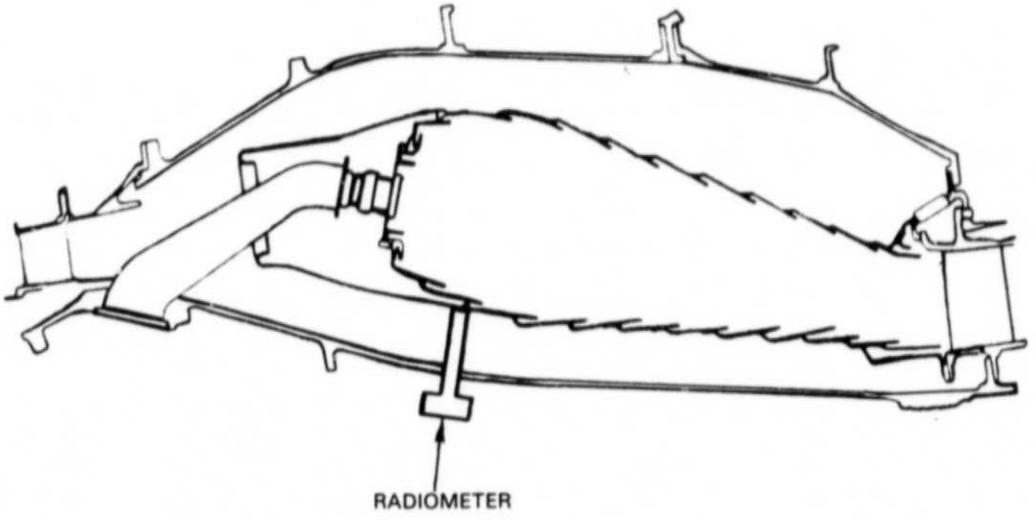

Figure 50 Schematic of Radiometer Installation

SECTION 7.0
DESCRIPTION OF TEST PLAN

TEST FACILITIES

The majority of the testing under this program was conducted in the Pratt & Whitney X-902 high pressure combustor facility, located in the four-stand Combustion Test Facility Complex at the Pratt & Whitney Middletown Plant. A schematic of the air supply system for this complex is shown in Figure 51 while the test stand is shown in Figure 52. Mass airflows and pressures up to 11 Kg/sec and 40 atmospheres, respectively, are provided by three multi-stage steam-turbine-driven compressors. Non-vitiated airflow with temperatures up to 925K can be provided by a gaseous or liquid fuel fired heat exchanger. A compressor intercooler and aftercooler provide the test facility with air containing approximately 0.002 kilogram of water or less per kilogram of dry air.

The stand is provided with an automatic control systems which monitors and maintains preselected rig inlet condtions. A wide range of fuels can be supplied at pressures and flows ranging up to 100 atmospheres and 0.7 Kg/sec, respectively.

Limited running was done in the United Technologies Research Center high pressure burner facility. While this facility does have high pressure capability, it is limited in flow capacity compared to X-902 stand.

RUN PROGRAM

The run program in X-902 was similar for both the baseline combustor and the variable geometry combustor. The purpose of this test was to determine the effect of combustor set point and fuel type on the total heat flux through, and the radiant heat flux incident on, the combustor liner walls. The combustors were tested over a range of points with four different fuels: 1) JET-A (13.62 % hydrogen by weight), 2) experimental referee broad spectrum fuel (Erbs) (12.93% hydrogen), 3) commodity fuel (Comm) (12.25% hydrogen), and 4) 11.8% hydrogen fuel.

The run program at UTRC was performed to compare the performance of the baseline combustor when run on Jet A and Methane.

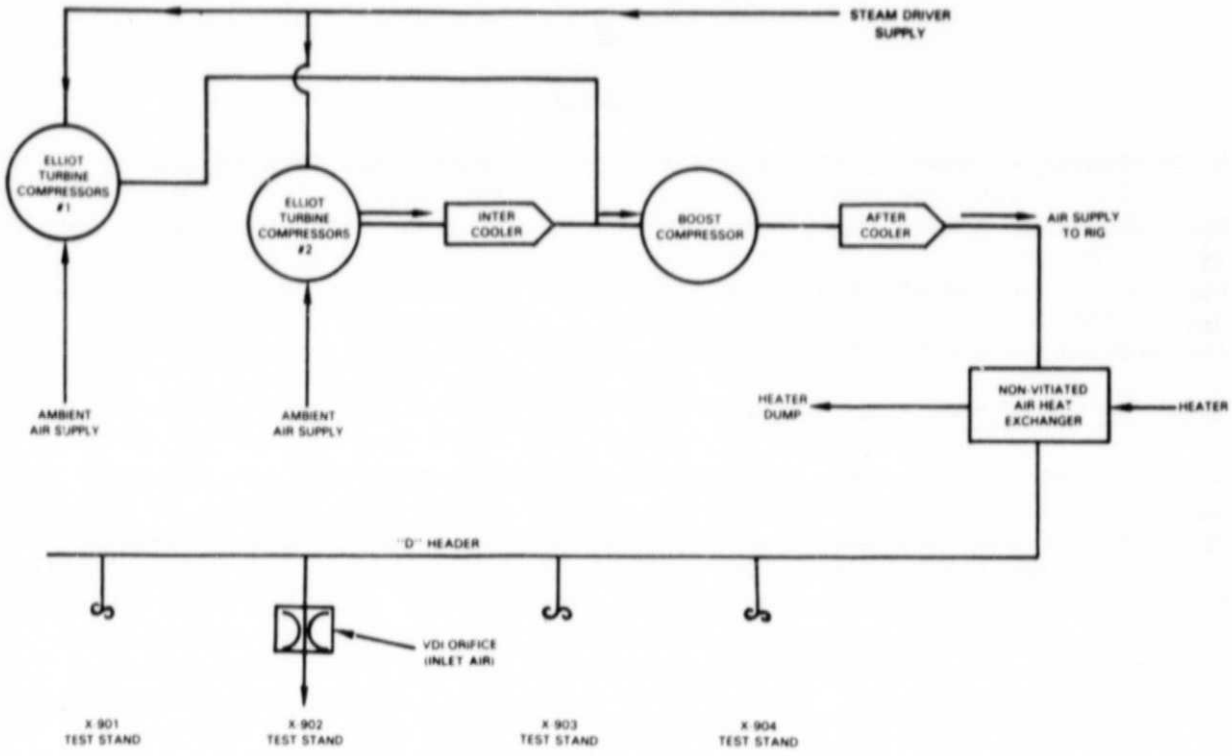

Figure 51 Schematic of Combustion Test Facility

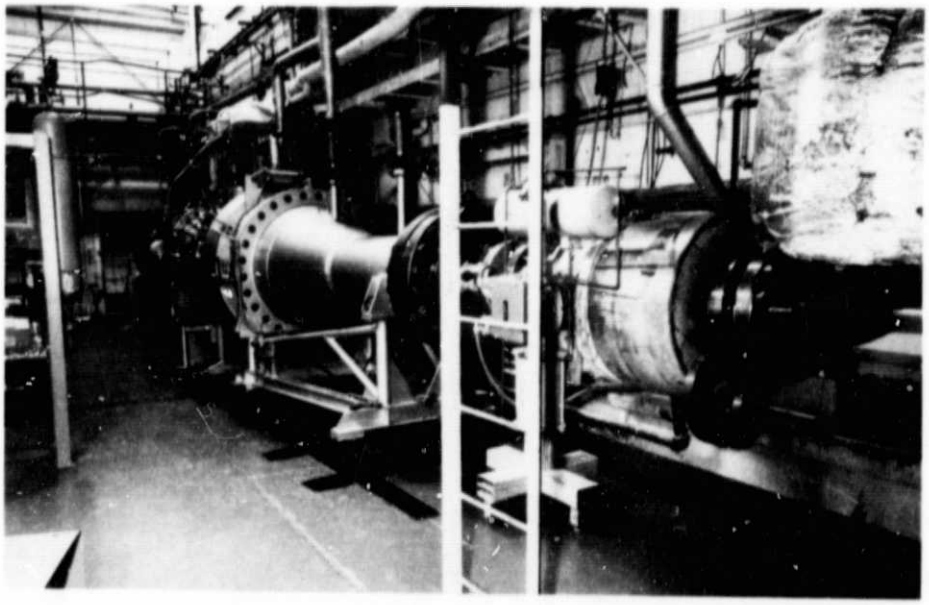

Figure 52 X-902 Test Stand

SECTION 8.0
TEST RESULTS

Both combustor segments tested are typical of modern gas turbine engine combustors. The main heat load to the combustor liner walls is radiation from the combustion zone. The primary method of combustor liner cooling is hot side film cooling. It is, therefore, expected that only a relatively small portion of the radiant heat flux incident on the combustor wall will actually be transmitted through the combustor wall. The majority of the heat will be carried off by the hot side film.

BASELINE COMBUSTOR- X-902 STAND

After it was instrumented, the baseline combustor underwent considerable handling before installation in X-902 stand. After installation, it remained inactive for over two months due to other test programs at the Middletown combustion facility. During that period, the test chamber was inadvertently filled with the acidic exhaust from one of the other combustor rigs. During rig cleanup, the sensor leads were subjected to more handling and flexing. The end result of the handling was that three of the eight sensors failed before the test started. Three more of the sensors failed almost immediately at the start of the test, so that data was obtained from only two sensors. Both radiometers continued to function throughout the test program. It was clear from the data, however, that the Medtherm radiometer was becoming fouled as the test progressed. Near the start of the test, the porous plug radiometer read approximately 35% higher than the Medtherm and by the end of the test, the porous plug reading was approximately 125% higher. The data obtained during the test program is contained in Table I. Due to data system problems, there is some question concerning the absolute level of the heat flux sensor data, however, the trends observed should be valid.

TABLE I
BASELINE BURNER - X-902 STAND

POINT NO.	BURNER PRESSURE· ATMOSPHERES	FUEL % H_2	EMBEDDED TC SENSOR D-62-3 MW/m^2	LAMINATED SENSOR L-ARI-6 MW/m^2	POROUS PLUG RADIOMETER MW/m^2	MEDTHERM RADIOMETER MW/m^2
1	13.7	13.62	.170	.108	1.06	0.79
2	13.7	12.93	.186	.128	1.25	0.78
3	13.7	11.80	.183	.143	1.35	0.80
4	13.7	12.25	.201	.138	1.33	0.76
5	21.3	13.62	.216	.177	1.34	0.65
6	21.3	12.93	.247	.186	1.43	0.71
7	21.9	13.62	.208	.178	1.35	0.65
8	21.9	12.93	.233	.199	1.43	0.64
9	21.9	11.80	.253	.216	1.55	0.67
10	21.9	12.25	.244	.198	1.49	0.66

Figure 53 shows the variation with combustor pressure of both the radiant heat load on the combustor wall as well as the heat flux transmitted through the liner. The radiant heat load data shown is from the porous plug radiometer. This data was taken with the combustor operating on Jet A fuel. Similar data taken with the combustor running on ERBS fuel is shown in Figure 54. Figure 55 shows the effect of fuel hydrogen content on the radiant heat load to the liner. The effect of the fuel hydrogen content on heat flux transmitted through the liner is shown in Figure 56. All of the data trends look reasonable. Both the radiant and transmitted heat flux increase with increasing combustor pressure. At constant combustor pressure, both the radiant and transmitted heat flux decreased with increasing fuel hydrogen content. As the amount of hydrogen increased, the luminosity of the flame decreased resulting in lower radiant heat load on the combustor wall.

At the conclusion of the test program conducted at X-902 test stand, all indications showed that the porous plug radiometer was in good shape. The data looked reasonable and the screen pressure drop was unchanged from the start of the test. Testing continued with various idle and lean blowout tests. During the blowout tests the pressure drop across the screen increased dramatically indicating that the porous screen was becoming plugged. As soon as the X-902 test program was concluded, the baseline combustor was shipped to the United Technologies Research Center for testing in their high pressure combustor facility. The porous plug and Medtherm radiometers were returned to the laboratory for inspection which revealed the screen on the porous plug radiometer was plugged. The window in the Medtherm radiometer was very dirty and the calibration was down 58% compared with the pretest data.

BASELINE COMBUSTOR-UNITED TECHNOLOGIES RESEARCH CENTER (UTRC)

The test started with the same two sensors that were operational at X-902 stand and that were still functioning. Early in the test program, the laminated sensor failed and became erratic. Two Medtherm radiometers (S/N 821 and S/N 841) were used. The data from this test program is given in Table II. Figure 57 shows the results obtained at UTRC using JET-A fuel and Figure 58 shows the results using Methane fuel. An expanded plot of that data is shown in Figure 59. The data taken from the Jet A run at UTRC look similar to the X-902 data. Both the radiant and transmitted heat flux increased with increasing pressure, and the radiant heat load was several times higher than the heat flux transmitted through the liner. As expected, both the radiant and transmitted heat flux were much lower for the runs using Methane fuel, due to the high hydrogen content of Methane.

POST TEST INSPECTION OF BASELINE COMBUSTOR

Upon completion of the test program at UTRC, the baseline combustor was inspected to identify the cause of the sensor failures. Three sensors had failures in the leadwires and two sensors failed in or near the sensor bodies. Three sensors still had electrical continuity to the end of the leadwires, although only one was yielding apparently valid data at the end of the test program. Figure 60 shows the location of the three sensors that still had electrical continuity at the end of the test program. During post test checks, both radiometers showed no significant change from their pretest results.

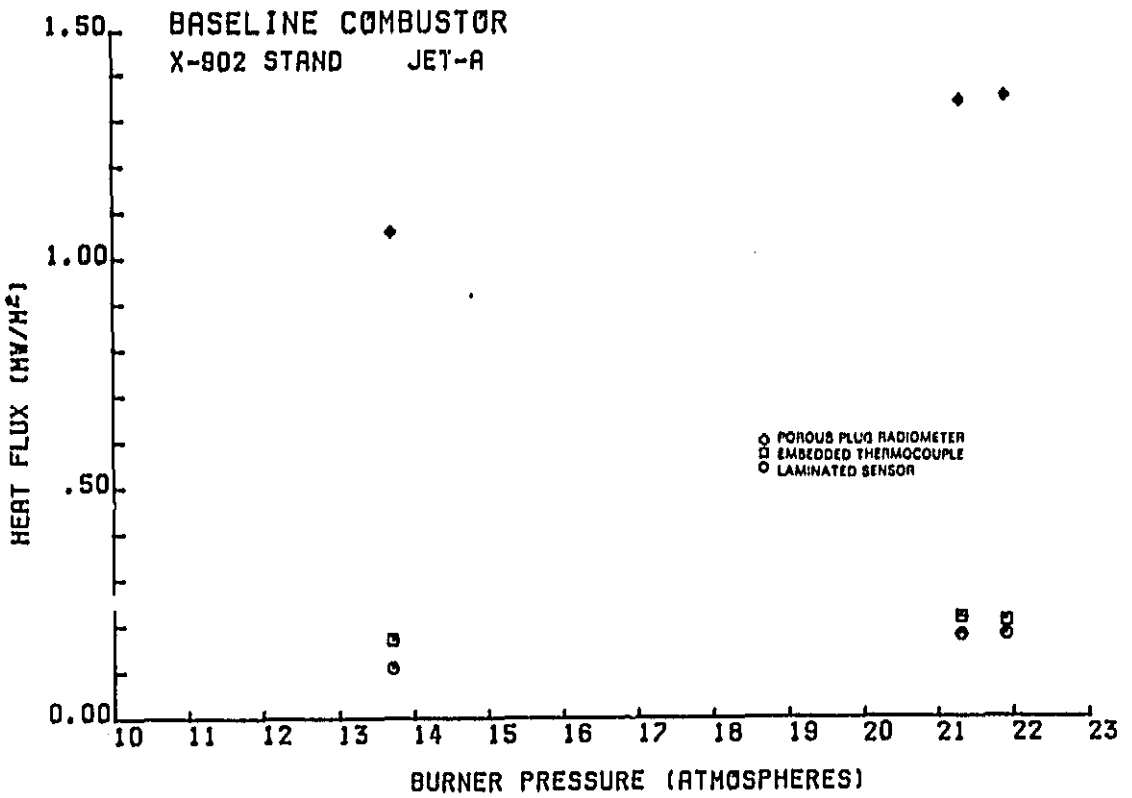

Figure 53 Baseline Combustor - Jet A Fuel

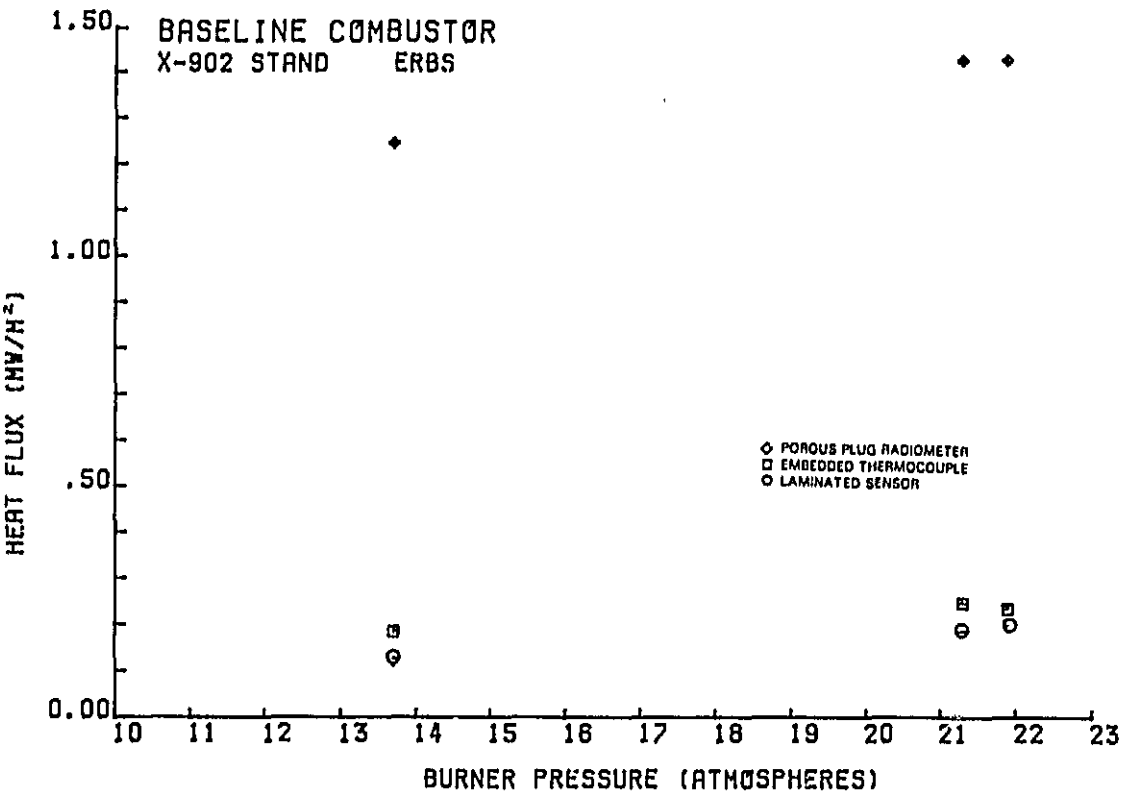

Figure 54 Baseline Combustor - ERBS Fuel

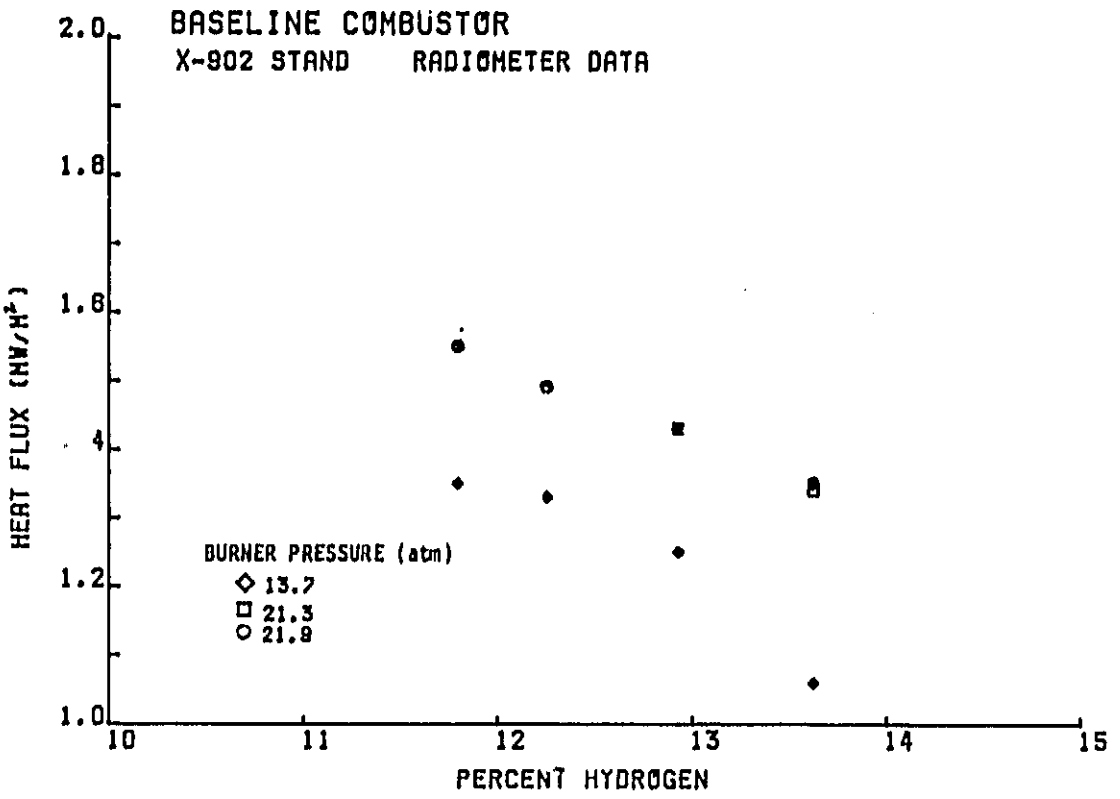

Figure 55 Baseline Combustor - Porous Plug Radiometer Data

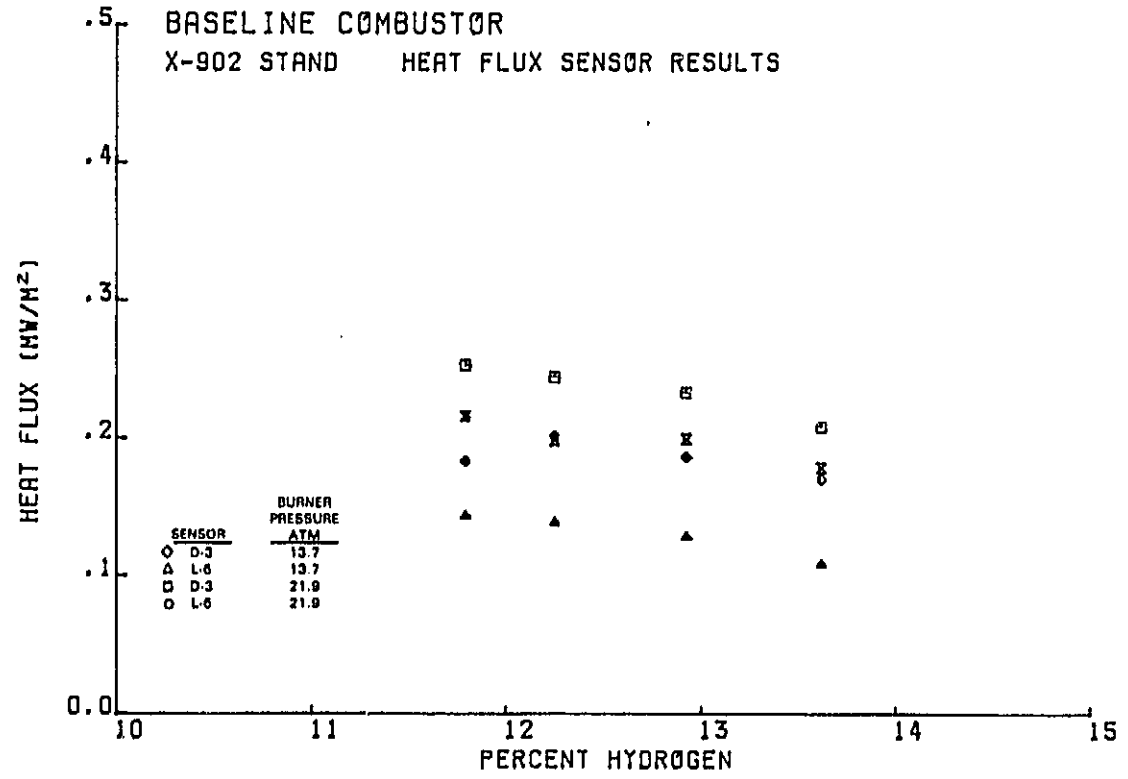

Figure 56 Baseline Combustor - Heat Flux Sensor Results

TABLE II
BASELINE BURNER UTRC

POINT NO.	BURNER PRESSURE ATMOSPHERES	FUEL	EMBEDDED TC SENSOR D-62-3 MW/m²	RADIOMETER MED 821 MW/m²	RADIOMETER MED 841 MW/m²
1	9.7	METHANE	.049	.088	.136
2	15.0	METHANE	.097	.118	.198
3	10.2	METHANE	.050	.090	.139
4	10.4	JET A	.125	.511	.636
5	14.8	JET A	.330	.693	.943
6	13.9	JET A	.295	.727	.920

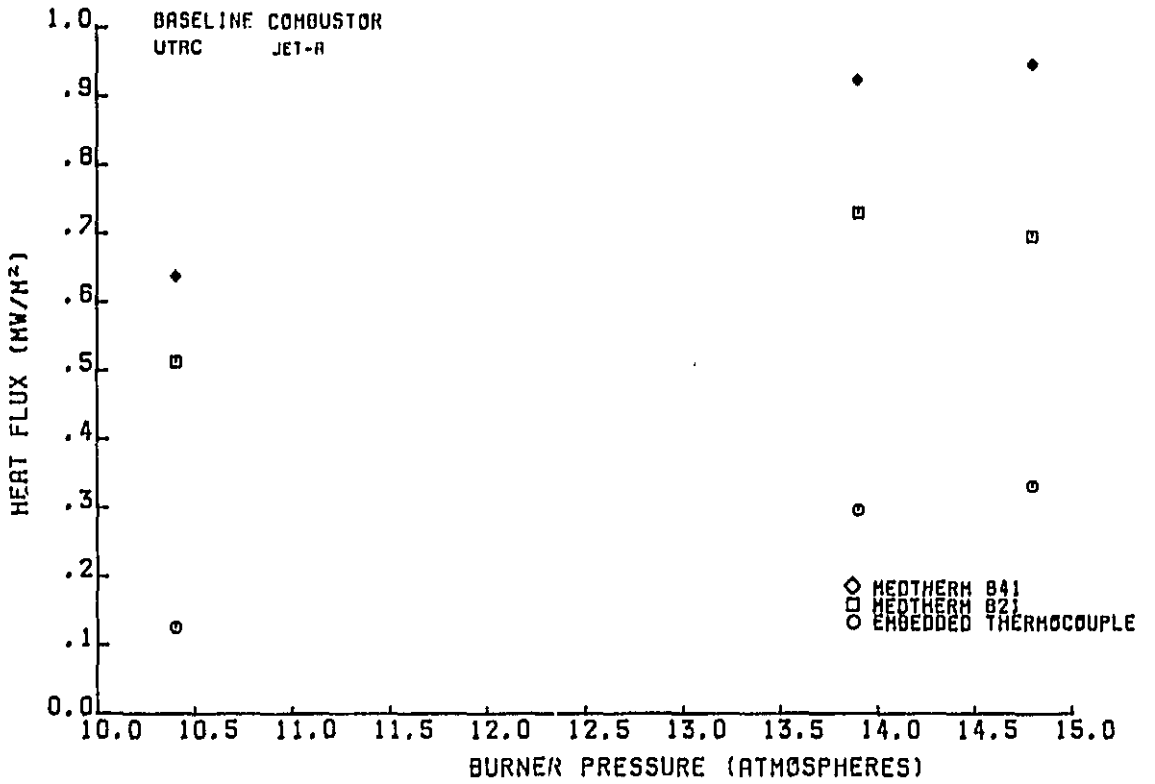

Figure 57 Baseline Combustor - UTRC - Jet A Fuel

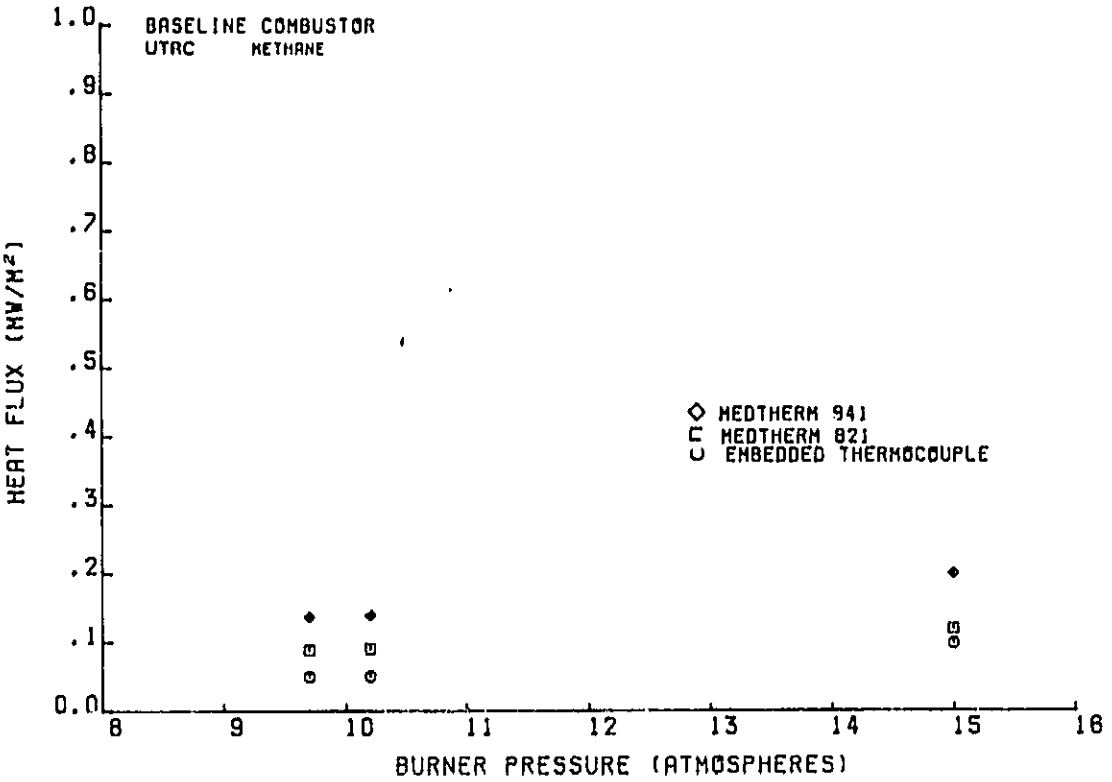

Figure 58 Baseline Combustor - UTRC - Methane

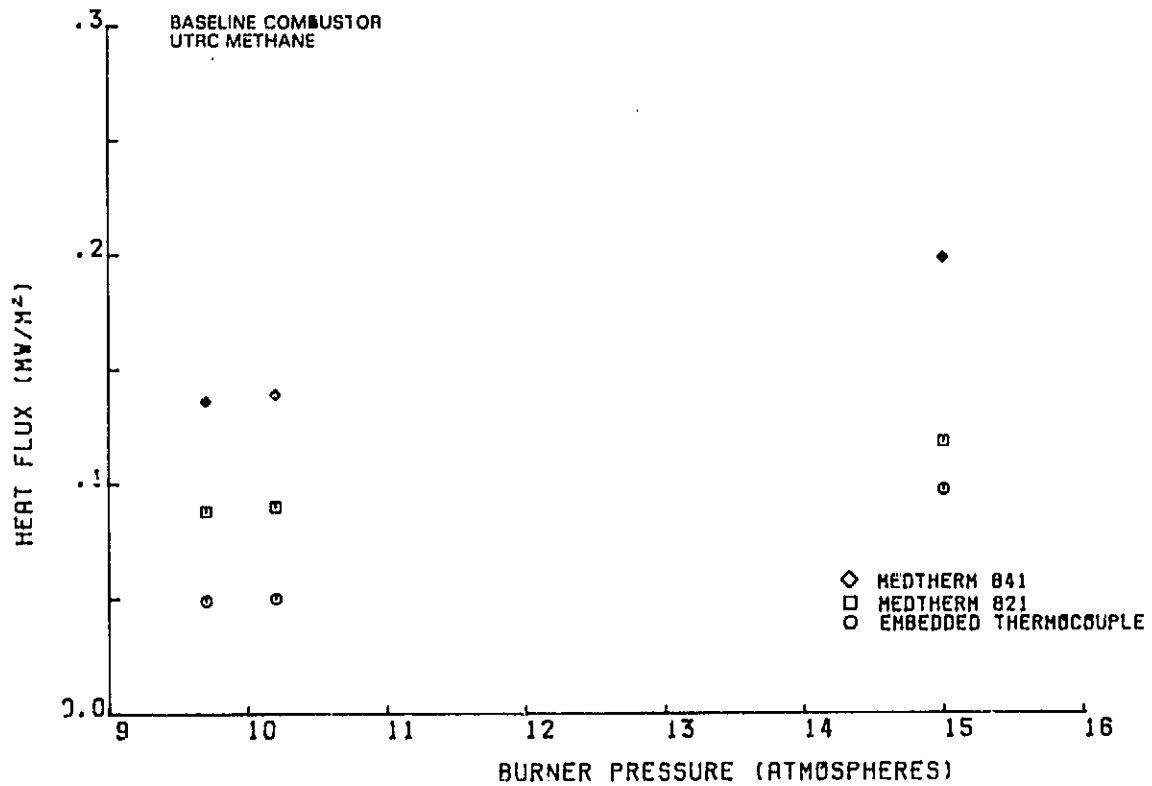

Figure 59 Baseline Combustor - UTRC - Methane-Expanded

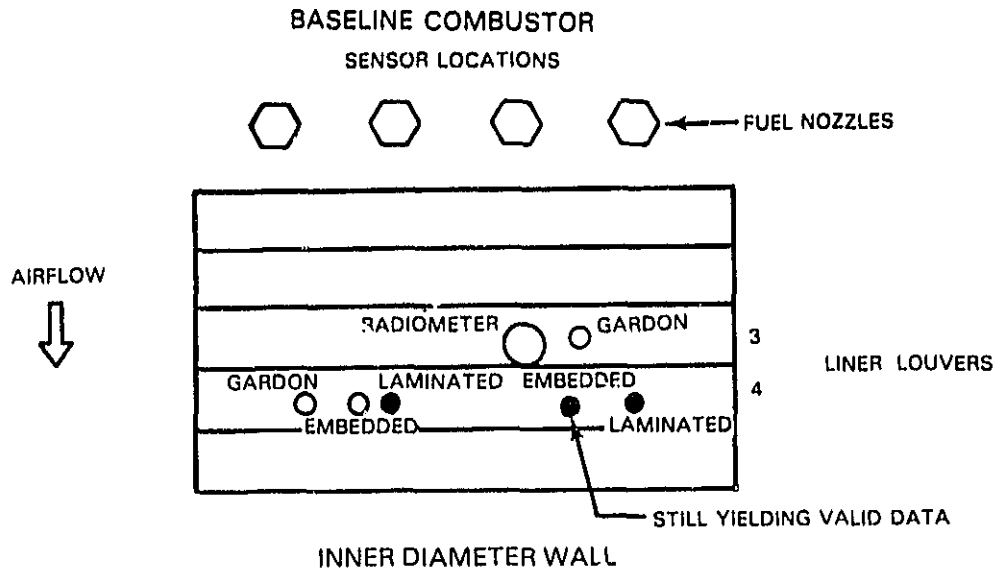

Figure 60 Schematic of Baseline Combustor Showing Surviving Sensors

VARIABLE GEOMETRY COMBUSTOR-X902 STAND

At the start of the variable geometry combustor run, all four sensors were operational. One sensor became erratic and failed part way through the test. The other three sensors survived the entire test program. Both the porous plug and Medtherm radiometers performed well throughout the test program. Data was obtained with the variable geometry vanes both open and closed. The data from this test program is given in Table III.

RADIOMETER RESULTS-VARIABLE AREA COMBUSTOR

Figures 61 and 62 show the variation in the radiant heat load measured by the porous plug radiometer vs. combustor pressure with the variable area vanes both open and closed. The data for Jet A fuel and for ERBS are shown in Figures 61 and 62, respectively. While data was not taken at exactly the same points with the vanes open and closed, the trends are clear. In general, the radiant heat load increased with increased burner pressure. With the vanes open, however, the heat load measured at 22.6 atmospheres was higher than the data taken at 23.1 atmospheres. This effect was observed for both Jet A and ERBS fuels. As burner pressure decreased, there was little change in the radiant heat load when the vanes were open. When the vanes were closed, the radiant heat load on the combustor wall fell rapidly with decreasing combustor pressure.

Figures 63 and 64 show the effect of fuel hydrogen content on the variation in radiant heat load measured by the porous plug radiometer, with the exception that the measured radiant heat load always increased with increasing combustor pressure. The data taken with the variable geometry vanes open and closed are shown in Figures 63 and 64, respectively. As expected, the data showed the radiant heat load decreased slightly with increasing fuel hydrogen content.

TABLE III
VARIABLE GEOMETRY COMBUSTOR X-902 STAND

POINT NO.	BURNER PRESSURE ATMOSPHERES	FUEL % H_2	GARDON GAUGE SENSOR G-62-10 MW/m^2	EMBEDDED TC SENSOR D-62-70 MW/m^2	GARDON GAUGE SENSOR G-62-13 MW/m^2	LAMINATED SENSOR L-62-30 MW/m^2	POROUS PLUG RADIOMETER MW/m^2	MEDTHERM RADIOMETER MW/m^2	VANE POSITION
1	23.2	13.62	.210	.309	.119	.275	1.29	1.09	OPEN
2	23.0	12.25	.236	.312	.123	.302	1.29	1.19	
3	23.1	12.93	.230	.313	.113	.303	1.28	1.17	
4	23.1	11.80	.247	.322	.110	.310	1.29	1.25	
5	13.7	13.62	.164	.227	.115	.127	1.23	.96	
6	13.7	12.93	.185	.245	.105	.193	1.28	1.05	
7	13.7	11.80	.201	.264	.114	.212	1.34	1.11	
8	13.7	12.25	.189	.251	.124	.194	1.30	1.09	
9	22.9	13.62	.198	.295	.157	.296	1.42	1.06	
10	22.5	12.93	.205	.307	.170	.308	1.45	1.12	
11	10.3	13.62	.079	.059	----	.057	0.36	0.15	CLOSED
12	10.3	12.93	.088	.070	----	.066	0.38	0.17	
13	13.7	12.93	.138	.178	----	.196	0.88	0.66	
14	20.3	13.62	.186	.461	----	.578	0.97	0.93	
15	20.3	12.93	.191	.364	----	.480	1.03	0.96	
16	20.3	12.25	.196	.424	----	.528	1.09	1.01	

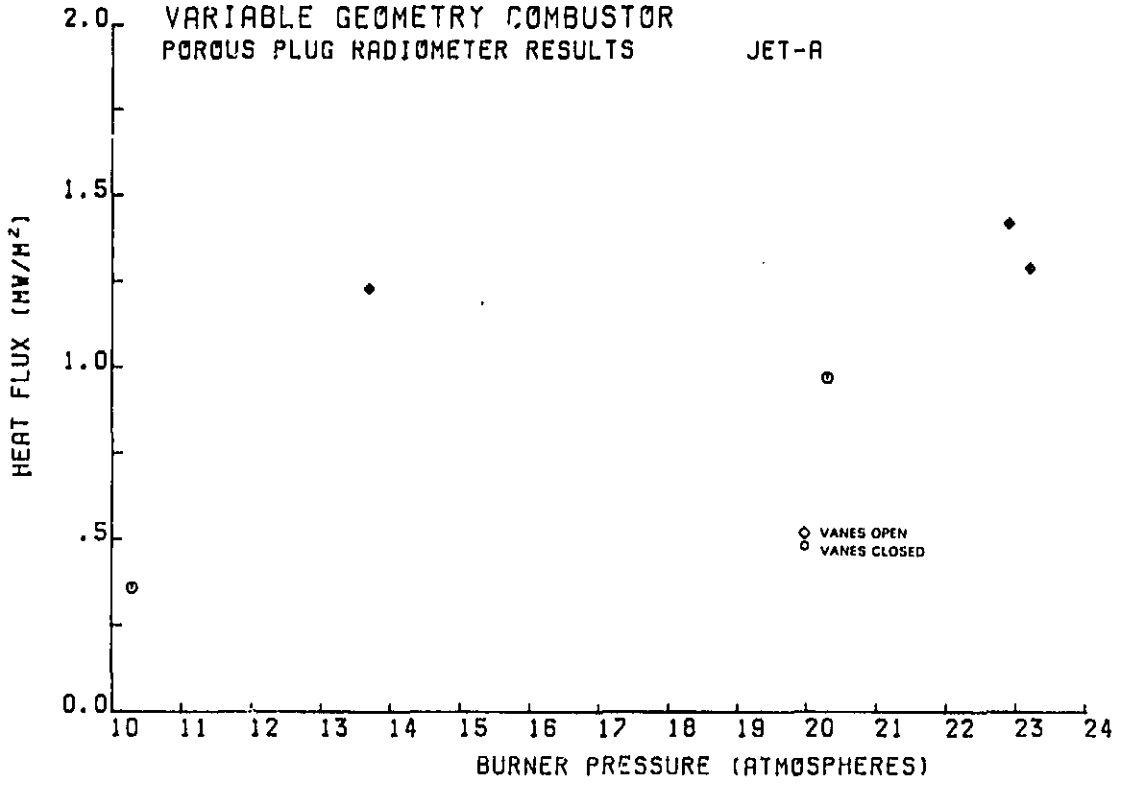

Figure 61 Variable Geometry Combustor - Porous Plug Radiometer Results Jet-A Fuel

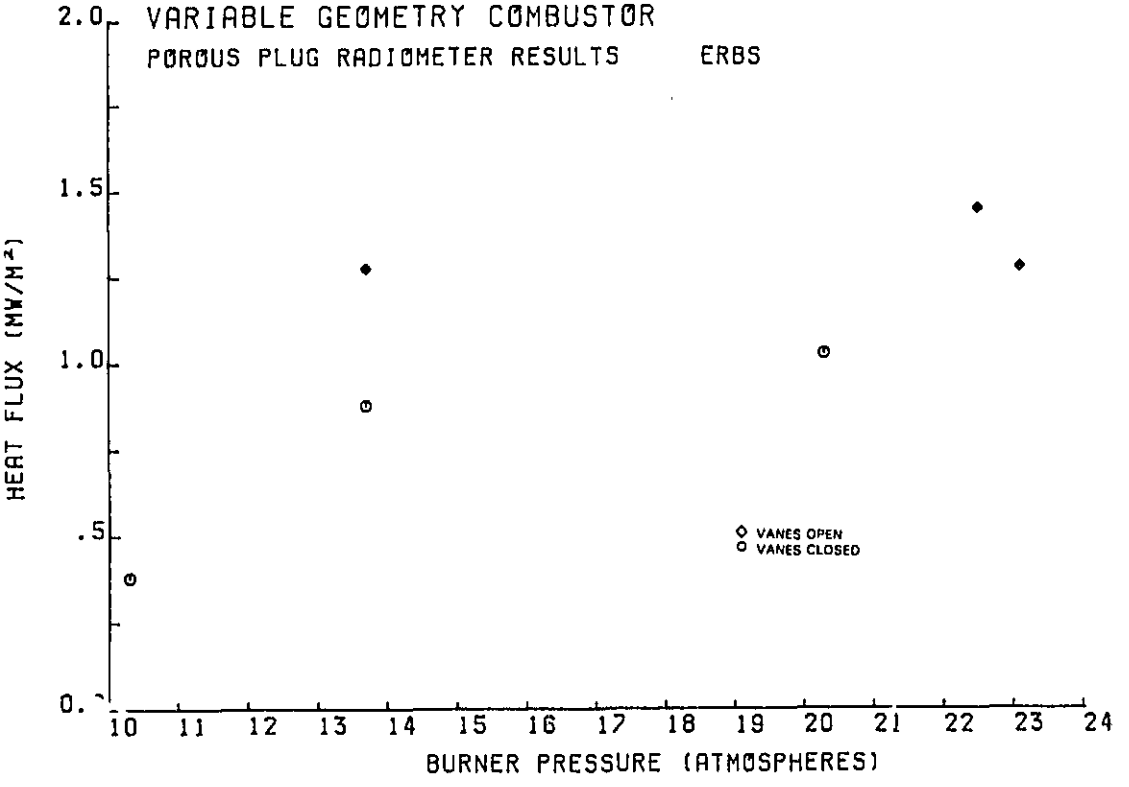

Figure 62 Variable Geometry Combustor - Porous Plug Radiometer Results ERBS

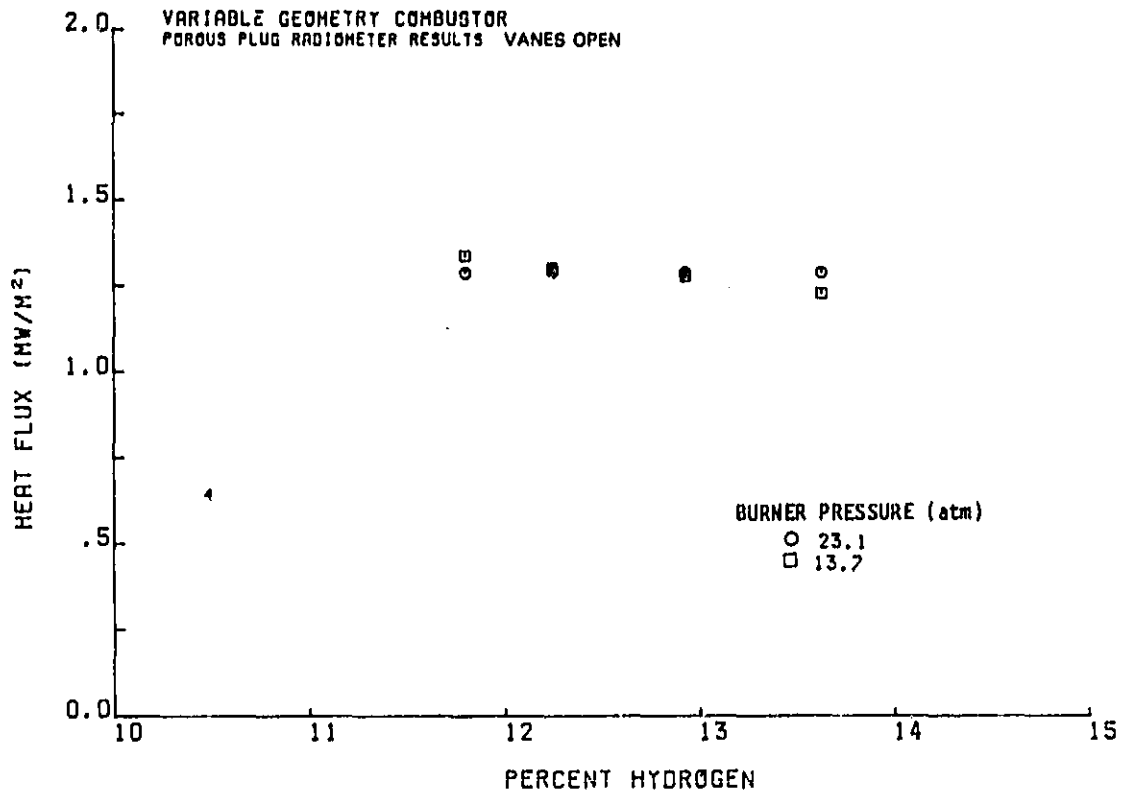

Figure 63 Variable Geometry Combustor - Porous Plug Results - Vanes Open

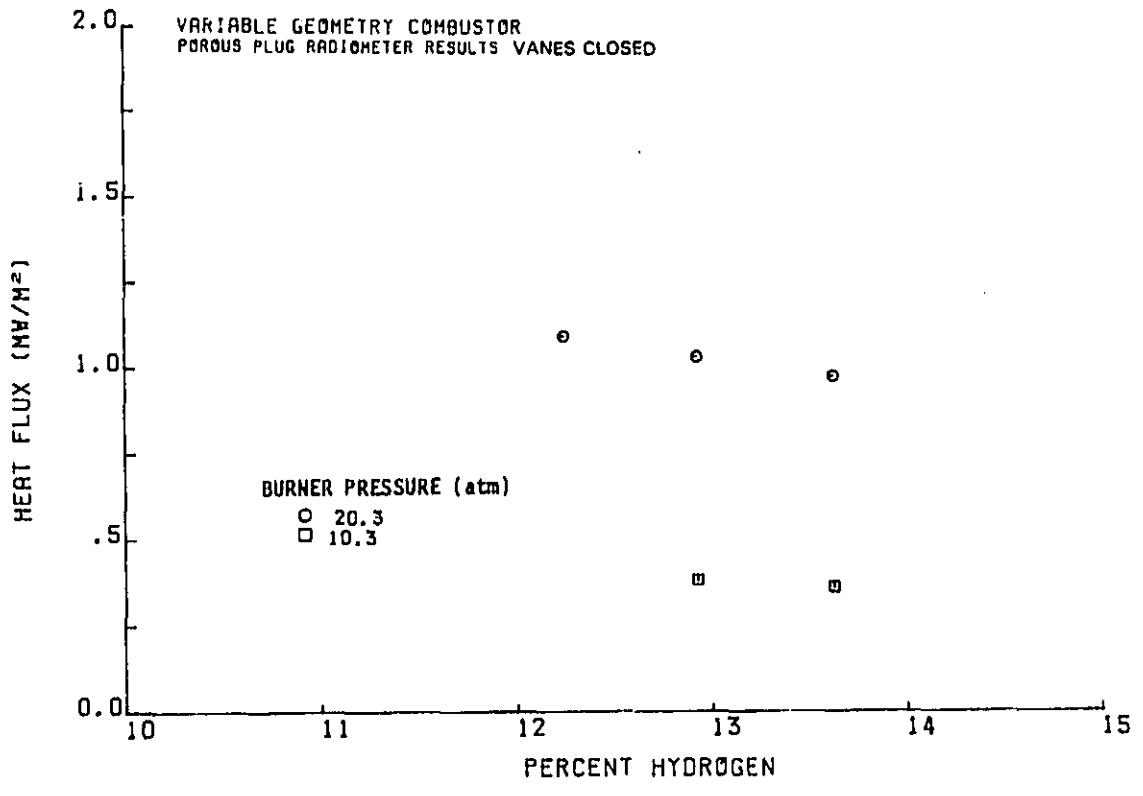

Figure 64 Variable Geometry Combustor - Porous Plug Results - Vanes Closed

Comparable data are shown in Figures 65 to 68 for the Medtherm radiometer. This data shows the same general trends seen in the porous plug data. Figure 69 shows the variation in the ratio between the Medtherm and the porous plug radiometers with burner pressure. The porous plug radiometer read higher than the Medtherm at all points. At high combustor pressure, the Medtherm read approximately 90% of the porous plug readings. At lower pressure, the Medtherm fell to less than 50% of the porous plug reading. The relatively large amount of scatter at approximately 23 atmospheres is due to the high porous plug reading at 22.6 atmospheres. The probable cause of the change, as power level (burner pressure) is reduced, is that the flame moves forward in the combustor. Since the Medtherm has a narrower field of view than the porous plug, it would be more affected by the flame moving away from the front of the radiometer.

HEAT FLUX SENSOR RESULTS VARIABLE GEOMETRY COMBUSTOR

The data from the heat flux sensors taken with the variable geometry vanes open using Jet A fuel is shown in Figure 70. Figure 71 shows the data with the vanes open using ERBS fuel. The data from both fuels were similar with the sensors on louver 3 reading higher than those on louver 2 and the sensor in line with the nozzles reading higher than the sensors between nozzles. The transmitted heat flux showed only a small variation with combustor pressure, which agreed with the radiant heat flux data with the vanes open. The radiometers were located in the third louver almost in-line with the nozzles (Figure 50). Figure 72 shows a comparison of the radiometer results with the heat flux sensor also on the third louver in line with a nozzle. They are in good agreement with the transmitted heat flux being 23-27% of the radiant heat flux incident on the liner.

Figure 73 shows heat flux data taken using ERBS fuel after the variable geometry vanes were closed. The heat flux through louver three was generally higher than through louver two, but the sensor between nozzles read higher than the sensor in line with the nozzle. Both sensors on louver 3 also showed a strong variation in transmitted heat flux with changes in combustor pressure. This agreed with the trend seen earlier in the radiant heat load data. Figure 74 shows a comparison of the radiant results with the data from the heat flux sensor on the third louver in line with a nozzle for the vanes closed condition. The trends were in good agreement with the transmitted heat flux being 27-41% of the radiant heat flux incident on the liner.

The variation in the heat flux transmitted through the liner with varying fuel hydrogen content is shown in Figures 75 through 78. The data for the sensors on louver 2, with the variable geometry vanes open, and the data with the vanes closed are shown in Figures 75 and 76, respectivly. As expected, the data shows the transmitted heat flux decreased slightly with increasing fuel hydrogen content. Comparable data for louver 3 is given in Figures 77 and 78. The data with the vanes open look as expected, with the heat flux decreasing with increasing fuel hydrogen content. The data with the vanes closed was unusual, with a higher transmitted heat flux being obtained at the highest fuel hydrogen content. Since this result was obtained from both sensors on louver 3, it is believed that this effect is real and not the result of an error in the sensors.

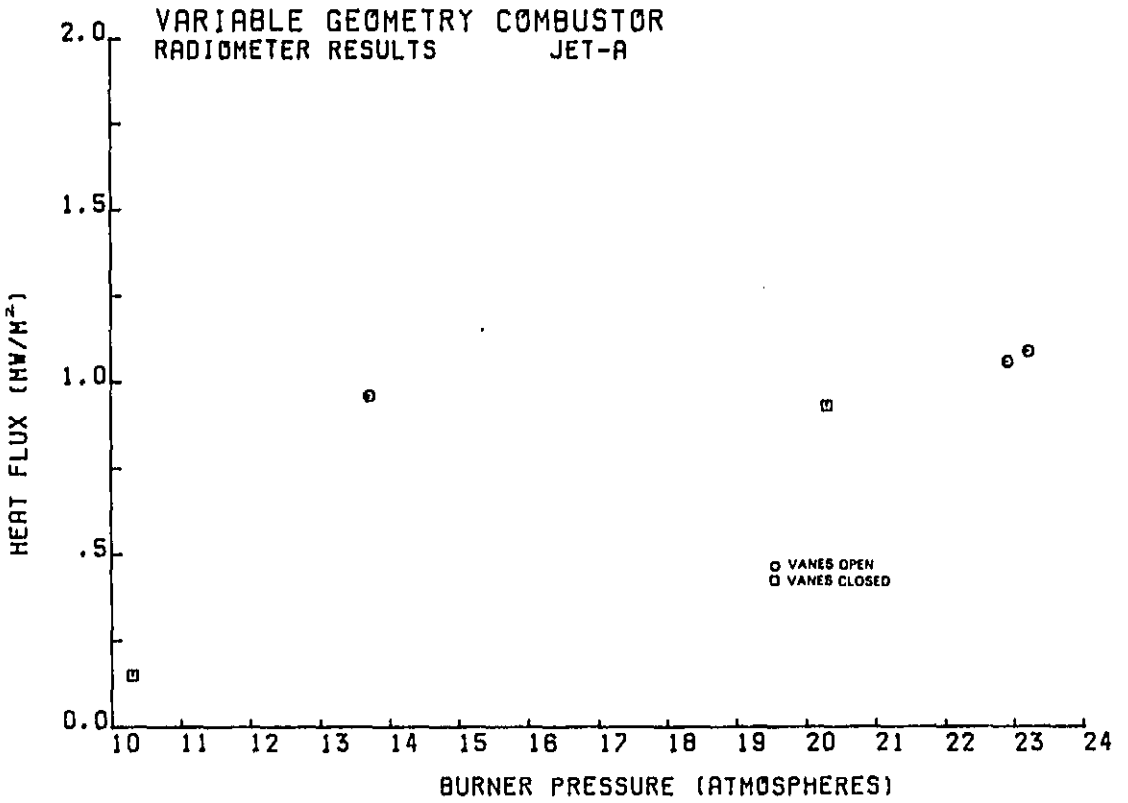

Figure 65 Variable Geometry Combustor - Medtherm Radiometer Results - Jet-A

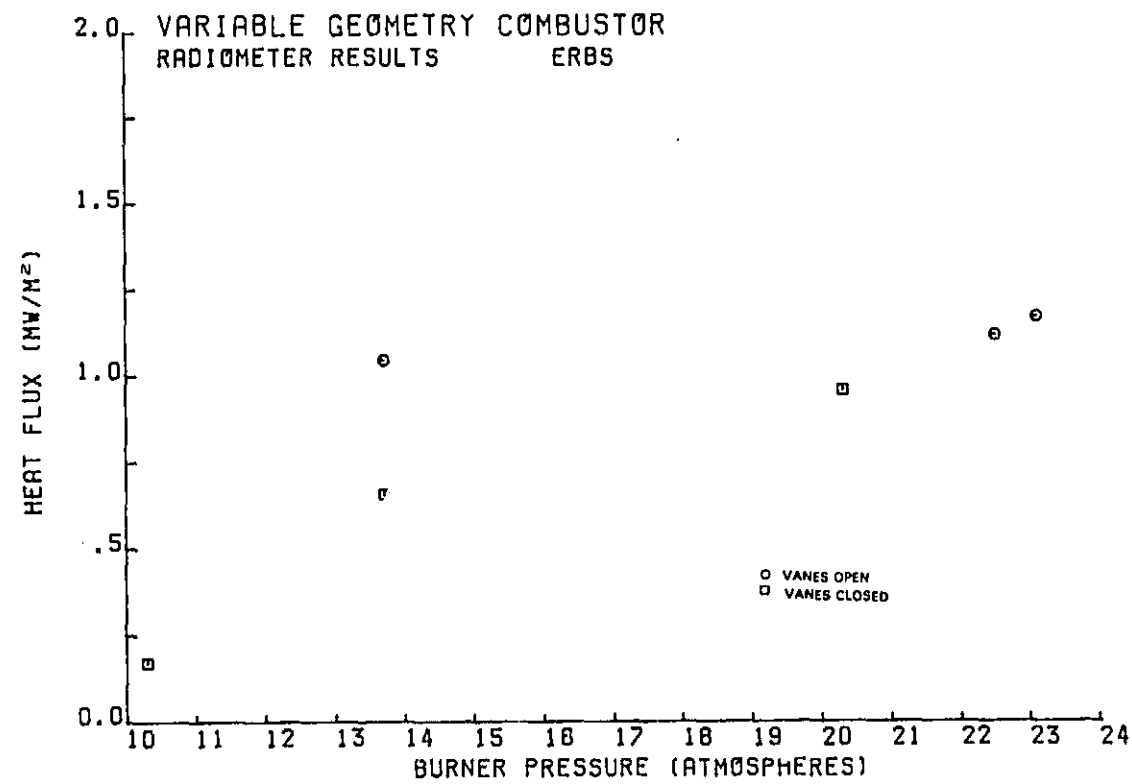

Figure 66 Variable Geometry Combustor - Medtherm Radiometer Results - ERBS

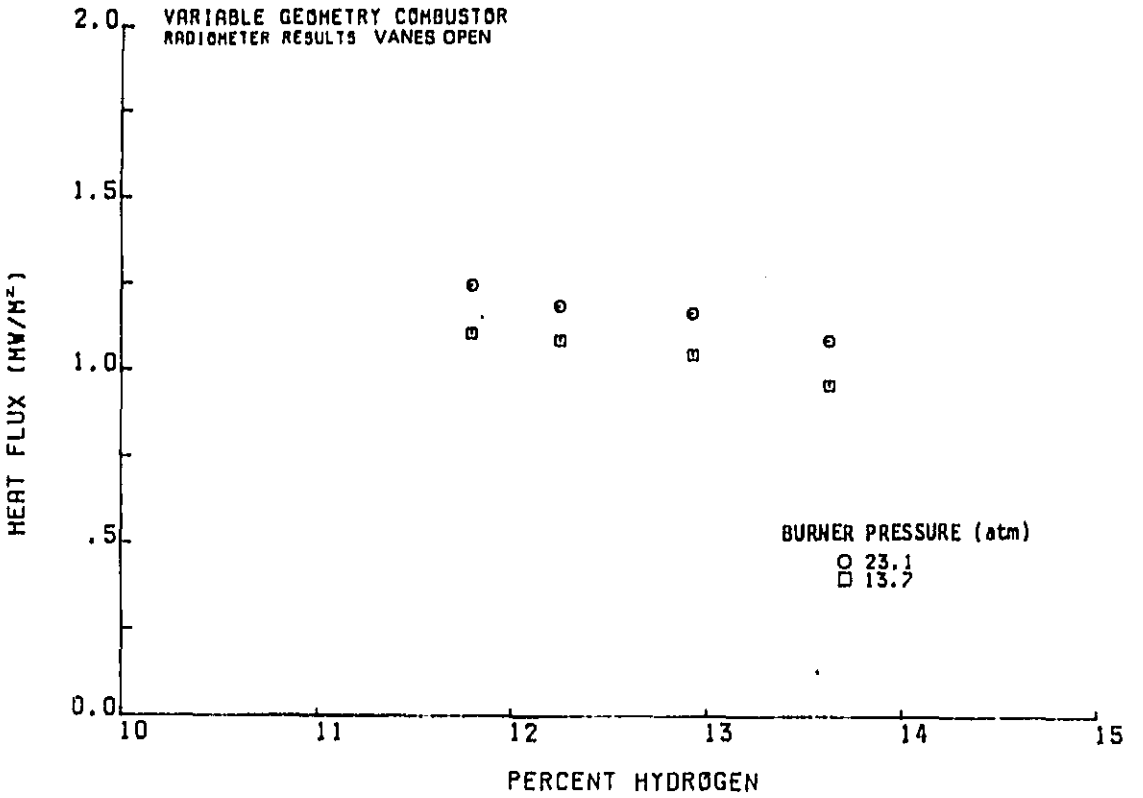

Figure 67 Variable Geometry Combustor - Medtherm Radiometer Results - Vanes Open

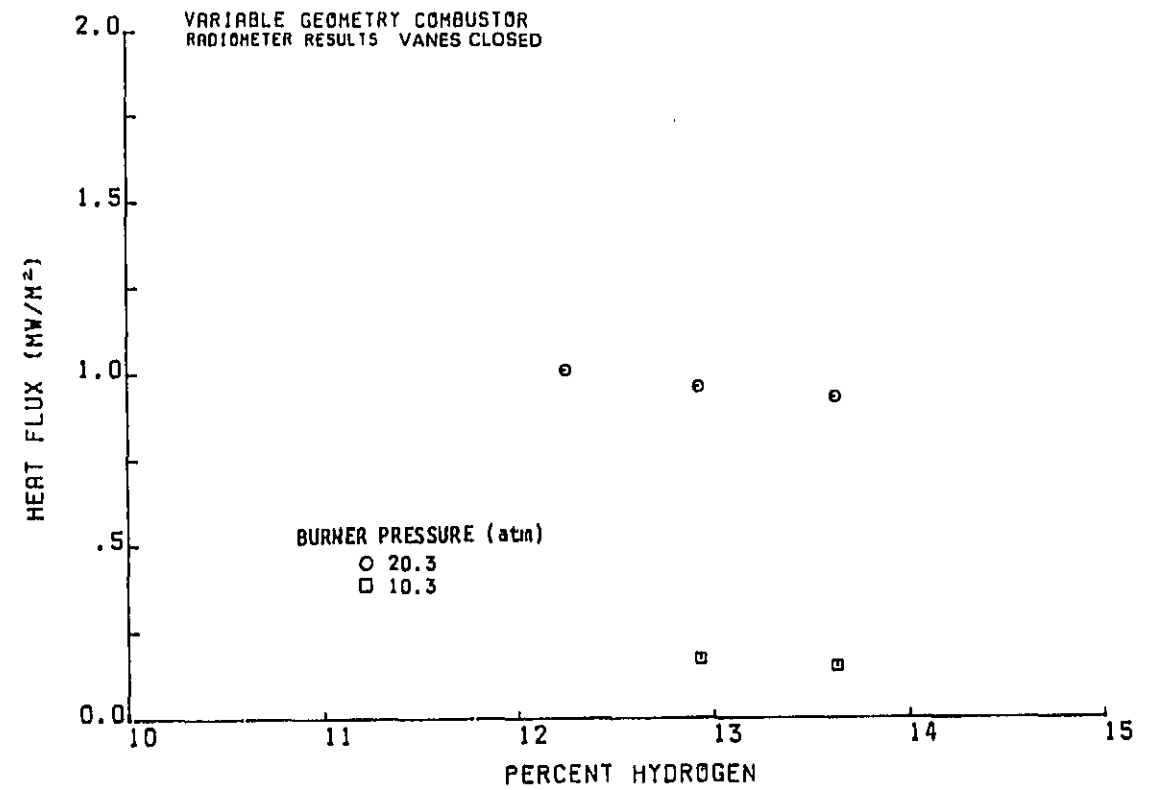

Figure 68 Variable Geometry Combustor - Medtherm Radiometer Results - Vanes Closed

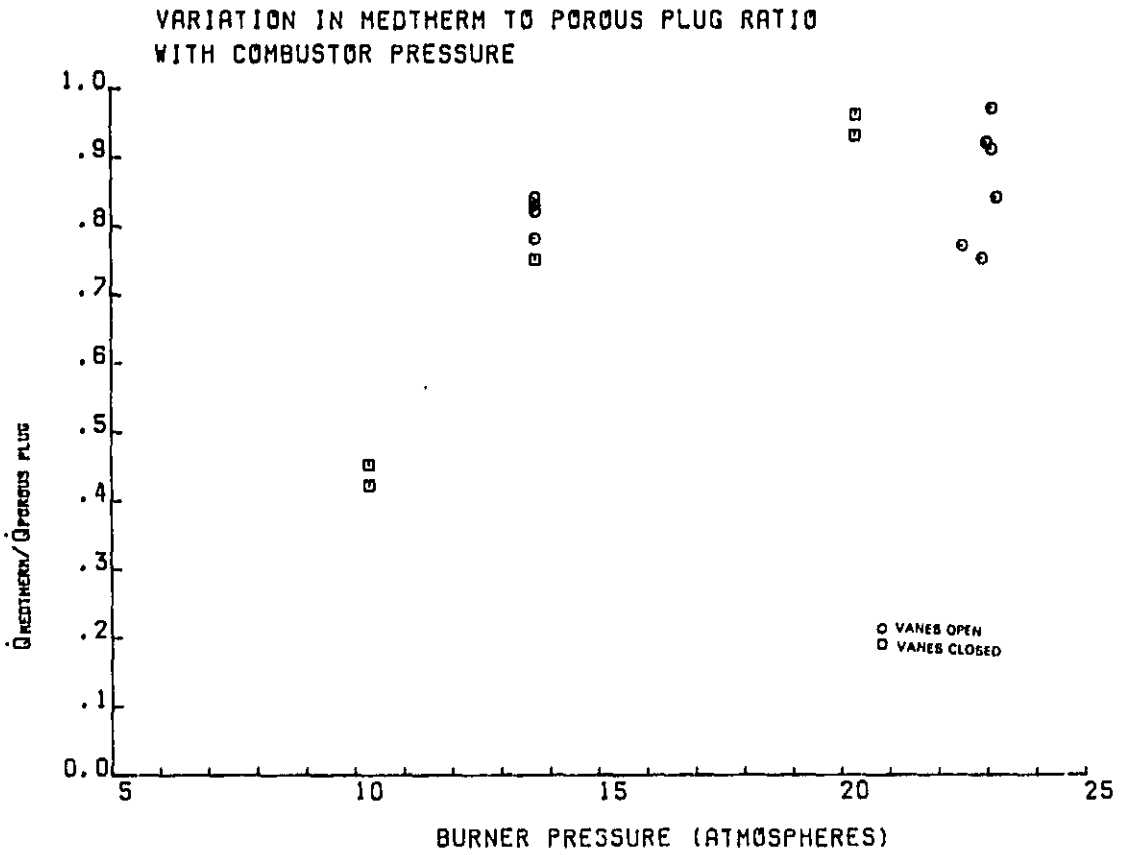

Figure 69 Variable Geometry Combustor - Variation in Medtherm to Porous Plug Ratio

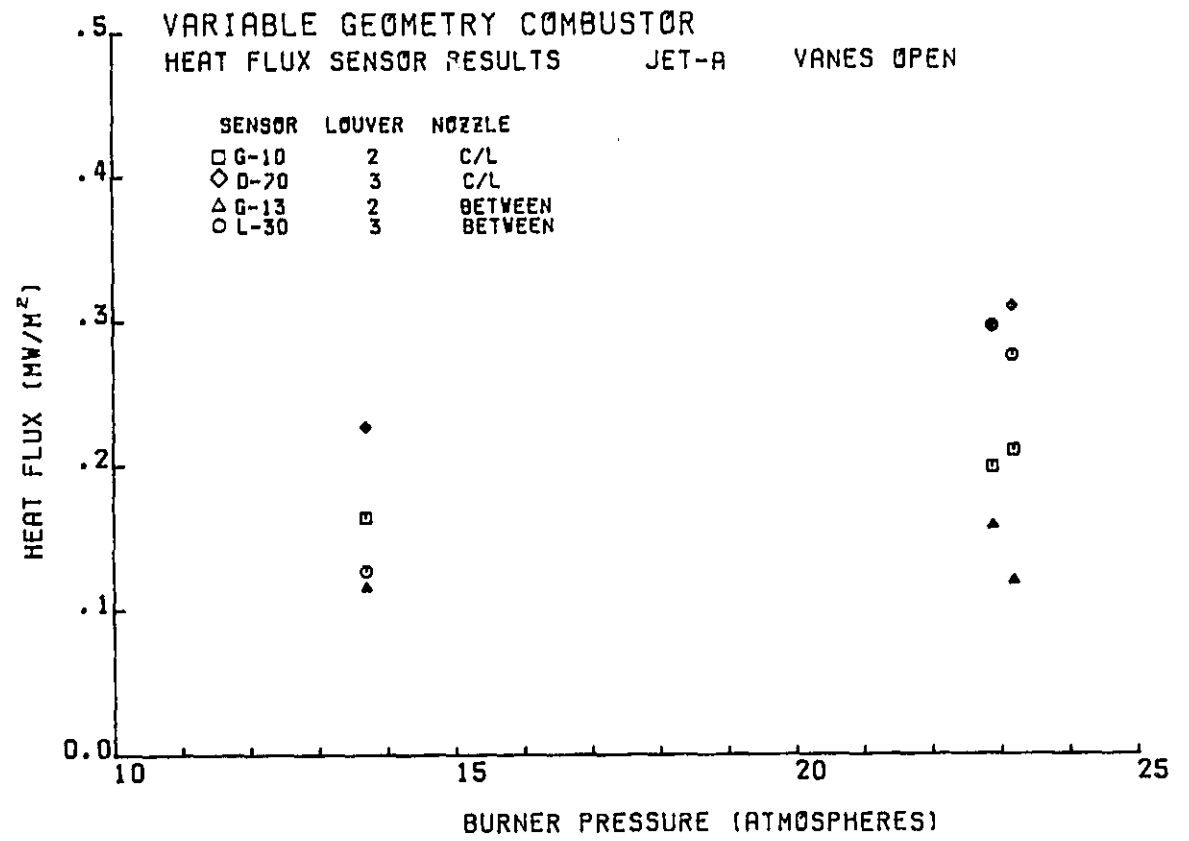

Figure 70 Variable Geometry Combustor - Heat Flux Sensor Results - Jet-A

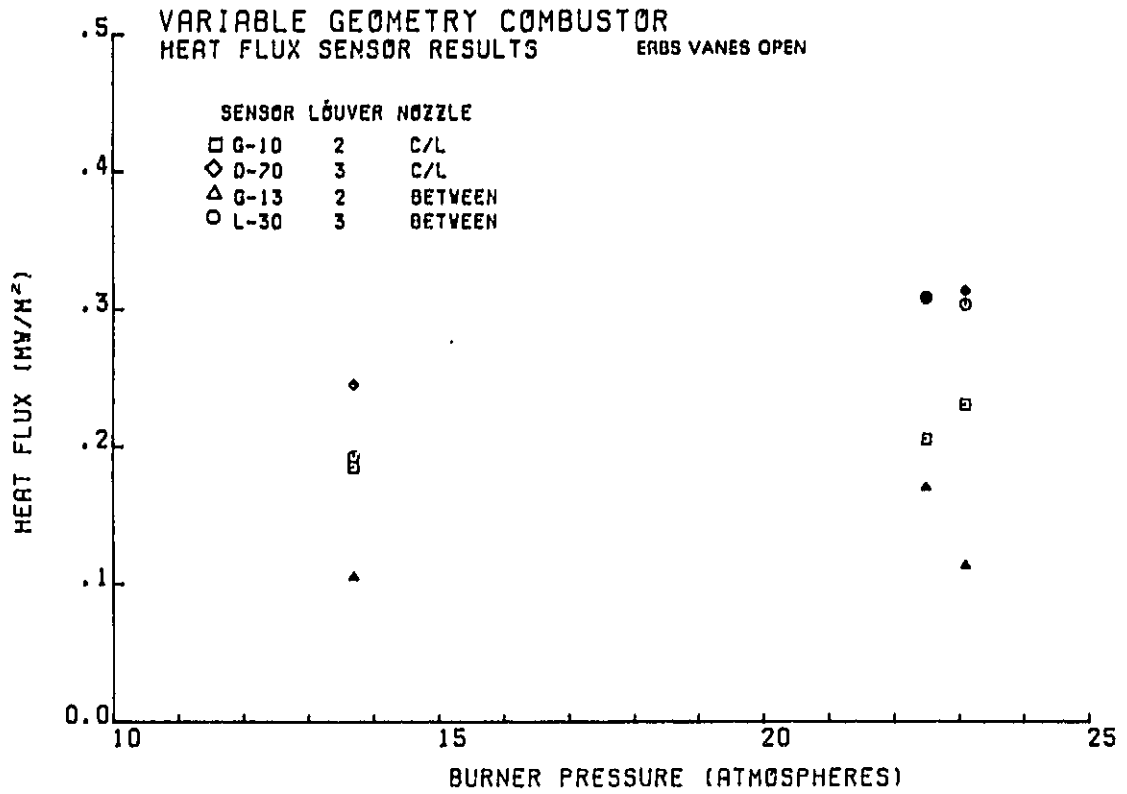

Figure 71 Variable Geometry Combustor - Heat Flux Sensor Results - ERBS

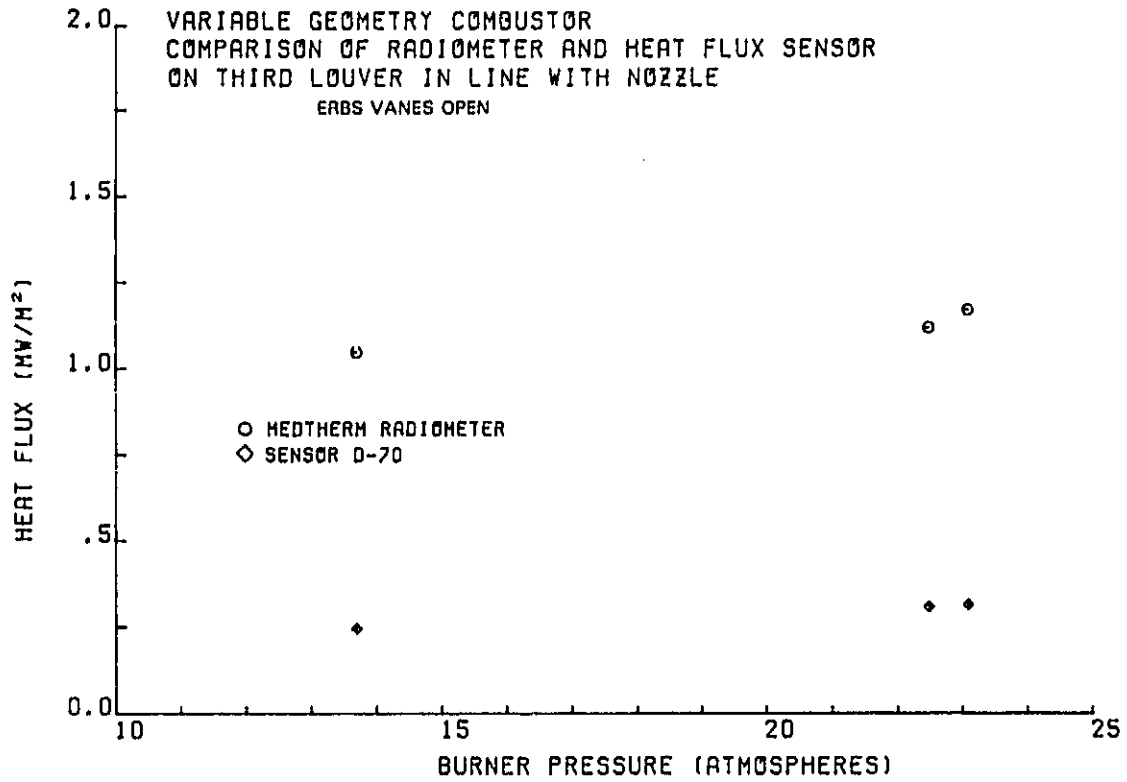

Figure 72 Variable Geometry Combustor - Comparison of Radiometer and Heat Flux Sensors on Third Louver - Vanes Open

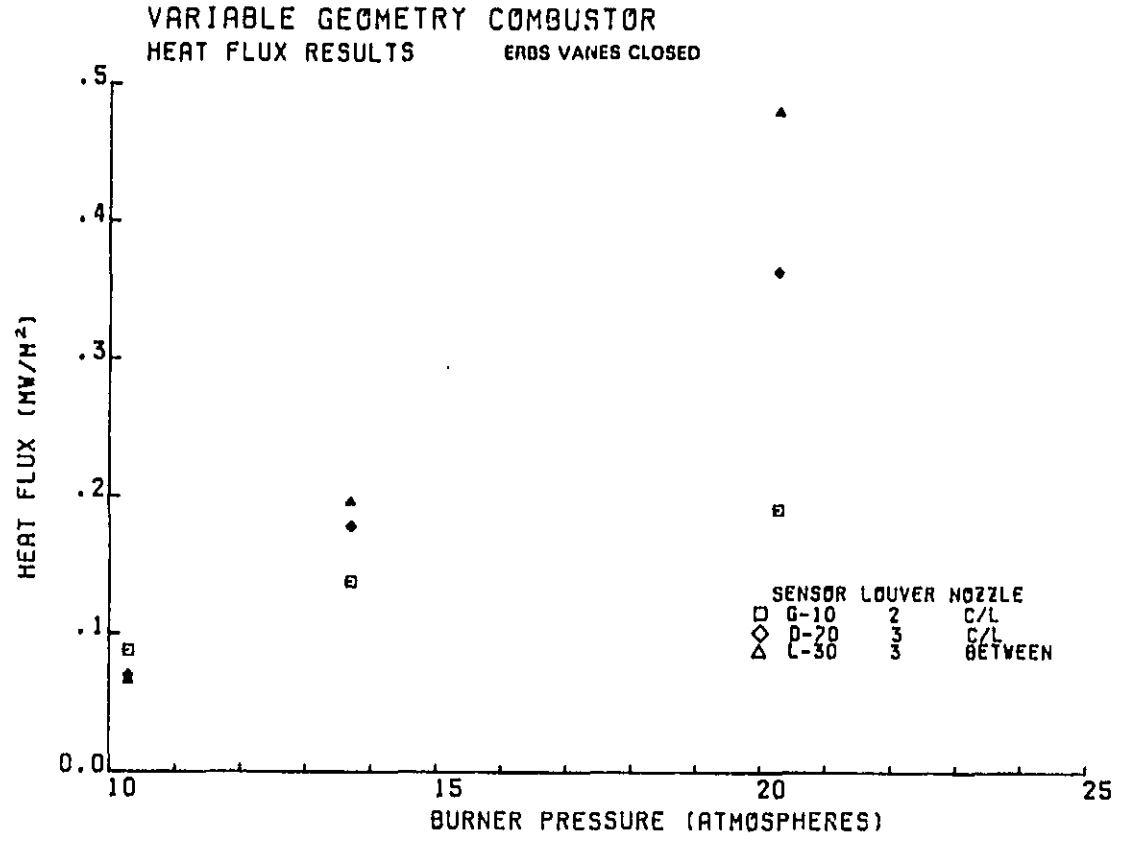

Figure 73 Variable Geometry Combustor - Heat Flux Sensor Results - ERBS - Vanes Closed

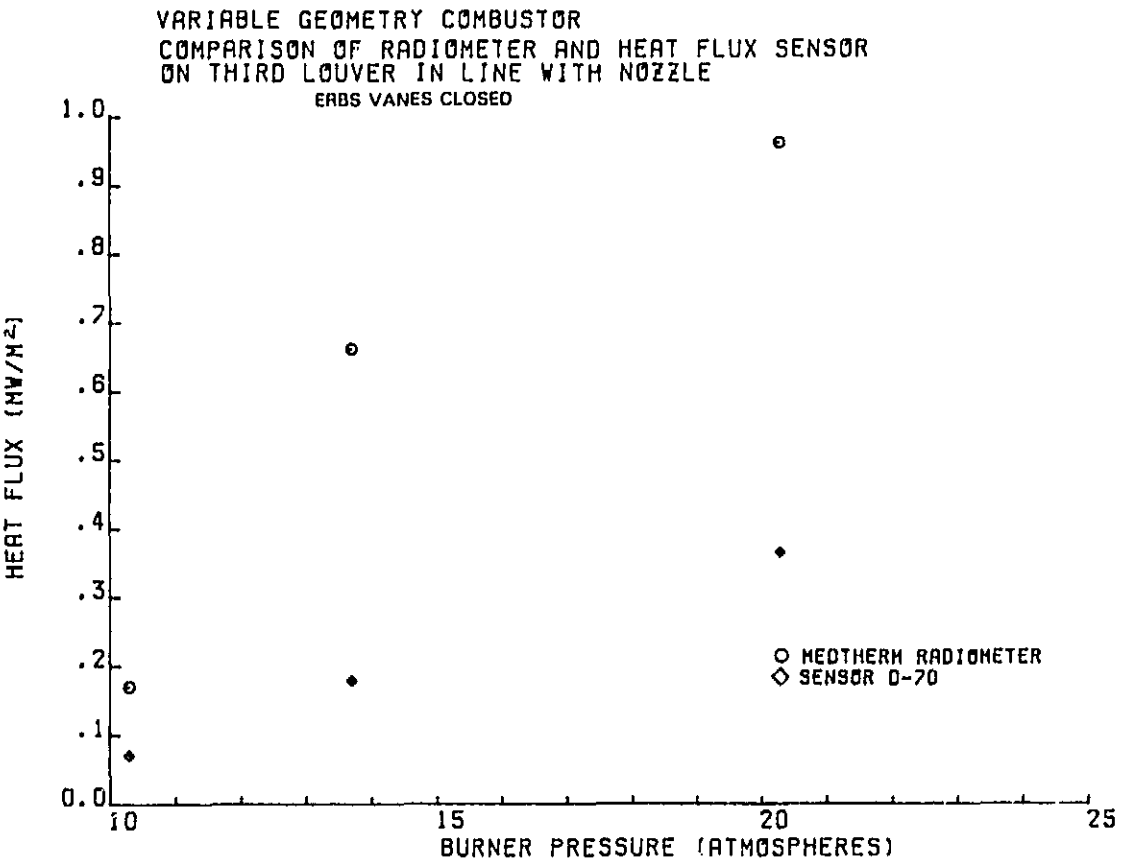

Figure 74 Variable Geometry Combustor - Comparison of Radiometer and Heat Flux Sensors on Third Louver - Vanes Closed

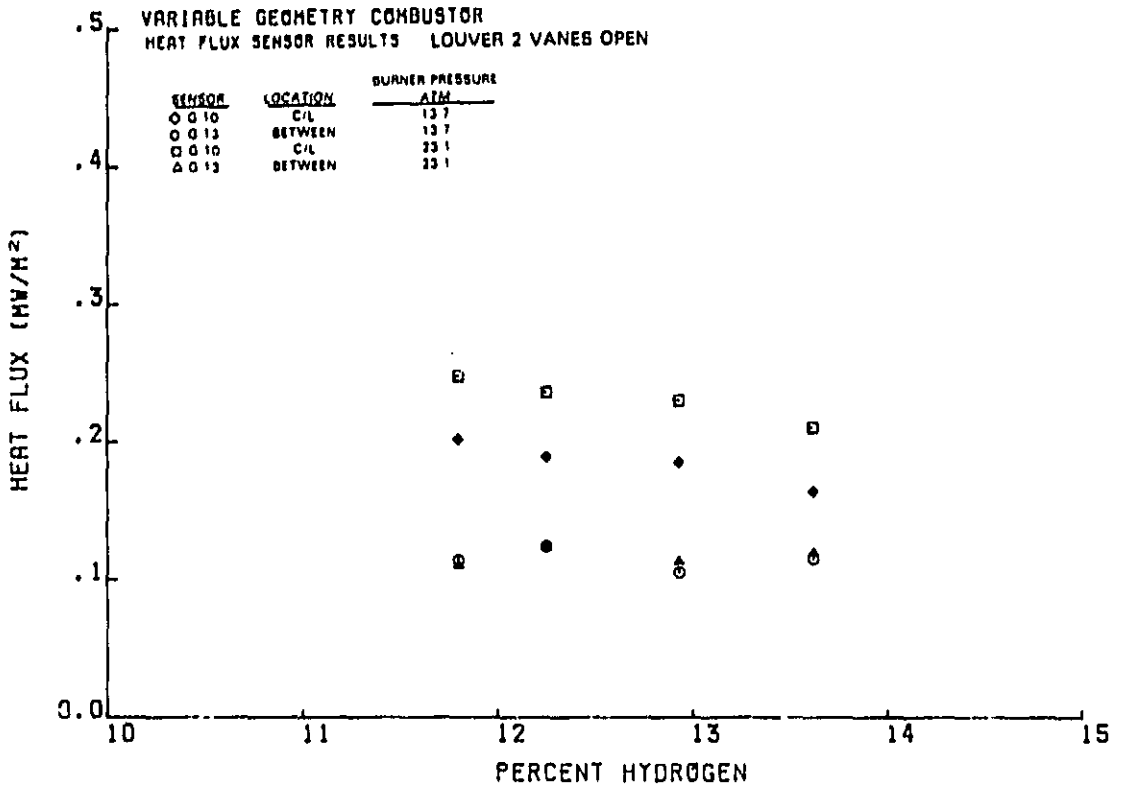

Figure 75 Variable Geometry Combustor - Heat Flux Sensor Results - Louver 2-Vanes Open

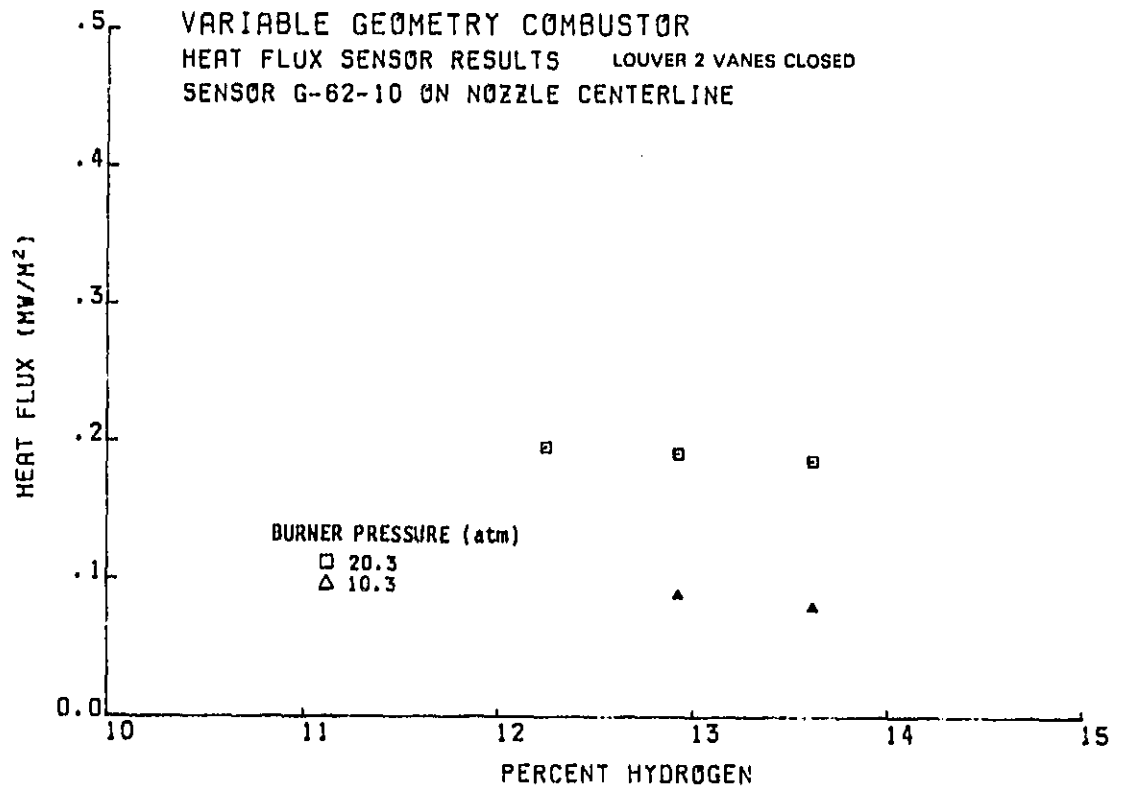

Figure 76 Variable Geometry Combustor - Heat Flux Sensor Results - Louver 2-Vanes Closed - Sensor 6-62-10

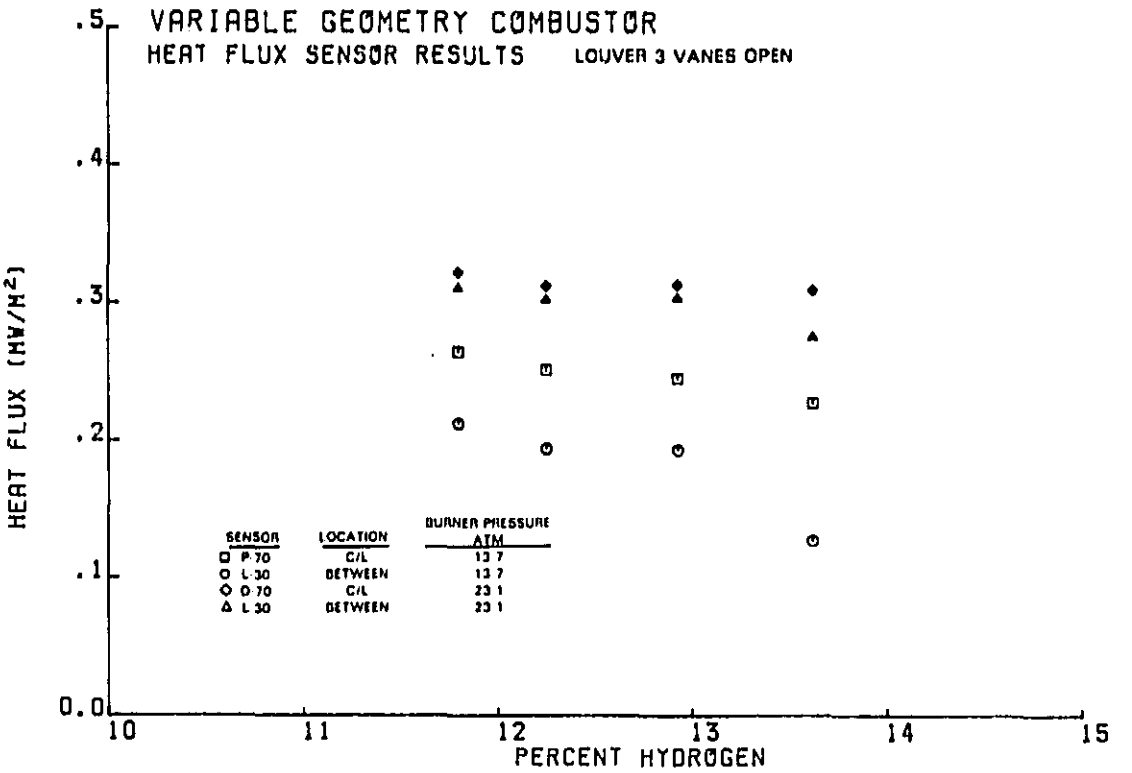

Figure 77 Variable Geometry Combustor - Heat Flux Sensor Results - Louver 3-Vanes Open

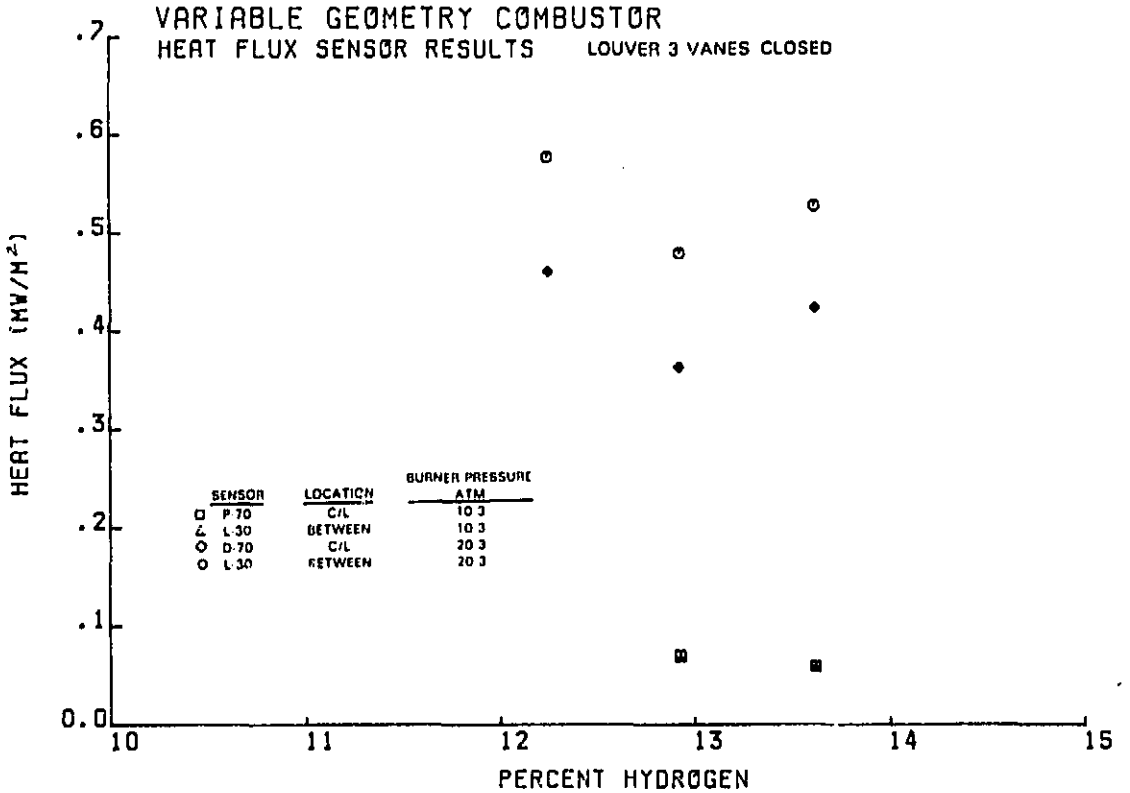

Figure 78 Variable Geometry Combustor - Heat Flux Sensor Results - Louver 3-Vanes Closed

SECTION 9.0
CONCLUSIONS AND RECOMMENDATIONS

Heat transfer tests were successfully completed in the high pressure combustor runs. Data was obtained from two different combustor installations, using five different fuels. Both the radiant heat load incident on the liners and the heat load transmitted through the liners were measured. The trends in the data looked as expected. Both radiant and transmitted heat flux increased with increasing combustor pressure or decreasing fuel hydrogen content. In the variable geometry combustor test, changing the combustor geometry altered the radiant heat load. The transmitted heat load changed in response to the modified incident heat load. Data was obtained simultaneously from radiometers with different fields of view. The data looks good and the data trends can be explained by the different fields of view of the two radiometers. On the baseline combustor, there was a high failure rate of the heat flux sensors. This appears to be due primarily to excessive handling rather than an inherent sensor design flaw. Overall, the heat flux sensors and radiometers were shown capable of producing data valuable in combustor studies. Based on the experience gained during the program, the following recommendations are made:

- Improved methods to protect the sensor leadwires from excessive handling should be developed.
- Sensors of these types should be utilized in combustor development programs to support development of improved combustor design codes.
- The radiometers used in the program gave good time average data. Their use should be continued and dynamic radiometers should be developed to investigate temporal variation in the combustor fireball.

REFERENCES

1. Atkinson, W. H.; Strange, R. R.,"Development of Advanced High-Temperature Heat Flux Sensors: NASA CR-165618, September 1982.
2. Moffat, R. J.; Hunn, B. D.; Ayers, J. F.; "Development of a Transpiration Radiometer:, Transaction of Instrument Society of America - Volume 4, 1971.
3. Atkinson, W. H.; Cyr, M. A.; Strange, R. R.; "Turbine Blade and Vane Heat Flux Sensor Development Phase I Final Report" NASA CR-168297, August 1984.